

RESCATTERING EFFECTS IN INCOHERENT  
PHOTOPRODUCTION OF  $\pi$ -MESONS OFF DEUTERIUM  
IN THE  $\Delta(1232)$  RESONANCE REGION

DISSERTATION  
ZUR ERLANGUNG DES GRADES  
„DOKTOR DER NATURWISSENSCHAFTEN“  
AM FACHBEREICH PHYSIK  
DER JOHANNES GUTENBERG-UNIVERSITÄT MAINZ

VORGELEGT VON  
EED M. DARWISH  
GEBOREN IN SOHAG, ÄGYPTEN

INSTITUT FÜR KERNPHYSIK  
JOHANNES GUTENBERG-UNIVERSITÄT MAINZ  
MAI 2002

Dekan: Professor Dr. Hartmut Backe  
1. Berichterstatter: Professor Dr. Hartmuth Arenhövel  
2. Berichterstatter: Professor Dr. Martin Reuter  
Datum der Einreichung: 27. Mai 2002  
Datum der mündlichen Prüfung: 10. Juli 2002

### **Hinweis**

Gegenüber der ursprünglichen, am 27. Mai 2002 im Dekanat des Fachbereichs Physik der Johannes Gutenberg-Universität Mainz eingereichten Arbeit sind in der vorliegenden Version einige zwischenzeitlich gefundene Druckfehler entfernt worden.

Mainz, Juli 2002

Eed M. Darwish

IN THE NAME OF GOD

*most Gracious and most Merciful*

DEDICATED TO THE MEMORY OF MY PARENTS

&

TO MY WIFE AND MY CHILDREN

*for their Patience, Forbearance and Encouragement*



# ABSTRACT

Incoherent photoproduction of pions on the deuteron in the  $\Delta(1232)$  resonance region is investigated in order to study the effect of nucleon-nucleon ( $NN$ ) and pion-nucleon ( $\pi N$ ) rescattering in the final state. The elementary  $\gamma N \rightarrow \pi N$  production amplitude is taken in the effective Lagrangian approach and contains besides the standard pseudovector Born terms the resonance contribution from the  $\Delta(1232)$  excitation. It yields for the elementary reaction a good agreement with the experimental data from MAMI, TRIUMF and TAPS.

Pion photoproduction on the deuteron is dominated by the impulse approximation where the pion is produced on one of the nucleons neglecting all final state interactions. The comparison of the impulse approximation with the available experimental data shows a significant overestimation of the data.

Therefore, the major point of concern of this thesis was the inclusion of rescattering effects in the final  $\pi NN$  system which we have limited to the leading order contributions of two-particle interactions in the  $NN$ - and  $\pi N$ -subsystems. As models for the relevant two-body interactions we have used separable approximations which fit the phase shift data for  $NN$  and  $\pi N$  scattering. We found that the influence of  $NN$ - and  $\pi N$ -rescattering effects on total and differential cross sections is significant. Inclusion of such effects leads to a much improved agreement with the existing experimental data.

Since several experiments to measure the spin asymmetry of the total photoabsorption cross section, which determines the Gerasimov-Drell-Hearn (GDH) sum rule, are now being performed or planned at different laboratories around the world (MAMI, ELSA, LEGS, GRAAL and TJNAF), the contribution of incoherent pion photoproduction to the spin asymmetry for the deuteron is evaluated with inclusion of  $NN$  and  $\pi N$  rescattering contributions. The effect of final state rescattering on the spin asymmetry for the deuteron is found to be quite important and should be included in forthcoming theoretical studies.

Mainz, May 27, 2002

Supervisor: Prof. Dr. H. Arenhövel



## ZUSAMMENFASSUNG

In der vorliegenden Arbeit wurde die inkohärente Photoproduktion von  $\pi$ -Mesonen am Deuteron im Bereich der  $\Delta(1232)$ -Resonanz unter Berücksichtigung der Endzustandswechselwirkung von Nukleon-Nukleon ( $NN$ ) und Pion-Nukleon ( $\pi N$ )-Rückstreuung untersucht. Die verwendete elementare Amplitude der Photopionproduktion am freien Nukleon berücksichtigt Born-Terme in pseudovektorieller  $\pi N$ -Kopplung sowie den  $\Delta(1232)$ -Resonanzbeitrag. Durch Anpassung der Modellparameter erhält man eine gute Übereinstimmung mit den experimentellen Daten von MAMI, TRIUMF und TAPS.

Bezüglich der inkohärenten Reaktion am Deuteron ergibt sich im Rahmen der Stoßnäherung qualitativ eine zufriedenstellende Übereinstimmung mit dem Experiment für geladene Pionen hinsichtlich der totalen und differentiellen Wirkungsquerschnitte. Es zeigt sich aber eine systematische Überschätzung von etwa 30 Prozent für neutrale Pionen. Daher ist es das Ziel dieser Arbeit, den Einfluß der bisher vernachlässigten  $NN$ -Endzustandswechselwirkung und der  $\pi N$ -Rückstreuung auf die Pionphotoproduktion zu untersuchen.

Bei der Behandlung der Drei-Teilchen-Dynamik im Endzustand beschränken wir uns auf Beiträge von Zwei-Teilchen-Wechselwirkungen in den  $NN$ - bzw.  $\pi N$ -Subsystemen. Als Modell für die  $NN$ - und  $\pi N$ -Wechselwirkung haben wir separable Potentiale benutzt, wobei die freien Parameter durch einen Fit der Streuphasendaten bestimmt sind. Dabei zeigt es sich, daß der Einfluß der  $NN$ - und  $\pi N$ -Rückstreueffekte auf die totalen und differentiellen Wirkungsquerschnitte signifikant ist. Die Einbeziehung solcher Effekte führt zu einer verbesserten Beschreibung der experimentellen Daten.

Als Beispiel einer Polarisationsobservablen haben wir die in die Gerasimov-Drell-Hearn-Summenregel (GDH) einfließende Beiträge der inkohärente  $\pi$ -Produktion zur Spin-Asymmetrie des totalen Absorptionsquerschnitts am Deuteron unter Berücksichtigung der  $NN$ - und  $\pi N$ -Endzustandswechselwirkung untersucht. Wir haben gefunden, dass der Einfluß der Endzustandswechselwirkungen für die Spin-Asymmetrie und das GDH-Integral wichtig ist und in den zukünftigen theoretischen Arbeiten berücksichtigt werden muß.

Mainz, Mai 27, 2002

Betreuer: Prof. Dr. H. Arenhövel



# Contents

<b>List of Figures</b>	<b>iii</b>
<b>List of Tables</b>	<b>vi</b>
<b>1 Introduction and Motivation</b>	<b>1</b>
1.1 Introduction . . . . .	1
1.2 Review of Previous Work . . . . .	2
1.3 Motivation . . . . .	4
1.4 Outline of this Thesis . . . . .	6
<b>2 Pion Photoproduction on the Nucleon</b>	<b>9</b>
2.1 The Photoproduction Operator . . . . .	11
2.2 Interaction Hamiltonian . . . . .	12
2.2.1 The Electromagnetic Interaction . . . . .	13
2.2.2 The $\pi N$ Interaction . . . . .	16
2.2.3 The $\pi N\Delta$ -Vertex . . . . .	17
2.3 Construction of the Amplitude . . . . .	18
2.3.1 The Born Terms . . . . .	18
2.3.2 The $\Delta(1232)$ Resonance Term . . . . .	19
2.4 Results for Elementary Process . . . . .	21
2.4.1 Differential Cross Section . . . . .	22
2.4.2 Total Cross Section . . . . .	24
<b>3 Photoproduction of <math>\pi</math>-Mesons on the Deuteron</b>	<b>27</b>
3.1 Kinematics . . . . .	28
3.2 Two-Nucleon Wave Function . . . . .	31
3.3 Matrix Elements for $\gamma d \rightarrow \pi NN$ . . . . .	32
3.3.1 The Impulse Approximation (IA) . . . . .	33
3.3.2 The $NN$ Final State Interaction . . . . .	35
3.3.3 The $\pi N$ Final State Interaction . . . . .	38

<b>4 Results and Discussion</b>	<b>43</b>
4.1 Total Cross Section . . . . .	44
4.1.1 Comparison with Experimental Data . . . . .	47
4.1.2 Comparison with other Theoretical Predictions . . . . .	48
4.2 Differential Cross Section . . . . .	52
4.2.1 Comparison with Experimental Data . . . . .	55
4.2.2 Comparison with other Theoretical Predictions . . . . .	58
4.3 Spin Asymmetry and Gerasimov-Drell-Hearn Sum Rule . . . . .	61
<b>5 Summary and Outlook</b>	<b>67</b>
5.1 Summary . . . . .	67
5.2 Future Extensions . . . . .	69
<b>Appendices</b>	<b>71</b>
<b>A General Notations and Conventions</b>	<b>73</b>
A.1 Dirac Algebra . . . . .	73
A.2 Normalization of States . . . . .	76
A.3 Spherical Basis . . . . .	76
<b>B Useful Formulas for the Elementary Process</b>	<b>79</b>
B.1 Kinematics and Relevant Formulas . . . . .	79
B.2 Multipole Decomposition of Amplitudes . . . . .	81
<b>C Field Operators</b>	<b>85</b>
<b>D Parametrization of the Deuteron Wave Functions</b>	<b>87</b>
<b>E Transformation of Differential Cross Section</b>	<b>89</b>
<b>F Two-Body Subsystems</b>	<b>91</b>
F.1 The $NN$ Subsystem . . . . .	91
F.1.1 $NN$ Scattering Equation . . . . .	91
F.1.2 Separable $NN$ Potential Model . . . . .	95
F.1.3 $NN$ Phase Shifts . . . . .	97
F.2 The $\pi N$ Subsystem . . . . .	99
F.2.1 $\pi N$ -Scattering Equation . . . . .	99
F.2.2 Separable $\pi N$ Potential Model . . . . .	101
F.2.3 $\pi N$ Phase Shifts . . . . .	104
<b>G Parameters of the <math>NN</math> Separable Potential</b>	<b>107</b>

H Parameters of the $\pi N$ Separable Potential	115
Bibliography	116



# List of Figures

1.1	Differential cross section for $\pi^-$ photoproduction on the deuteron in the impulse approximation from [23] a	
1.2	Total cross section for $\pi^0$ photoproduction on the deuteron in the impulse approximation from [23] a	
2.1	The elementary process $\gamma N \rightarrow \pi N$ . A solid, dashed and wavy line represents a nucleon, pion and ph	
2.2	Diagrams for the elementary process $\gamma N \rightarrow \pi N$ : (a) the Kroll-Rudermann graph, (b) and (c) the tw	
2.3	The $\gamma N$ - and $\gamma\pi$ -vertices. . . . .	13
2.4	The $\pi\gamma$ -vertex. . . . .	14
2.5	The $\gamma\pi N$ -vertex. . . . .	15
2.6	The $\gamma N \Delta$ -vertex. . . . .	15
2.7	The $\pi N$ -vertices. . . . .	17
2.8	The $\pi N$ -vertex in case of the pion absorption. . . . .	17
2.9	The $\pi N \Delta$ -vertex. . . . .	18
2.10	Real and imaginary parts of the $M_{1+}^{3/2}$ multipole in comparison with the calculation using the MAID	
2.11	Differential cross section for $\gamma n \rightarrow p\pi^-$ at six different values of the photon energy in the laboratory	
2.12	Differential cross section for $\gamma p \rightarrow n\pi^+$ . Lines description as in Fig. 2.11. The experimental data are	
2.13	Differential cross section for $\gamma p \rightarrow p\pi^0$ . Lines description as in Fig. 2.11. The experimental data are	
2.14	Total cross sections for pion photoproduction on the nucleon as a function of photon energy for the f	
3.1	Kinematics in the laboratory frame for the reaction $\gamma d \rightarrow \pi NN$ . . . . .	29
3.2	Diagrammatic representation of the $\gamma d \rightarrow \pi NN$ amplitude including rescattering in the final state and	
3.3	Diagrammatic representation of final state interactions of the reaction $\gamma d \rightarrow \pi NN$ : (a) and (b) are "dr	
3.4	Feynman diagrams for the reaction $\gamma d \rightarrow \pi NN$ in the impulse approximation. 34	
3.5	Feynman diagram for the reaction $\gamma d \rightarrow \pi NN$ including $NN$ -rescattering in the final state. 35	
3.6	Feynman diagram for the reaction $\gamma d \rightarrow \pi NN$ including $\pi N$ -rescattering in the final state. 38	
4.1	Total cross sections for $\gamma d \rightarrow \pi NN$ reaction obtained within the impulse approximation (dotted curv	
4.2	The ratio $\sigma_{tot}^{IA+NN+\pi N} / \sigma_{tot}^{IA}$ as a function of the photon energy in the laboratory frame. The left, mid	
4.3	The ratio $\sigma_{tot}^{IA+NN+\pi N} / \sigma_{tot}^{IA+NN}$ as a function of the photon energy. The left, middle and right panels	
4.4	Total cross sections for $\pi^-$ (left panel) and $\pi^0$ (right panel) photoproduction on the deuteron. Solid	
4.5	Total cross sections for pion photoproduction on the deuteron obtained within the impulse approxim	
4.6	Differential cross sections for pion photoproduction on the deuteron within the impulse approximatio	

---

4.7	Differential cross section for $\pi^-$ photoproduction on the deuteron in the impulse approximation at different photon energies. The left panel shows the differential cross section for $\pi^-$ photoproduction on the deuteron as a function of the pion angle in the laboratory frame at different photon energies. The right panel shows the ratio $d\sigma^{IA+NN+\pi N}/d\sigma^{IA}$ as a function of the pion angle at different photon energies. The legend indicates that the solid line is for $\pi^-$ and the dashed line is for $\pi^0$ .	
4.8	The ratio $d\sigma^{IA+NN+\pi N}/d\sigma^{IA}$ as a function of the pion angle in the laboratory frame at different photon energies. The left panel shows the differential cross section for $\pi^-$ photoproduction on the deuteron as a function of the pion angle in the laboratory frame at different photon energies. The right panel shows the ratio $d\sigma^{IA+NN+\pi N}/d\sigma^{IA+NN}$ as a function of the pion angle at different photon energies. The legend indicates that the solid line is for $\pi^-$ and the dashed line is for $\pi^0$ .	
4.9	The ratio $d\sigma^{IA+NN+\pi N}/d\sigma^{IA+NN}$ as a function of the pion angle at different photon energies. The left panel shows the differential cross section for $\pi^-$ photoproduction on the deuteron as a function of the pion angle in the laboratory frame at different photon energies. The right panel shows the ratio $d\sigma^{IA+NN+\pi N}/d\sigma^{IA+NN}$ as a function of the pion angle at different photon energies. The legend indicates that the solid line is for $\pi^-$ and the dashed line is for $\pi^0$ .	
4.10	Differential cross sections for $\pi^-$ (left panels) and $\pi^0$ (right panels) photoproduction on the deuteron as a function of pion angle in the $\gamma N$ c.m. frame for the reaction $\gamma N \rightarrow \pi N$ . The left panel shows the differential cross section for $\pi^-$ photoproduction on the deuteron as a function of the pion angle in the $\gamma N$ c.m. frame for the reaction $\gamma N \rightarrow \pi N$ . The right panel shows the ratio $d\sigma^{IA+NN+\pi N}/d\sigma^{IA+NN}$ as a function of the pion angle at different photon energies. The legend indicates that the solid line is for $\pi^-$ and the dashed line is for $\pi^0$ .	
4.11	Differential cross section for $\pi^0$ photoproduction on the deuteron as a function of pion angle in the $\gamma N$ c.m. frame for the reaction $\gamma N \rightarrow \pi N$ . The left panel shows the differential cross section for $\pi^0$ photoproduction on the deuteron as a function of the pion angle in the $\gamma N$ c.m. frame for the reaction $\gamma N \rightarrow \pi N$ . The right panel shows the ratio $d\sigma^{IA+NN+\pi N}/d\sigma^{IA+NN}$ as a function of the pion angle at different photon energies. The legend indicates that the solid line is for $\pi^-$ and the dashed line is for $\pi^0$ .	
4.12	Differential cross sections for pion photoproduction on the deuteron in comparison with the results from the impulse approximation. The left panel shows the differential cross section for $\pi^-$ photoproduction on the deuteron as a function of the pion angle in the $\gamma N$ c.m. frame for the reaction $\gamma N \rightarrow \pi N$ . The right panel shows the ratio $d\sigma^{IA+NN+\pi N}/d\sigma^{IA+NN}$ as a function of the pion angle at different photon energies. The legend indicates that the solid line is for $\pi^-$ and the dashed line is for $\pi^0$ .	
4.13	Differential cross section for $\pi^-$ photoproduction on the deuteron in the impulse approximation. The left panel shows the differential cross section for $\pi^-$ photoproduction on the deuteron as a function of the pion angle in the $\gamma N$ c.m. frame for the reaction $\gamma N \rightarrow \pi N$ . The right panel shows the ratio $d\sigma^{IA+NN+\pi N}/d\sigma^{IA+NN}$ as a function of the pion angle at different photon energies. The legend indicates that the solid line is for $\pi^-$ and the dashed line is for $\pi^0$ .	
4.14	Differential cross section for $\pi^-$ photoproduction on the deuteron in the impulse approximation. The left panel shows the differential cross section for $\pi^-$ photoproduction on the deuteron as a function of the pion angle in the $\gamma N$ c.m. frame for the reaction $\gamma N \rightarrow \pi N$ . The right panel shows the ratio $d\sigma^{IA+NN+\pi N}/d\sigma^{IA+NN}$ as a function of the pion angle at different photon energies. The legend indicates that the solid line is for $\pi^-$ and the dashed line is for $\pi^0$ .	
4.15	Illustration of the relative spin orientation of the incoming photon and the target nuclei in the GDH formalism. The left panel shows the relative spin orientation of the incoming photon and the target nuclei in the GDH formalism. The right panel shows the ratio $d\sigma^{IA+NN+\pi N}/d\sigma^{IA+NN}$ as a function of the pion angle at different photon energies. The legend indicates that the solid line is for $\pi^-$ and the dashed line is for $\pi^0$ .	
4.16	Total absorption cross sections for circularly polarized photons on a target with spin parallel $\sigma^P$ (upper panel) and antiparallel $\sigma^A$ (lower panel) to the incoming photon. The left panel shows the total absorption cross sections for circularly polarized photons on a target with spin parallel $\sigma^P$ (upper panel) and antiparallel $\sigma^A$ (lower panel) to the incoming photon. The right panel shows the ratio $d\sigma^{IA+NN+\pi N}/d\sigma^{IA+NN}$ as a function of the pion angle at different photon energies. The legend indicates that the solid line is for $\pi^-$ and the dashed line is for $\pi^0$ .	
4.17	The Gerasimov-Drell-Hearn integral (see Eq. (4.3)) as a function of the upper limit of integration for the $\pi^-$ channel. The left panel shows the Gerasimov-Drell-Hearn integral as a function of the upper limit of integration for the $\pi^-$ channel. The right panel shows the ratio $d\sigma^{IA+NN+\pi N}/d\sigma^{IA+NN}$ as a function of the pion angle at different photon energies. The legend indicates that the solid line is for $\pi^-$ and the dashed line is for $\pi^0$ .	
4.18	Summation of the contributions of the three channels of incoherent single pion photoproduction to the total cross section. The left panel shows the summation of the contributions of the three channels of incoherent single pion photoproduction to the total cross section. The right panel shows the ratio $d\sigma^{IA+NN+\pi N}/d\sigma^{IA+NN}$ as a function of the pion angle at different photon energies. The legend indicates that the solid line is for $\pi^-$ and the dashed line is for $\pi^0$ .	
B.1	Kinematics in the $\pi N$ c.m. frame for the reaction $\gamma N \rightarrow \pi N$ . . . . .	80
F.1	The graphical diagram of the Lippmann-Schwinger equation for $NN$ interaction. . . . .	92
F.2	$^1S_0$ phase shift using a rank-3 separable potential from [49] (solid curve) in comparison with the original phase shift (dashed curve). . . . .	92
F.3	Same notation as in Fig. F.2 but for the $^3P_0$ , $^1P_1$ and $^3P_1$ and single channels using a rank-2 separable potential. . . . .	92
F.4	Same notation as in Fig. F.2 but for the $^1D_2$ and $^3D_2$ single channels using a rank-2 separable potential. . . . .	92
F.5	Same notation as in Fig. F.2 but for the coupled channel $^3S_1$ - $^3D_1$ using a rank-4 separable potential. . . . .	92
F.6	Same notation as in Fig. F.2 but for the coupled channel $^3P_2$ - $^3F_2$ using a rank-3 separable potential. . . . .	92
F.7	Same notation as in Fig. F.2 but for the coupled channel $^3D_3$ - $^3G_3$ using a rank-4 separable potential. . . . .	92
F.8	The $\pi N$ phase shifts of the $S$ partial waves obtained from the LS equation using the separable potential. . . . .	105
F.9	Same as Fig. F.8 but for the $P$ partial waves. . . . .	105
F.10	Same as Fig. F.8 but for the $D$ partial waves. . . . .	106

# List of Tables

4.1	Contributions of incoherent single pion photoproduction to the GDH integral for the deuteron integrals	
D.1	Coefficients of the parametrized deuteron wave functions for the Bonn OBE-potential (full model)	[4]
G.1	Parameters of the PEST3 potential in the $^1S_0$ partial wave.	108
G.2	Parameters of the PEST2 potential in the uncoupled $P$ waves.	109
G.3	Parameters of the PEST2 potential in the uncoupled $D$ waves.	110
G.4	Parameters of the PEST4 potential in the coupled $^3S_1$ - $^3D_1$ partial wave.	111
G.5	Parameters of the PEST3 potential in the coupled $^3P_2$ - $^3F_2$ partial wave.	112
G.6	Parameters of the PEST4 potential in the coupled $^3D_3$ - $^3G_3$ partial wave.	113
H.1	Parameters of the $\pi N$ separabel potential of Nozawa <i>et al.</i> [15] for the $\pi N$ partial waves. These parameters	



# Chapter 1

## Introduction and Motivation

### 1.1 Introduction

The present work is concerned with photoproduction of  $\pi$ -meson on deuterium. The  $\pi$ -meson or pion is the lightest of all the strongly interacting particles and plays a central role in the physics of strong interactions. It was proposed in 1935 by Yukawa [1] as the carrier of the strong interaction between nucleons (proton, neutron) in analogy with the photon in the electromagnetic interaction. The existence of the  $\pi$ -meson was experimentally confirmed in 1947 by Powell and his collaborators [2] and the pion is now known to exist in three charge states,  $\pi^+$ ,  $\pi^-$  and  $\pi^0$ , with masses of  $139.6 \text{ MeV}/c^2$  for charged pions and  $135.0 \text{ MeV}/c^2$  for the neutral pion.

Photo- and electroproduction of pions on a proton have been studied thoroughly both theoretically and experimentally. Beyond the pion threshold energy almost all reactions on the nucleon, either initiated by photons, pions or other hadrons with energies of a few hundred MeV (in the center-of-mass) are dominated via the formation of the first excited state of the nucleon, the  $\Delta(1232)$  resonance ( $J = 3/2$ ,  $I = 3/2$ ), which almost exclusively decays into a pion plus a nucleon.

During the last years, pseudoscalar meson production in electromagnetic reactions on light nuclei has become a very active field of research in medium-energy nuclear physics with respect to the study of hadron structure. For the following reasons the deuteron plays an outstanding role besides the free nucleon. The first one is that the deuteron is the simplest nucleus on whose structure we have abundant information and a reliable theoretical understanding, i.e. the structure of the deuteron is very well understood in comparison to heavier nuclei. Furthermore, the small binding energy of nucleons in the deuteron, which from the kinematical point of view provides the case of a nearly free neutron target, allows one to compare the contributions of its constituents to the electromagnetic and hadronic reactions to those from free

nucleons in order to estimate interaction effects.

The basic interaction in photoproduction is as follows: a photon is incident on a target nucleus and interacts with its constituents. As a result, a pseudoscalar meson is produced along with other particles. Two kinds of processes depending on the nature of the other particles produced in this interaction are found: coherent and incoherent processes.

In the coherent process, the meson is produced with the target nucleus maintaining its initial character. Thus, the interaction starts with a photon and some nucleus, and ends up with a meson and the same nucleus, i.e.  $\gamma X_A \rightarrow \pi X_A$ , where  $A$  is the mass number of the target nucleus. The process is labeled “coherent” because all nucleons in the nucleus participate in the process coherently, leading to a coherent sum of the individual nucleon contributions.

In the incoherent process, the nucleus ruptures and thus fails to maintain its initial identity. The meson is produced in association with a nucleon (or an excited state of the nucleon) and some new recoil “daughter” hadronic system. Thus, the interaction starts with a photon and some nucleus and ends up with a meson, a free nucleon (or an excited state of it) and a new hadronic system, i.e.  $\gamma X_A \rightarrow \pi N X_{A-1}$ . The process is labeled as “incoherent” because it occurs in kinematic and physical circumstances similar to those of the process that produces a meson from a free nucleon.

## 1.2 Review of Previous Work

The electromagnetic production of pions on the free nucleon, including photoproduction and electroproduction, has long been studied since the pioneering work of Chew, Goldberger, Low and Nambu (CGLN) [3]. As a result, an enormous amount of knowledge has been accumulated. Recently, theoretical interest in these reactions was revived by the new generation of high-intensity and high duty-cycle electron accelerators. With the developments of these new facilities, it is now possible to obtain accurate data for meson electromagnetic production, including spin-dependent observables. Extensive work during these more than forty years (see for example [4]-[17]) indicates that, below 500 MeV incident photon energy, the mechanisms of the  $\gamma N \rightarrow \pi N$  reaction are dominated by the Born terms and the  $\Delta(1232)$  excitation.

In this work, we go a step further by studying photoproduction of pions on the deuteron. First investigations on photoproduction of pions on the deuteron go back to the early fifties [18, 19] with view on the general structure of spin flip and no spin flip amplitudes. Later, a more systematic calculation of pion photoproduction

on the deuteron was done by Laget [12, 13, 20] and Blomqvist and Laget [11]. In their work the influence of pion rescattering and  $NN$  final state interaction is included within a diagrammatic ansatz. They used the elementary photoproduction operator of Blomqvist and Laget [11] as input in their calculations. At the time of these calculations, a comparison with experimental data was possible only for  $\pi^-$  production since data for  $\pi^+$  and  $\pi^0$  production in the  $\Delta(1232)$  resonance region were not available. The agreement of their predictions including final state interactions with the experimental data of the reaction  $\gamma d \rightarrow \pi^- pp$  [21] is quite good. They found that the final state interaction effects are small for the charged pion photoproduction reactions in comparison to the neutral channel. In recent years, experimental data for  $\pi^0$  photoproduction on the deuteron have become available [22]. As mentioned in Ref. [22], the predictions from [11, 12, 13, 20] are significantly above the data. A possible reason for this may be that they used the Blomqvist and Laget parametrization [11] of the elementary photoproduction amplitude which is not able to describe the neutral pion photoproduction from the proton.

Pion photoproduction on the deuteron in the impulse approximation has been studied by Schmidt *et al.* [23] neglecting all kinds of final state interactions and other two-body operators. They constructed an effective Lagrangian model for the process on the free nucleon and used it in their calculations on the deuteron. Since data for  $\pi^+$  and  $\pi^0$  photoproduction on the deuteron were absent at the time of these calculations, the authors could not compare their predictions with experimental data for these channels. A comparison with experimental data for  $\pi^-$  production, showed a slight overestimation of the data. They reported that the reason for that is an overestimation of the elementary reaction on the neutron. A comparison between their predictions and the recently measured experimental data for  $\pi^0$  photoproduction on the deuteron [22] is now possible. One can see in [22] that this prediction can hardly provide a reasonable description of the data for this channel. As already noted in [12, 24, 25], the effect of  $NN$  rescattering is important in the incoherent pion photoproduction on the deuteron, especially for  $\pi^0$  production.

Levchuk *et al.* [24] studied quasifree  $\pi^0$  photoproduction from the neutron via the  $d(\gamma, \pi^0)np$  reaction using the elementary photoproduction operator of Blomqvist and Laget [11]. The contributions from the pole diagrams as well as one-loop diagrams both with  $np$  and  $\pi N$  rescattering were taken into account. They wanted to explore the possibility of measuring the  $E_{1+}/M_{1+}$  ratio via photoproduction from quasifree production on the neutron. The isospin  $I = 3/2$  component of this ratio characterizes the relative strength of the recently much discussed (see e.g. [26, 27]) quadrupole  $E2$ -excitation of the  $\Delta$  resonance. The idea was that the  $n(\gamma, \pi^0)n$  reaction would be very useful for the isospin separation of the multipoles. In agreement with the results from the Laget model [12], Levchuk *et al.* find that the largest

effects disturbing the extraction of the multipoles for quasifree neutrons arise from the  $np$  final state interaction. They predict that these effects lead to a strong reduction of the cross section at pion forward angles, but are much less important for backward angles. They found also that the correction due to  $np$  rescattering decreases with increasing pion angle and becomes to be less than 8% at  $\theta_\pi \geq 90^\circ$ . Furthermore, they pointed out that the contribution of the proton pole diagram and the one of  $\pi N$  rescattering are negligible. The experimental data from Ref. [22] for the  $d(\gamma, \pi^0)np$  reaction qualitatively support this prediction since the disagreement with the spectator approach is most severe at pion forward angles but less pronounced at backward angles. However, a comparison of the data to the Laget model including final state interactions shows some unexplained reduction of the cross section at backward angles.

Recently and during the calculations of this work, Levchuk *et al.* [25] modified their theoretical predictions which have been done in [24] using a more realistic version of the elementary production operator and including the charged pion production channels which are not included in their old calculations [24]. The elementary production operator is taken in on-shell form and calculated using the SAID [28] and MAID [17] multipole analyses. The authors in [25] studied the semi-inclusive reaction  $d(\gamma, \pi)NN$  in the  $\Delta$  resonance region including pole diagrams and one-loop diagrams with  $NN$  and  $\pi N$  rescattering in the final state. Their predictions for total and differential cross sections including final state interactions show good agreement with the experimental data. However, Fig. 1.1 shows that a big difference between the theoretical predictions from [25] (dashed curve) and [23] (solid curve) is found for charged pion production reactions at pion forward angles in the impulse approximation. Furthermore, the predictions from [23] for the total cross sections for charged pion channels are found to be higher than the ones from [25] in the impulse approximation.

### 1.3 Motivation

The main motivation for studying photoproduction of pions on light nuclei is to obtain information on the elementary process on the neutron. The main goal of this thesis is to investigate incoherent pion photoproduction on the deuteron in the  $\Delta(1232)$  resonance region in order to study the effect of  $NN$  and  $\pi N$  rescattering in the final state. We include besides the pure impulse approximation, the two-body  $t$ -matrices from  $NN$  and  $\pi N$  rescattering in the final state.

As already mentioned above, a big difference is found between the theoretical predictions from [25] and [23] in the impulse approximation. Therefore, it is interesting

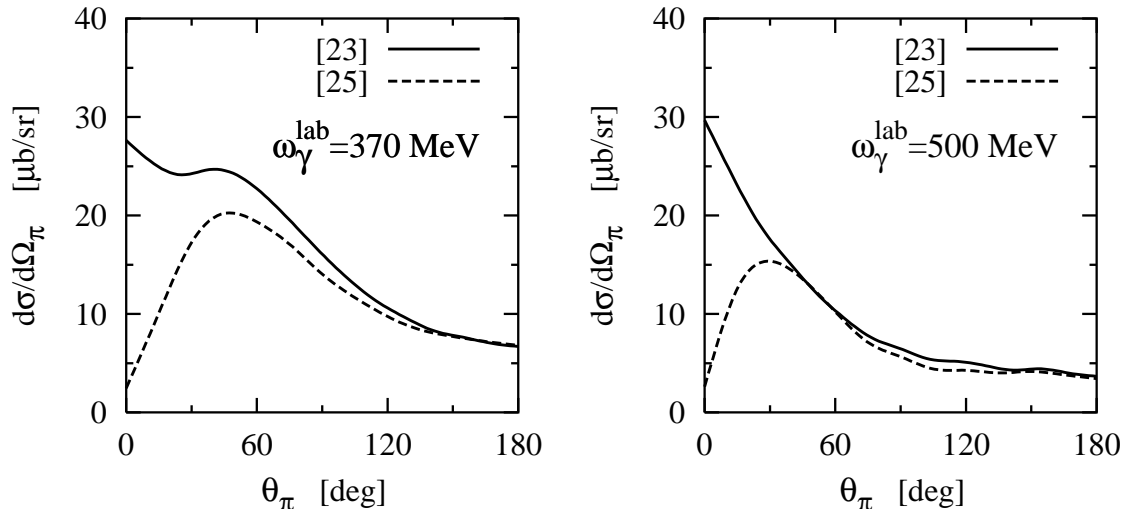


Figure 1.1: Differential cross section for  $\pi^-$  photoproduction on the deuteron in the impulse approximation from [23] (solid curve) in comparison with the results from [25] (dashed curve).

to check in this work where this big difference comes from. Since the authors in [25] pointed out that the main difference between their calculation and the one of Ref. [12] is that a more realistic version of the elementary production operator is used, we will also examine in this work the use of different pion photoproduction operators.

Furthermore, the comparison between the theoretical prediction from [23] for the total cross section of  $\pi^0$  photoproduction on the deuteron in the impulse approximation and the TAPS data [22] (see Fig. 1.2) gives a clear indication that the effects of final state interaction may be important. It was found that the final state interaction effects are significant in the case of coherent pion photoproduction on the deuteron (see for example [14, 29, 30, 31]). This means that one needs a reliable description for the rescattering process.

Recently, several experiments to measure the spin asymmetry of the total photoabsorption cross section, which determines the Gerasimov-Drell-Hearn (GDH) sum rule, on the proton and on the deuteron are now performed or planned at different laboratories around the world (MAMI, ELSA, LEGS, GRAAL and TJNAF). The A2 collaboration has prepared an experiment on the proton and on the deuteron at the Mainzer Microtron MAMI, that shall be completed for the higher photon energies at ELSA in Bonn. This makes the theoretical investigation of the spin asymmetry and the corresponding GDH integral particularly interesting. Therefore,

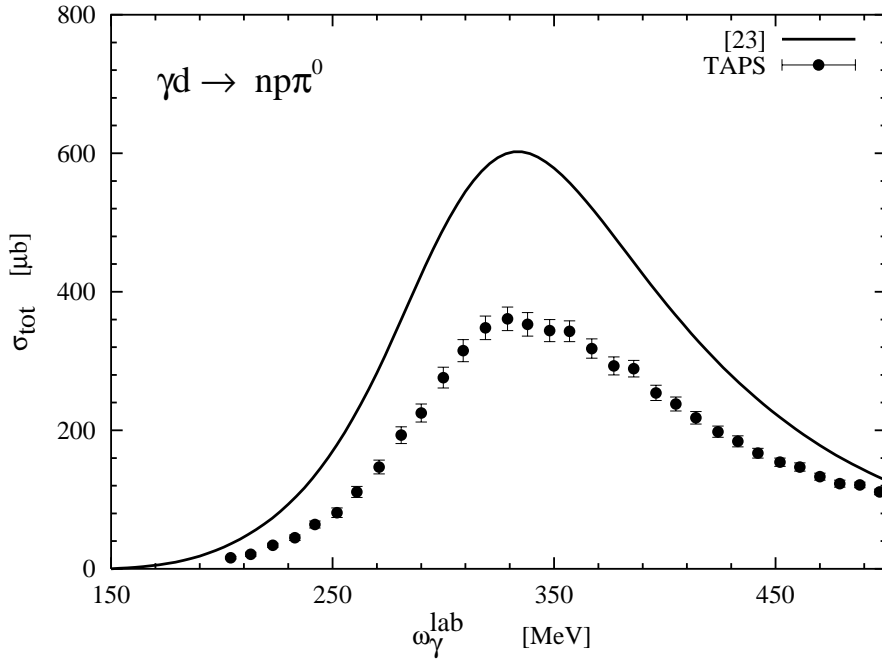


Figure 1.2: Total cross section for  $\pi^0$  photoproduction on the deuteron in the impulse approximation from [23] as a function of the photon energy in the laboratory frame. Data points are from TAPS [22].

we investigate in this work the influence of  $NN$  and  $\pi N$  rescattering effects on the spin asymmetry and GDH sum rule for the deuteron.

Therefore, our aim is to construct a model for the reaction  $\gamma d \rightarrow \pi NN$  in the  $\Delta(1232)$  resonance region by incorporating the leading contributions from  $NN$  and  $\pi N$  final state interactions in time-ordered perturbation theory.

## 1.4 Outline of this Thesis

This thesis is organized as follows. In chapter 2, we present the effective Lagrangian model of the elementary pion photoproduction process on the free nucleon which we use as input in our calculations on the deuteron. We explain how the reaction operator for this process is constructed. The nonresonant amplitudes and the contribution of the  $\Delta(1232)$  resonance are given in an arbitrary frame of reference. We end this chapter with a discussion of our results for differential and total cross sections and compare with experimental data.

Chapter 3 is devoted to the central topic of this work. The treatment of the

$\gamma d \rightarrow \pi NN$  amplitude, based on time-ordered perturbation theory with the inclusion of  $NN$  and  $\pi N$  final state interactions is developed in this chapter. The transition matrix element is explicitly described with the inclusion of the  $NN$ - and  $\pi N$ -rescattering.

In chapter 4, we will present our main results together with a comparison with experimental data and other theoretical predictions. We discuss in this chapter the effects of rescattering on total and differential cross sections. The contribution of incoherent single pion photoproduction to the spin asymmetry and the corresponding GDH sum rule for the deuteron is also discussed. Finally, we conclude and summarize our results in chapter 5. Future considerations are also given in this chapter.

For the convenience of the reader, eight appendices are given at the end of the thesis. Appendix A, B and C contain the general notations, formalism and useful formulas for the process on the nucleon. In appendix D, we give the parametrization of the deuteron wave functions for the Bonn potential which we use in our calculations. In order to compare our results for differential cross section of  $\pi^0$  photoproduction reaction on the deuteron with the experimental data from Ref. [22], transformation formulas from the laboratory frame of the deuteron to the  $\gamma N$  center-of-mass frame are given in appendix E. In appendix F, we study in detail the  $NN$  and  $\pi N$  scattering matrices which we use as input in our predictions and also give a solution for the two-body scattering matrix using separable two-body interactions. The parameters of the form factors of these separable models are given in appendix G and H.



# Chapter 2

## Pion Photoproduction on the Nucleon

Starting point of the construction of an operator for pion photoproduction in the two-nucleon space is the study of the elementary process, i.e. pion photoproduction on the free nucleon. This process is usually labeled as "elementary" to distinguish it from the same process from a nucleus. In the elementary process a photon is absorbed by a free nucleon (a proton or a neutron) to yield a  $\pi$ -meson in addition to a nucleon.

The electromagnetic production of pions on the free nucleon, including photoproduction and electroproduction, has long been studied since the pioneering work of Chew, Goldberger, Low and Nambu (CGLN) [3]. An enormous amount of knowledge has been accumulated as a result. Kroll and Rudermann [4] were the first to derive model-independent predictions in the threshold region, so-called low-energy theorems (LET), by applying gauge and Lorentz invariance to the reaction  $\gamma N \rightarrow \pi N$ . The general formalism for this process was developed by Chew *et al.* [3] (CGLN-amplitudes). Fubini *et al.* [5] extended the earlier predictions of LET by including also the hypothesis of a partially conserved axial current (PCAC). In this way they succeeded in describing the threshold amplitude as a power series in the ratio  $m = \frac{m_\pi}{M_N}$  up to terms of order  $m^2$ . Berends *et al.* [6] analysed the existing data in terms of a multipole decomposition and presented tables of the various multipole amplitudes constructing in the region up to excitation energies of 500 MeV.

For more than twenty years, the standard model for pion photoproduction on the nucleon has been the model of Olsson and Osypowski [7, 8], who emphasized the importance of Watson's theorem as a requirement to be obeyed by the electromagnetic multipoles below  $\pi\pi$ -threshold. In practice, a model that has been more extensively used for comparison with data is the one of Blomqvist and Laget [11] which is a

non-relativistic reduction of the model of Olsson and Osypowski. It has been constructed in a general frame of reference, but Blomqvist and Laget used different  $\Delta$  parametrizations for neutral and charged pion photoproduction. These parametrizations give a satisfactory fit to the amplitude for charged pion photoproduction, but it is not able to describe the neutral pion photoproduction from the proton. More than ten years ago, another model for pion photoproduction on the nucleon in the  $\Delta$  region has been proposed by Nozawa, Blankleider and Lee [15]. This model has been extended to pion electroproduction and has also proved to be successful for photo- and electroproduction on the free nucleon.

Garcilazo and Moya de Guerra [16] have been constructed a model for photo- and electroproduction on the nucleon. This model is applicable from threshold through the first and second resonance regions. It contains the Born terms, the  $\rho$  and  $\omega$  vector mesons, the  $\Delta$  and the Roper resonances as well as the resonances  $S_{11}$ ,  $D_{13}$ ,  $S_{31}$  and  $D_{33}$ . They found a good agreement with experimental data up to 1 GeV. Recently, a unitary isobar model for pion photo- and electroproduction off the nucleon has been developed for nuclear applications at photon energies up to 1 GeV [17]. This model contains Born terms, vector mesons and nucleon resonances and is constructed in the  $\pi N$  center-of-mass frame. Within this model they have obtained good agreement with experimental data for pion photo- and electroproduction on the free nucleon.

In this work we will examine the various observables for pion photoproduction on the free nucleon using the effective Lagrangian model of Schmidt *et al.* [23] which we will briefly outline in this chapter. The main advantage of this model is that it has been constructed in a general frame of reference and therefore can be applied directly to the electromagnetic photoproduction of  $\pi$ -mesons on nuclei. This model contains besides the standard pseudovector Born terms the resonance contribution from the  $\Delta(1232)$  excitation. Kinematical and other useful formulas for pion photoproduction on the free nucleon, which diagrammatically shown in Fig. 2.1, are given in appendix B.

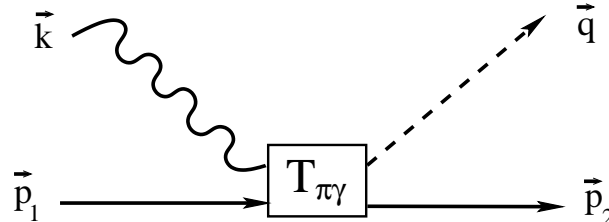


Figure 2.1: The elementary process  $\gamma N \rightarrow \pi N$ . A solid, dashed and wavy line represents a nucleon, pion and photon, respectively.

## 2.1 The Photoproduction Operator

The  $\mathcal{T}$ -operator describing transitions between asymptotically free states is given in terms of the interaction Hamiltonian  $\mathcal{H}_{int}$  between all the involved particles as follows [32]

$$\mathcal{T} = \mathcal{H}_{int} + \mathcal{H}_{int} \frac{1}{E - \mathcal{H} + i\epsilon} \mathcal{H}_{int}, \quad (2.1)$$

which can also be re-written as

$$\mathcal{T} = \mathcal{H}_{int} + \mathcal{H}_{int} \frac{1}{E - \mathcal{H}_0 + i\epsilon} \mathcal{T}, \quad (2.2)$$

where  $\mathcal{H}_0$  is the free Hamiltonian. The on-shell matrix element  $T_{fi}$  of Eq. (2.2) is given in terms of the Hamilton operator  $\mathcal{H}_{int}$  by

$$T_{fi} = \langle f | \mathcal{T} | i \rangle = \langle f | \mathcal{H}_{int} | i \rangle + \sum_{\alpha} \langle f | \mathcal{H}_{int} | \alpha \rangle \frac{1}{E - E_{\alpha} + i\epsilon} T_{\alpha i}, \quad (2.3)$$

where the energy eigenvalues  $E_{\alpha}$  are given by

$$\mathcal{H}_0 | \alpha \rangle = E_{\alpha} | \alpha \rangle. \quad (2.4)$$

Making one-iteration approximation and keeping terms from the second order we obtain the following expression for the  $T_{fi}$ -matrix

$$T_{fi}^{(2)} = \langle f | \mathcal{H}_{int} | i \rangle + \sum_{\alpha} \langle f | \mathcal{H}_{int} | \alpha \rangle \frac{1}{E - E_{\alpha} + i\epsilon} \langle \alpha | \mathcal{H}_{int} | i \rangle. \quad (2.5)$$

The complete Fock space of the system contains  $N$ -,  $\pi N$ -,  $\pi\pi N$ -,  $NN\bar{N}$ -,  $\pi NN\bar{N}$ -,  $\Delta$ -,  $\pi\Delta$ -, etc states.

For the process in our case, the form of the initial photon-nucleon state  $|i\rangle$  and the final pion-nucleon state  $|f\rangle$  is specified by the asymptotical states as follows

$$|i\rangle = |N, \gamma; \vec{p}_1 m_t, \vec{k} \vec{\epsilon}\rangle, \quad (2.6)$$

$$|f\rangle = |N', \pi; \vec{p}_2 m_{t'}, \vec{q} \mu\rangle, \quad (2.7)$$

where  $\vec{p}_1$ ,  $\vec{p}_2$ ,  $\vec{k}$  and  $\vec{q}$  are the momenta of initial and final nucleon, photon and meson, respectively. The isospin projection of the produced pion is given by  $\mu$ , the polarization vector of the incoming photon by  $\vec{\epsilon}$  and  $m_t$  and  $m_{t'}$  are the isospin projection of the initial and final nucleon, respectively. The states of all particles are covariantly normalized (see appendix A.2). The individual terms of the  $T_{fi}$ -matrix for pion photoproduction on the free nucleon are shown in Fig. 2.2. In the following we will evaluate the full interaction Hamiltonian of Eq. (2.5) in more details.

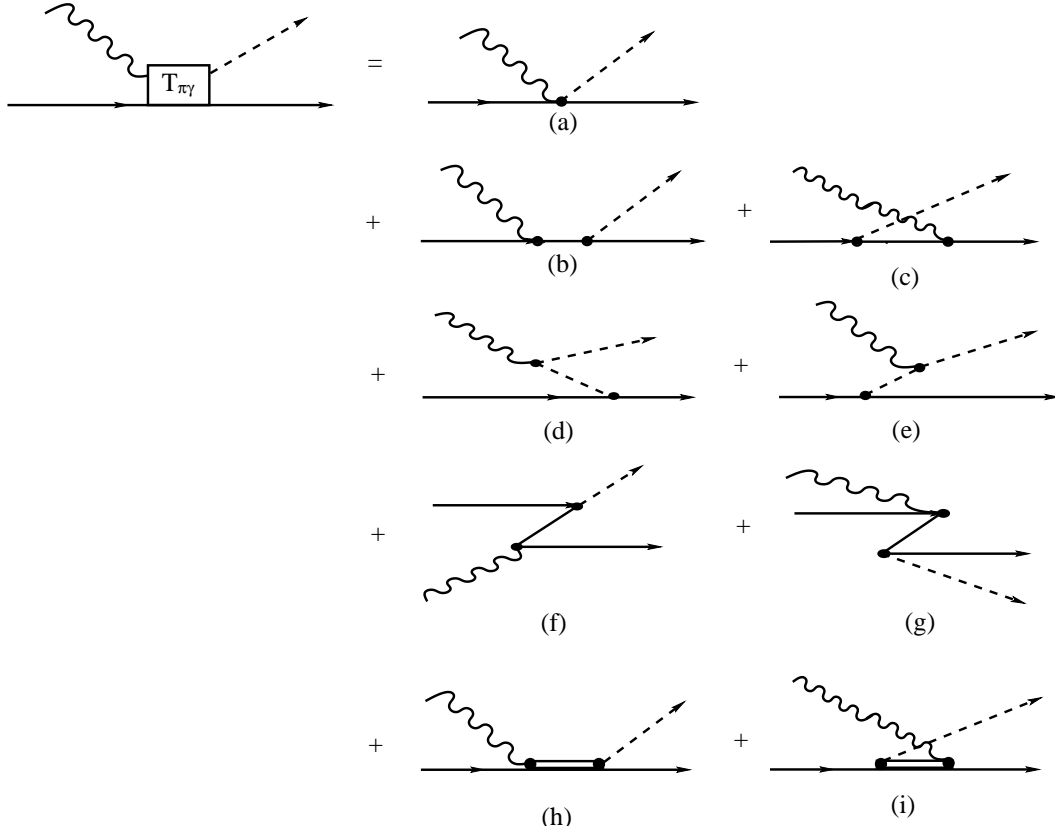


Figure 2.2: Diagrams for the elementary process  $\gamma N \rightarrow \pi N$ : (a) the Kroll-Rudermann graph, (b) and (c) the two time-ordered contributions to the direct and crossed nucleon pole graph, (d) and (e) the two time-ordered contributions to the pion pole graph, (f) and (g) the Z-graphs and (h) and (i) the  $\Delta(1232)$  resonance graphs. Lines descriptions as in Fig. 2.1.

## 2.2 Interaction Hamiltonian

The general form of the interaction Hamiltonian of the involved particles, i.e. nucleon,  $\Delta$ , pion and photon is described by the operator  $\mathcal{H}_{int}$  which is given by

$$\mathcal{H}_{int} = \mathcal{H}_{em} + \mathcal{H}_{\pi N} + \mathcal{H}_{\pi N \Delta}, \quad (2.8)$$

where  $\mathcal{H}_{em}$ ,  $\mathcal{H}_{\pi N}$  and  $\mathcal{H}_{\pi N \Delta}$  are the Hamiltonians of the electromagnetic interaction, the  $\pi N$ -coupling and the coupling of the  $\Delta$  resonance to the  $\pi N$  system, respectively. In the following we begin by evaluating the Hamiltonians which describe the interaction between pions, nucleons and photons as well as the contribution of the  $\Delta(1232)$  resonance.

### 2.2.1 The Electromagnetic Interaction

The electromagnetic interaction  $\mathcal{H}_{em}$  contains in our case the coupling of the photon field to the free nucleon, pion and  $\Delta$  fields

$$\mathcal{H}_{em} = \mathcal{H}_{\gamma N} + \mathcal{H}_{\gamma\pi} + \mathcal{H}_{\gamma\pi N} + \mathcal{H}_{\gamma N\Delta}. \quad (2.9)$$

The Hamiltonian corresponding to the absorption of a photon at a nucleon or a pion (see Fig. 2.3) are given, respectively, by

$$\mathcal{H}_{\gamma N} = -e \int d^3x \bar{\Psi}(\vec{x}) \vec{A}(\vec{x}) \cdot \vec{\gamma} \Psi(\vec{x}) \quad (2.10)$$

and

$$\mathcal{H}_{\gamma\pi} = \frac{1}{2} \int d^3x \sum_{\mu} (-)^{\mu} ie \mu \vec{A}(\vec{x}) \left[ \left( \vec{\nabla} \Phi_{\mu}(\vec{x}) \right) \Phi_{-\mu}(\vec{x}) - \left( \vec{\nabla} \Phi_{-\mu}(\vec{x}) \right) \Phi_{\mu}(\vec{x}) \right], \quad (2.11)$$

where  $\vec{A}(\vec{x})$ ,  $\Psi(\vec{x})$  and  $\Phi_{\mu}(\vec{x})$  are the field operators of the photon, nucleon and pion, respectively. More information about these operators is given in appendix C.  $\vec{\gamma}$  represent the Dirac matrices and  $e$  denotes the elementary charge.

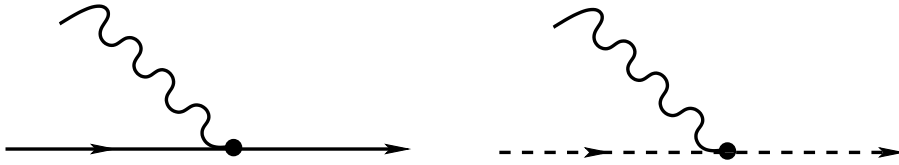


Figure 2.3: The  $\gamma N$ - and  $\gamma\pi$ -vertices.

Using field quantization (see appendix C) the matrix elements corresponding to the two diagrams of Fig. 2.3 are given by

$$\begin{aligned} \langle N'; \vec{p}_2 m'_t | \mathcal{H}_{\gamma N} | N, \gamma; \vec{p}_1 m_t, \vec{k} \vec{\epsilon} \rangle &= -(2\pi)^3 \delta^3(\vec{p}_2 - \vec{p}_1 - \vec{k}) \\ &\times \frac{1}{2M_N} \langle m'_t | \left( \hat{e}(\vec{p}_2 + \vec{p}_1) + i(\hat{e} + \hat{\kappa}) \vec{\sigma} \times \vec{k} \right) \cdot \vec{\epsilon} | m_t \rangle \end{aligned} \quad (2.12)$$

and

$$\langle \pi; \vec{q}' \mu' | \mathcal{H}_{\gamma\pi} | \pi, \gamma; \vec{q} \mu, \vec{k} \vec{\epsilon} \rangle = -(2\pi)^3 \delta^3(\vec{q}' - \vec{q} - \vec{k}) \delta_{\mu\mu'} e \mu (\vec{q} + \vec{q}') \cdot \vec{\epsilon}, \quad (2.13)$$

where  $M_N$  is the nucleon mass and  $\vec{\sigma}$  are the Pauli spin matrices.  $\hat{e}$  and  $\hat{\kappa}$  denote nucleon charge and anomalous part of the nucleon magnetic moment, respectively.

These are isospin operators of the nucleon and are given by

$$\begin{aligned}\hat{e} &= \frac{e}{2}(\mathbb{1} + \tau_0) , \\ \hat{\kappa} &= \frac{e}{2}[\kappa_p(\mathbb{1} + \tau_0) + \kappa_n(\mathbb{1} - \tau_0)] ,\end{aligned}\quad (2.14)$$

where  $\kappa_p = \frac{1}{2}(\kappa_s + \kappa_v) = 1.79$  and  $\kappa_n = \frac{1}{2}(\kappa_s - \kappa_v) = -1.91$  are the anomalous magnetic moments of the proton and the neutron<sup>1</sup> in units of nuclear magnetons, respectively, and  $\kappa_s = -0.12$  and  $\kappa_v = 3.70$ . The coupling constant  $\frac{e^2}{4\pi} = \frac{1}{137}$ .

In addition to the matrix elements of Eqs. (2.12) and (2.13), the following matrix element of  $\mathcal{H}_{\pi\gamma}$  between a state of two-pion and one photon (see Fig. 2.4) is considered

$$\langle \pi, \pi'; \vec{q}\mu, \vec{q}'\mu' | \mathcal{H}_{\pi\gamma} | \gamma; \vec{k}\vec{\epsilon} \rangle = -(2\pi)^3 \delta^3(\vec{q}' + \vec{q} - \vec{k}) \delta_{-\mu\mu'} e \mu(\vec{q} + \vec{q}') \cdot \vec{\epsilon}. \quad (2.15)$$

This matrix element will be used later in the construction of the amplitude of diagrams (d) and (e) in Fig. 2.2. The pionic current terms, which are given in Eqs. (2.13) and (2.15), contribute only to the photoproduction of charged pions.

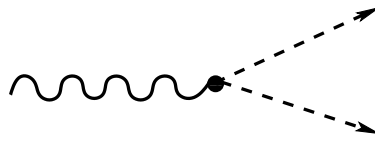


Figure 2.4: The  $\pi\gamma$ -vertex.

The  $\gamma\pi N$  Hamiltonian is given by

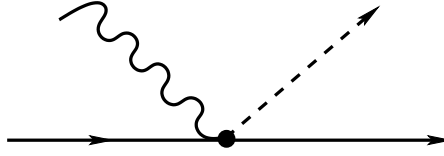
$$\mathcal{H}_{\gamma\pi N} = \frac{if_{\pi N}}{m_\pi} \sum_{\mu=\pm 1,0} \int d^3x \bar{\Psi}(\vec{x}) \vec{\gamma} \cdot \vec{A}(\vec{x}) \gamma_5 [\hat{e}, \tau_\mu^+] \Psi(\vec{x}) \Phi_\mu(\vec{x}), \quad (2.16)$$

where  $m_\pi$  is the pion mass and  $\vec{\gamma}$  represent the isospin matrices. We used the  $\pi N$  coupling constant  $\frac{f_{\pi N}^2}{4\pi} = 0.0735$  which is given in Ref. [33] by fitting the  $\pi N$  scattering data. The  $\gamma\pi N$  Hamiltonian is linear in photon and pion fields. This leads to a vertex, in which both photon and pion couple to the nucleon. The matrix element of  $\mathcal{H}_{\gamma\pi N}$  for the diagram in Fig. 2.5 is given by<sup>2</sup>

$$\begin{aligned}\langle N', \pi; \vec{p}_2 m'_t, \vec{q}\mu | \mathcal{H}_{\gamma\pi N} | N, \gamma; \vec{p}_1 m_t, \vec{k}\vec{\epsilon} \rangle &= (2\pi)^3 \delta^3(\vec{p}_2 + \vec{q} - \vec{p}_1 - \vec{k}) \\ &\times \frac{if_{\pi N}}{m_\pi} \langle m'_t | \vec{\sigma} \cdot \vec{\epsilon} [\hat{e}, \tau_\mu^+] | m_t \rangle.\end{aligned}\quad (2.17)$$

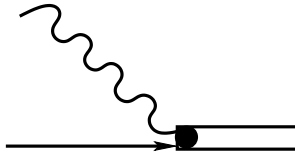
<sup>1</sup>The magnetic moments of the proton and neutron are  $\mu_p = 1 + \kappa_p$  and  $\mu_n = \kappa_n$ , respectively.

<sup>2</sup>This term contributes only to the photoproduction of charged pions.

Figure 2.5: The  $\gamma\pi N$ -vertex.

Now we evaluate the fourth term in Eq. (2.9). In the description of the  $\gamma N\Delta$ -vertex (see Fig 2.6) one has to take into account the magnetic dipole  $M1$  and a possible electric quadrupole  $E2$  excitation of the  $\Delta$  resonance

$$\mathcal{H}_{\gamma N\Delta} = \mathcal{H}_{\gamma N\Delta}^{M1} + \mathcal{H}_{\gamma N\Delta}^{E2}. \quad (2.18)$$

Figure 2.6: The  $\gamma N\Delta$ -vertex.

Since the strength of the electric quadrupole excitation  $E2$  is much smaller than the magnetic dipole one (see for example [30, 34]) we will neglect it in this work. Following Weber and Arenhövel [35], Wilhelm and Arenhövel [30] and Schmidt *et al.* [23], the  $\gamma N\Delta$  vertex reads

$$\mathcal{H}_{\gamma N\Delta} = \frac{ieG_{\Delta N}^{M1}(W_{\pi N})}{2M_N} \vec{\sigma}_{\Delta N} \cdot (\vec{k} \times \vec{\epsilon}) \tau_{\Delta N,0}. \quad (2.19)$$

Here  $W_{\pi N}$  denotes the invariant mass of the  $\pi N$ -subsystem and it is given by

$$W_{\pi N} = E_N(q_{c.m.}) + \omega_{\pi}(q_{c.m.}), \quad (2.20)$$

where  $E_N = \sqrt{M_N^2 + q_{c.m.}^2}$  and  $\omega_{\pi} = \sqrt{m_{\pi}^2 + q_{c.m.}^2}$  with the c.m. pion momentum  $q_{c.m.}$ . The transition spin (isospin) operator  $\vec{\sigma}_{N\Delta} = \vec{\sigma}_{\Delta N}^{\dagger}$  ( $\vec{\tau}_{N\Delta} = \vec{\tau}_{\Delta N}^{\dagger}$ ) is normalized as

$$\langle \frac{3}{2} || \sigma_{\Delta N}(\tau_{\Delta N}) || \frac{1}{2} \rangle = -\langle \frac{1}{2} || \sigma_{N\Delta}(\tau_{N\Delta}) || \frac{3}{2} \rangle = 2. \quad (2.21)$$

The energy dependent and complex coupling  $G_{\Delta N}^{M1}(W_{\pi N})$  is given as in [30] by

$$G_{\Delta N}^{M1}(W_{\pi N}) = \begin{cases} \mu^{M1}(W_{\pi N}) e^{i\Phi^{M1}(W_{\pi N})} & \text{for } W_{\pi N} > m_\pi + M_N \\ 0 & \text{else} \end{cases}, \quad (2.22)$$

where  $\mu^{M1}(W_{\pi N})$  is given by

$$\mu^{M1}(W_{\pi N}) = \mu_0 + \mu_2 \left( \frac{q_\Delta}{m_\pi} \right)^2 + \mu_4 \left( \frac{q_\Delta}{m_\pi} \right)^4 \quad (2.23)$$

and the phase  $\Phi^{M1}(W_{\pi N})$  by [36]

$$\Phi^{M1}(W_{\pi N}) = \frac{q_\Delta^3}{a_1 + a_2 q_\Delta^2}. \quad (2.24)$$

$q_\Delta$  is the on-shell pion momentum in the  $\pi N$  c. m. frame on the top of the resonance, i.e., when the invariant mass  $W_{\pi N}$  of the  $\pi N$  state equals the mass of the  $\Delta$  resonance

$$W_{\pi N} = \omega_\pi(q_\Delta) + E_N(q_\Delta) = M_\Delta. \quad (2.25)$$

It is given by

$$q_\Delta = \sqrt{\frac{(W_{\pi N}^2 - m_\pi^2 - M_N^2)^2 - 4m_\pi^2 M_N^2}{4W_{\pi N}^2}}. \quad (2.26)$$

The free parameters  $\mu_0 = 4.16$ ,  $\mu_2 = 0.542$ ,  $\mu_4 = -0.0757$ ,  $a_1 = 0.185 \text{ fm}^{-3}$  and  $a_2 = 4.94 \text{ fm}^{-1}$  are fitted to the experimental data for the  $M_{1+}^{3/2}$ -multipole of pion photoproduction [28, 30].

## 2.2.2 The $\pi N$ Interaction

The  $\pi N$  interaction operator in pseudovector coupling is given by

$$\mathcal{H}_{\pi N} = -\frac{f_{\pi N}}{m_\pi} \int d^3x \bar{\Psi}(\vec{x}) \vec{\gamma} \cdot \gamma_5 \vec{\tau} \cdot \Psi(\vec{x}) \vec{\nabla} \vec{\Phi}(\vec{x}). \quad (2.27)$$

This operator is linear in the pion field operator  $\vec{\Phi}(\vec{x})$ . Therefore, only one pion can be produced or absorbed at the  $\pi N$ -vertex. Thus, only two possible diagrams as shown in Fig. 2.7 contribute. The evaluation of these two graphs yields the matrix elements

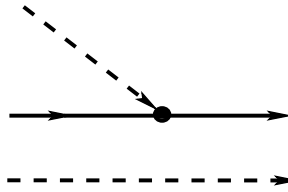
$$\begin{aligned} \langle N', \pi; \vec{p}_2 m'_t, \vec{q} \mu | \mathcal{H}_{\pi N} | N; \vec{p}_1 m_t \rangle &= -(2\pi)^3 \delta^3(\vec{p}_2 + \vec{q} - \vec{p}_1) \\ &\times \frac{if_{\pi N}}{m_\pi} \langle m'_t | \vec{q} \cdot \vec{\sigma} \tau_\mu^+ | m_t \rangle \end{aligned} \quad (2.28)$$

Figure 2.7: The  $\pi N$ -vertices.

for the emission of a pion and

$$\begin{aligned} \langle N', \pi; \vec{p}_2 m'_t, \vec{q} \mu | \mathcal{H}_{\pi N} | N, \pi_1, \pi_2; \vec{p}_1 m_t, \vec{q}_1 \mu_1, \vec{q}_2 \mu_2 \rangle &= -(2\pi)^6 \frac{2i f_{\pi N}}{m_\pi} \\ &\times [\delta^3(\vec{p}_2 - \vec{q}_1 - \vec{p}_1) \delta^3(\vec{q} - \vec{q}_2) \delta_{\mu\mu_2} \omega_{\vec{q}_2} (-)^{\mu_1} \langle m'_t | \tau_{\mu_1} \vec{q}_1 \cdot \vec{\sigma} | m_t \rangle \\ &+ \delta^3(\vec{p}_2 - \vec{q}_2 - \vec{p}_1) \delta^3(\vec{q} - \vec{q}_1) \delta_{\mu\mu_1} \omega_{\vec{q}_1} (-)^{\mu_2} \langle m'_t | \tau_{\mu_2} \vec{q}_2 \cdot \vec{\sigma} | m_t \rangle] \end{aligned} \quad (2.29)$$

for the absorption of a pion, where  $\omega_{\vec{q}_i} = \sqrt{m_\pi^2 + q_i^2}$  is the energy of the pion with momentum  $\vec{q}_i$ . Note, that in case of the pion absorption the vertex is evaluated for the transition of a two to a one pion state (see Fig. 2.8) which will appear later in the construction of the matrix elements.

Figure 2.8: The  $\pi N$ -vertex in case of the pion absorption.

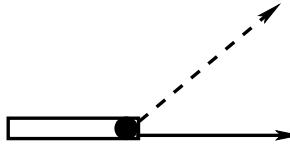
### 2.2.3 The $\pi N \Delta$ -Vertex

Here we will evaluate the  $\pi N \Delta$ -vertex which contribute to the amplitude of the  $\Delta$  resonance. For the  $\pi N \Delta$ -vertex which diagrammatically is given in Fig. 2.9 we use [30, 35]

$$\mathcal{H}_{\pi N \Delta} = -\frac{i}{m_\pi} F_\Delta(q^2) (-)^\mu \vec{\tau}_{N\Delta, -\mu} \vec{\sigma}_{N\Delta} \cdot \vec{q}. \quad (2.30)$$

We have introduced a hadronic monopole form factor

$$F_\Delta(q^2) = f_{\pi N \Delta} \frac{\Lambda_\Delta^2 + q_\Delta^2}{\Lambda_\Delta^2 + q^2}. \quad (2.31)$$

Figure 2.9: The  $\pi N \Delta$ -vertex.

The coupling constant  $\frac{f_{\pi N \Delta}^2}{4\pi} = 1.393$  and the cutoff  $\Lambda_\Delta = 315$  MeV are fixed in Refs. [30, 37] to fit the  $\pi N$  scattering phase shift in the  $P_{33}$  channel and is also used in the calculations of this work.

Now, using the Hamilton operator (2.8) and taking into account all possible intermediate states  $|\alpha\rangle$  in (2.5), we can calculate the on-shell  $T_{fi}$ -matrix for pion photoproduction on the free nucleon by constructing the lowest order diagrams as shown in Fig. 2.2.

## 2.3 Construction of the Amplitude

Using the previously mentioned electromagnetic and hadronic vertices, it is possible now to calculate the  $T_{fi}$ -matrix from Eq. (2.5) for photoproduction of pions on the free nucleon. Obviously, only the Kroll-Rudermann term<sup>3</sup> ( $T_{fi}^{\text{KR}}$ ) contributes to the first term of the right-hand side of Eq. (2.5).

### 2.3.1 The Born Terms

First, we consider the nonresonant amplitudes. These are referred to as the Born terms and they are dominant at low energy and for charged pion photoproduction still provide 50% of the cross section in the energy region of the  $\Delta(1232)$  resonance.

Using graphs (a) to (e) in Fig. 2.2 one finds in addition to the Kroll-Rudermann term (graph (a)) the direct and crossed nucleon pole terms (graphs (b) and (c)) and the two pion pole terms (graphs (d) and (e)). These terms are given, respectively, by

$$T_{fi}^{\text{KR}} = (2\pi)^3 \delta^3(\vec{p}_2 + \vec{q} - \vec{p}_1 - \vec{k}) \frac{if_{\pi N}}{m_\pi} \vec{\sigma} \cdot \vec{\epsilon} [\hat{e}, \tau_\mu^+], \quad (2.32)$$

$$T_{fi}^N = -(2\pi)^3 \delta^3(\vec{p}_2 + \vec{q} - \vec{p}_1 - \vec{k}) \frac{if_{\pi N}}{2m_\pi}$$

<sup>3</sup>Named also *seagull* or *contact* term.

$$\begin{aligned} & \times \left( \frac{\tau_\mu^+ \vec{\sigma} \cdot \vec{q} \left( 2(\vec{p}_2 + \vec{q}) \cdot \vec{\epsilon} \hat{e} + i \vec{\sigma} \cdot \vec{k} \times \vec{\epsilon} (\hat{e} + \hat{\kappa}) \right)}{E_{\vec{p}_2 + \vec{q}} (\omega_{\vec{q}} + E_{\vec{p}_2} - E_{\vec{p}_2 + \vec{q}})} \right. \\ & \left. + \frac{\left( 2\vec{p}_2 \cdot \vec{\epsilon} \hat{e} + i \vec{\sigma} \cdot \vec{k} \times \vec{\epsilon} (\hat{e} + \hat{\kappa}) \right) \tau_\mu^+ \vec{\sigma} \cdot \vec{q}}{E_{\vec{p}_2 - \vec{k}} (E_{\vec{p}_2} - E_{\vec{p}_2 - \vec{k}} - \omega_\gamma)} \right), \end{aligned} \quad (2.33)$$

$$\begin{aligned} T_{fi}^\pi &= (2\pi)^3 \delta^3(\vec{p}_2 + \vec{q} - \vec{p}_1 - \vec{k}) \frac{if_{\pi N}}{m_\pi} \frac{\vec{q} \cdot \vec{\epsilon} \vec{\sigma} \cdot (\vec{q} - \vec{k})}{\omega_{\vec{q} - \vec{k}}} \\ &\times \left( \frac{1}{\omega_{\vec{q}} - \omega_{\vec{q} - \vec{k}} - \omega_\gamma} + \frac{1}{\omega_\gamma - \omega_{\vec{q} - \vec{k}} - \omega_{\vec{q}}} \right) [\hat{e}, \tau_\mu^+], \end{aligned} \quad (2.34)$$

where  $E_{\vec{p}} = \sqrt{M_N^2 + \vec{p}^2}$  and  $\omega_{\vec{p}} = \sqrt{m_\pi^2 + \vec{p}^2}$  are the energies of a nucleon and a pion with momentum  $\vec{p}$ , respectively.

To take the anti-nucleon terms in the propagators of direct and crossed nucleon pole graphs into account, we consider also the two  $Z$ -graphs given by diagrams (f) and (g) in Fig. 2.2. The matrix element using these  $Z$ -graphs ( $T_{fi}^Z$ ) is given by

$$\begin{aligned} T_{fi}^Z &= (2\pi)^3 \delta^3(\vec{p}_2 + \vec{q} - \vec{p}_1 - \vec{k}) \frac{if_{\pi N}}{m_\pi} M_N \omega_{\vec{q}} \vec{\sigma} \cdot \vec{\epsilon} \\ &\times \left( \frac{\tau_\mu^+ \hat{e}}{E_{\vec{p}_2 + \vec{q}} (E_{\vec{p}_2 + \vec{q}} + E_{\vec{p}_2} + \omega_{\vec{q}})} + \frac{\hat{e} \tau_\mu^+}{E_{\vec{p}_2 - \vec{k}} (E_{\vec{p}_2 - \vec{k}} + E_{\vec{p}_2} - \omega_\gamma)} \right). \end{aligned} \quad (2.35)$$

We would like to note that for a better description of the real part of the  $M_{1+}^{3/2}$  multipole (see section 2.4) the suppression of the nonresonant background by the form factor is essential. Therefore, it is necessary to introduce a form factor

$$F_B(q) = \frac{\Lambda_B^2 - m_\pi^2}{\Lambda_B^2 + q^2}, \quad (2.36)$$

with the cutoff  $\Lambda_B = 800$  MeV to obtain a better description.

### 2.3.2 The $\Delta(1232)$ Resonance Term

The dominant non-Born contribution for photon energies up to 500 MeV is that of the  $P_{33}$  pion-nucleon resonance, the  $\Delta(1232)$  resonance. Now, we will evaluate the contribution of the  $\Delta(1232)$  resonance corresponding to the vertices given in Eqs. (2.19) and (2.30). Using the nonrelativistic form of the  $\Delta$  propagator, the various diagrams involving an intermediate  $\Delta(1232)$  (see graphs (h) and (i) in Fig.

2.2) can be calculated. We obtain the following expression for the  $s$  and  $u$  channel contributions in center-of-mass frame

$$\begin{aligned} T_{fi}^\Delta &= (2\pi)^3 \delta^3(\vec{p}_2 + \vec{q} - \vec{p}_1 - \vec{k}) \\ &\times \left( \frac{F_\Delta(q^2)}{m_\pi} \frac{ef_{\pi N \Delta} G_{\Delta N}^{M1}(W_{\pi N})}{2\sqrt{E_{\vec{p}_1} E_{\vec{p}_2}}} \frac{\{\tau_\mu^\dagger, \tau_0\} - \frac{1}{2}[\tau_\mu^\dagger, \tau_0]}{3} \frac{\vec{\sigma}_{N\Delta} \cdot \vec{q} \vec{\sigma}_{\Delta N} \cdot \vec{k} \times \vec{\epsilon}}{W_{\pi N} - M_\Delta + \frac{i}{2}\Gamma_\Delta(W_{\pi N})} \right. \\ &\quad \left. + \frac{F_\Delta(0)}{m_\pi} \frac{ef_{\pi N \Delta} G_{\Delta N}^{M1}(0)}{2\sqrt{E_{\vec{p}_1} E_{\vec{p}_2}}} \frac{\{\tau_\mu^\dagger, \tau_0\} + \frac{1}{2}[\tau_\mu^\dagger, \tau_0]}{3} \frac{\vec{\sigma}_{\Delta N} \cdot \vec{k} \times \vec{\epsilon} \vec{\sigma}_{N\Delta} \cdot \vec{q}}{E_{\vec{p}_2} - \omega_\gamma - E_{\vec{p}_2 - \vec{k}}^\Delta} \right), \quad (2.37) \end{aligned}$$

where  $M_\Delta$  is the mass of the  $\Delta$  resonance.

The energy dependent width of the  $\Delta$  resonance above pion threshold  $\Gamma_\Delta(W_{\pi N})$  is given by

$$\Gamma_\Delta(W_{\pi N}) = \begin{cases} \frac{1}{6\pi} \frac{M_N}{\omega_q + M_N} \frac{q^3}{m_\pi^2} f_{\pi N \Delta}^2 F_\Delta^2(q^2) & \text{for } W_{\pi N} > m_\pi + M_N \\ 0 & \text{else} \end{cases}. \quad (2.38)$$

In the  $u$  channel contribution which is given by the second part in Eq. (2.37) we take the values of the form factor  $F_\Delta$ , the electromagnetic coupling  $G_{\Delta N}^{M1}$  and the width of the resonance  $\Gamma_\Delta$  at pion threshold. In the expressions of the hadronic form factors (Eq. (2.31)), the complex coupling  $G_{\Delta N}^{M1}$  (Eq. (2.22)) and the width of the  $\Delta$  resonance (Eq. (2.38)) we use the c.m. pion momentum as given by the invariant mass of the  $\pi N$ -subsystem (see Eq. (2.20)).

In order to build the elementary pion photoproduction operator into the two-nucleon system, which will be necessary for the calculations on the two-nucleon space in the forthcoming chapters, we must construct the elementary amplitude in a general frame of reference. The Born terms given in section 2.3.1 are already constructed in an arbitrary frame. In order to build the resonance term of Eq. (2.37) into the two-nucleon system we must re-write Eq. (2.37) in an arbitrary frame of reference. In Ref. [30] the following Galilei invariant transformations are found for the photon and pion momenta which have to be replaced by the relative photon-nucleon momentum

$$\vec{k} \longrightarrow \vec{k}_{\gamma N}(\vec{k}, \vec{p}_1) := \frac{M_N \vec{k} - (M_\Delta - M_N) \vec{p}_1}{M_\Delta} \quad (2.39)$$

and respective pion-nucleon momentum

$$\vec{q} \longrightarrow \vec{q}_{\pi N}(\vec{q}, \vec{p}_2) := \frac{M_N \vec{q} - \omega_q \vec{p}_2}{M_N + \omega_q}. \quad (2.40)$$

Now, all contributions for the elementary photoproduction operator on the free

nucleon, which in Fig. 2.2 are graphically represented, are calculated. The full  $T_{fi}$ -matrix is then given in a simple form by<sup>4</sup>

$$T_{\pi\gamma} = T_{fi}^{\text{KR}} + T_{fi}^{\text{N}} + T_{fi}^{\pi} + T_{fi}^{\text{Z}} + T_{fi}^{\Delta}. \quad (2.41)$$

## 2.4 Results for Elementary Process

In this section we will examine the various observables for pion photoproduction on the free nucleon using the effective Lagrangian model of Schmidt *et al.* [23]. This model contains besides the standard pseudovector Born terms the resonance contribution from the  $\Delta(1232)$  excitation. The parameters of the  $\Delta$  resonance are fixed by fitting the experimental data [28] for the  $M_{1+}^{3/2}$  multipole which is dominant in the  $\Delta(1232)$  region. Due to the use of a constant  $\Delta$  mass in the  $\Delta$  propagator and a different cutoff  $\Lambda_{\Delta}$  we had to increase  $G_{\Delta N}^{M1}$  from [30] by a factor of 1.15 to fit the experimental  $M_{1+}^{3/2}$  multipole.

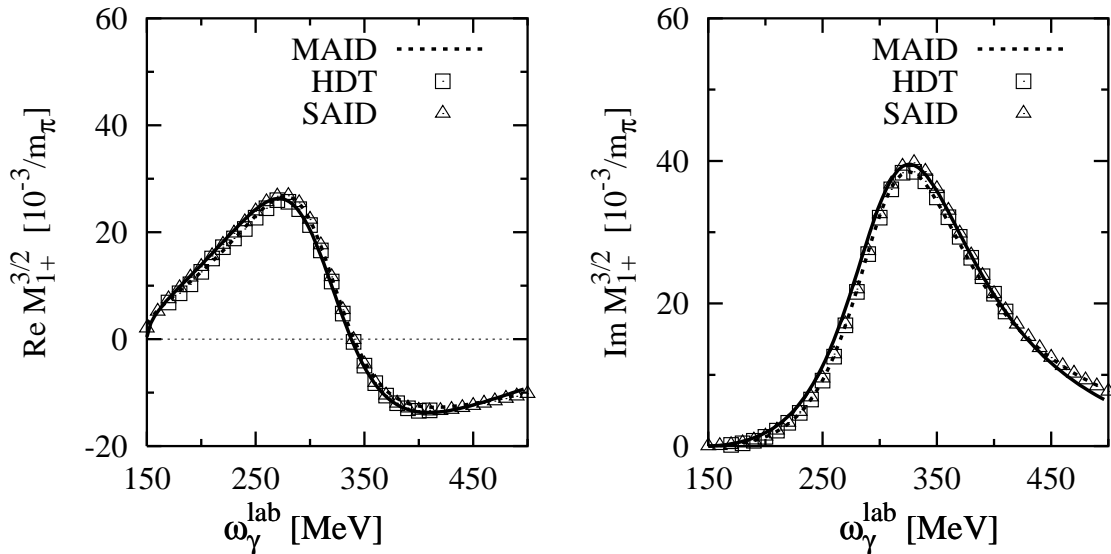


Figure 2.10: Real and imaginary parts of the  $M_{1+}^{3/2}$  multipole in comparison with the calculation using the MAID program [17]. The data points show the results of the VPI analysis [28] (solution: September 2000) and the Mainz dispersion analysis (HDT) [27].

Fig. 2.10 shows our fit for the real and imaginary parts of the  $M_{1+}^{3/2}$  multipole in comparison with the MAID analysis [17], the Mainz dispersion analysis (HDT) [27]

<sup>4</sup>In this work no further contributions are used. This means in particular that terms from the  $\omega$ - and  $\rho$ -meson exchange in the  $t$ -channel are not considered.

and the VPI analysis from the SAID program [28]. We see that the agreement of our results (solid curves) in comparison with data and theoretical calculation from MAID (dashed curves) is good.

### 2.4.1 Differential Cross Section

The c.m. differential cross section for the transition from an initial photon-nucleon state  $|i\rangle$  to a final pion-nucleon state  $|f\rangle$  is given by

$$\frac{d\sigma}{d\Omega_{\pi}^{c.m.}} = \frac{1}{64\pi^2} \frac{\tilde{q}M_N^2}{\omega_{\gamma}W_{\pi N}^2} \sum_{m_{\gamma}m_s m_{s'}} |T_{\pi\gamma}|^2, \quad (2.42)$$

where  $\omega_{\gamma}$  is the photon energy in the laboratory frame and  $m_{\gamma} = \pm 1$ . The magnetic quantum numbers of the target and the recoiling nucleons are respectively  $m_s$  and  $m_{s'}$ . The invariant  $\pi N$  mass  $W_{\pi N}$  is given in the c.m. frame as

$$W_{\pi N} = E_{\vec{p}_1} + \omega_{\gamma}, \quad (2.43)$$

and the absolute value of the pion momentum  $\tilde{q}$  is given by

$$\tilde{q} = \sqrt{\left(\frac{m_{\pi}^2 + 2\omega_{\gamma}W_{\pi N}}{2W_{\pi N}}\right)^2 - m_{\pi}^2}. \quad (2.44)$$

In Figs. 2.11–2.13 we compare our results (solid curves) for the differential cross sections with the MAID analysis [17] (dashed curves) and with old and new experimental data from Mainz and Bonn. Most interesting for our analysis are the recent experimental data from the Mainz Microtron MAMI. Differential cross sections of both  $\pi^+$  and  $\pi^0$  photoproduction off the proton have been measured [26, 38, 39], with high precision at all angles and photon energies for both channels. To get the full isospin decomposition we also had to include data for  $\pi^-$  photoproduction, for which we took the differential cross sections from [40]. In general, we obtain a good agreement with the experimental data for pion photoproduction on both the proton and neutron, especially in the energy range of the  $\Delta(1232)$  region.

For charged pion channels we see from Figs. 2.11 and 2.12 a similar shape, but we find a somewhat different situations. Fig. 2.11 shows the result of our calculation of  $\pi^-$  photoproduction on the neutron at six different values for the photon energy in comparison with the data from [40] and also with the MAID analysis [17]. It can be seen that we fit this experiment quite well, in particular for a photon energy of 330 MeV which is very near to the  $\Delta(1232)$  region. Furthermore, the comparison with the MAID analysis at this energy is good. For higher and lower photon energies

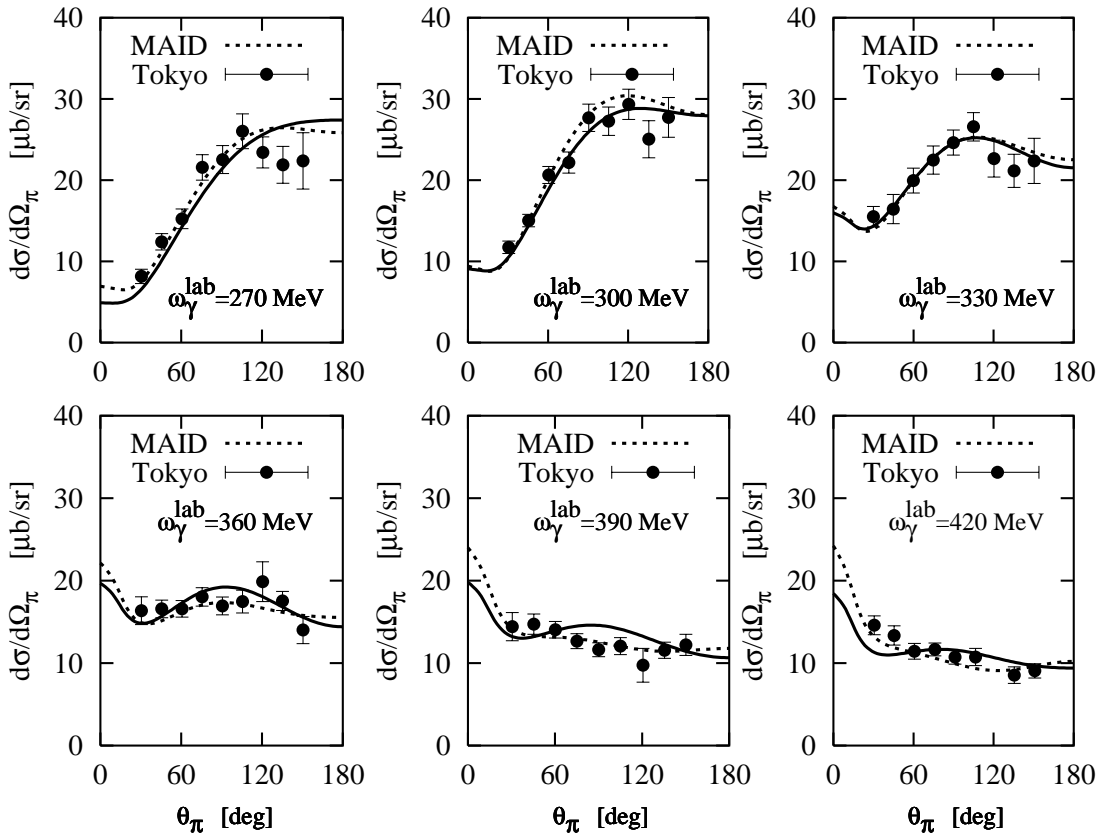


Figure 2.11: Differential cross section for  $\gamma n \rightarrow p\pi^-$  at six different values of the photon energy in the laboratory frame. The solid curve shows the result of our calculations and the dotted one shows the results using the MAID program [17]. The experimental data are from Tokyo [40].

we note small discrepancies. In the case of high energies these discrepancies come from the fact that no other resonances besides the  $\Delta(1232)$  are included in our calculation. It is also interesting to point out the importance of the Born terms in the charged pion photoproduction reactions in comparison to the contribution of the  $\Delta$  resonance. These terms play an important role in the case of low photon energies.

In Fig. 2.12 we compare our predictions for  $\pi^+$  photoproduction on the proton with the more recent experimental data from the Mainz experiment [26] and the GDH experiment [39] for different photon energies. We see that the agreement with both experiment and MAID analysis [17] is good. We think that the agreement with experiment is in our case better than the MAID analysis for low and intermediate photon energies. For high energies small discrepancies are found since we assume a pure magnetic dipole transition in the  $\gamma N \Delta$  coupling. Moreover, the  $D_{13}$  resonance

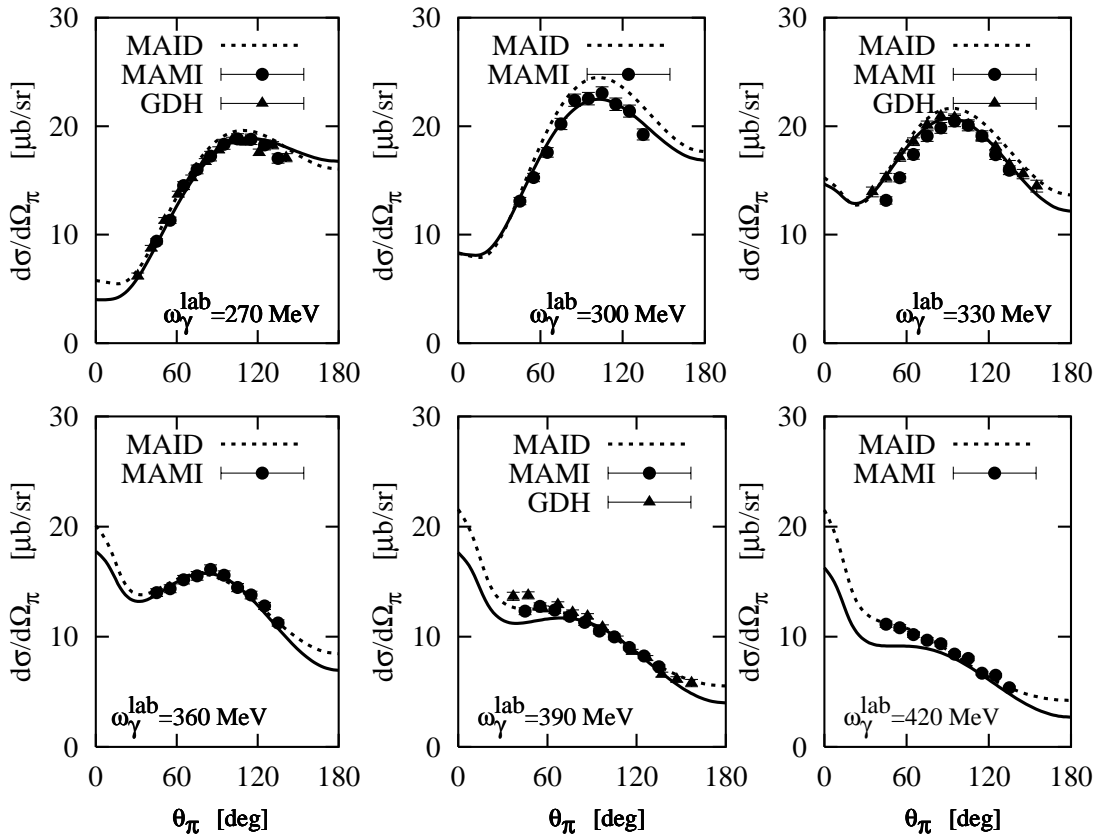


Figure 2.12: Differential cross section for  $\gamma p \rightarrow n\pi^+$ . Lines description as in Fig. 2.11. The experimental data are from GDH [39] and MAMI [26].

contributes with a non-vanishing term in this region.

In case of the  $\pi^0$  photoproduction on the proton, shown in Fig. 2.13, the situation is much more satisfactory. We see that the agreement of our calculation with the most recent experimental data from [38] and [39] is good. Small discrepancies between our calculation and the MAID analysis appear which very likely are due to the fact that no other resonances are included in our calculation.

### 2.4.2 Total Cross Section

The total cross sections for the different pion channels are shown in Fig. 2.14 and compared with experimental data. The total cross sections for  $\gamma p \rightarrow \pi^+ n$  and  $\gamma n \rightarrow \pi^- p$  have a similar structure. In particular, the  $\Delta$  peak is seen exactly at the same energy, 300 MeV.

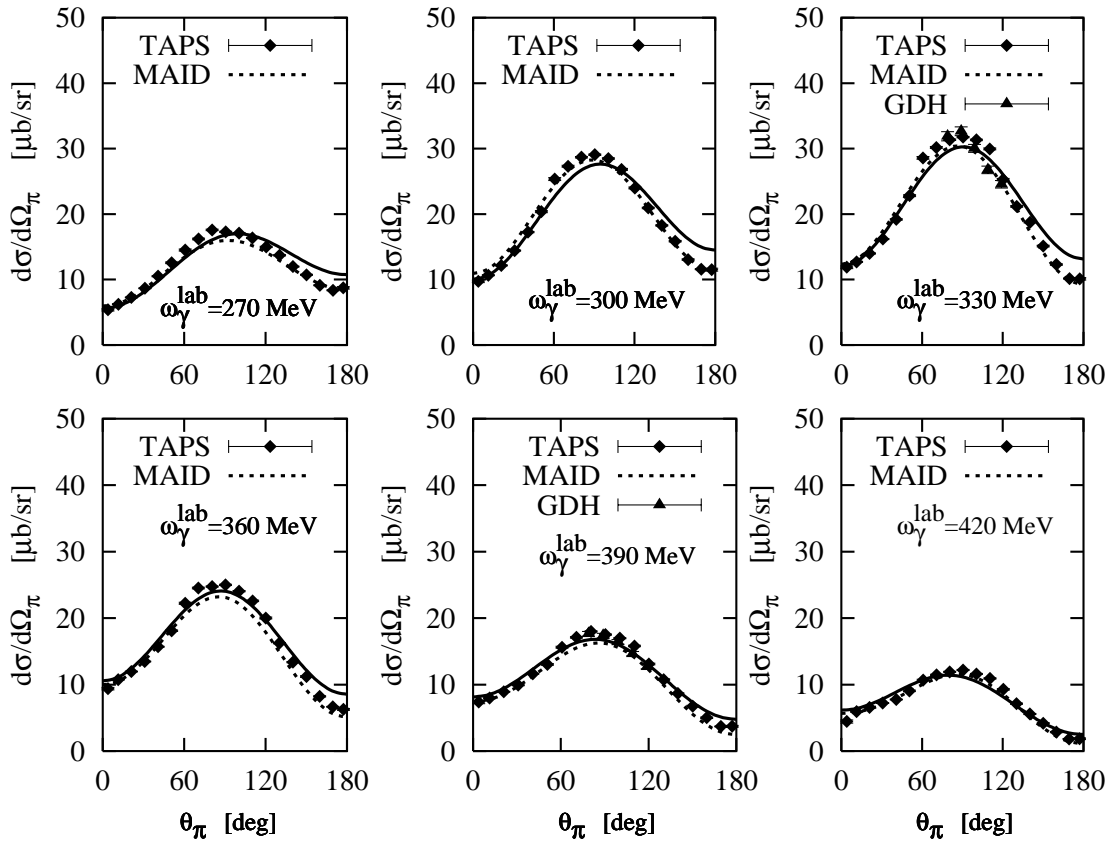


Figure 2.13: Differential cross section for  $\gamma p \rightarrow p\pi^0$ . Lines description as in Fig. 2.11. The experimental data are from TAPS [38] and GDH [39].

The comparison of our calculation with experimental data is carried out for photon energies up to 500 MeV. For higher photon energies the parameterization of the  $\Delta$  resonance possesses no more valid. In general, we obtain a good agreement with the recent experimental data using the small value  $\frac{f_{\pi N}^2}{4\pi} = 0.069$  for the pion-nucleon coupling constant. The agreement with the experimental data from [40] and [41] for  $\pi^-$  photoproduction on the neutron is satisfactory. In case of the  $\pi^+$  photoproduction, the agreement with the recent experimental data from [39] is good up to photon energy of about 400 MeV. For high energies the  $D_{13}$  resonance, which is not included in our calculation, has non-vanishing contribution. The  $\pi^+$  data from [40] are slightly overestimated in the resonance region by our calculation and also by the MAID analysis.

At low photon energies, the charged pion reactions differ significantly in magnitude from the neutral pion reactions due to the Kroll-Rudermann term which does not

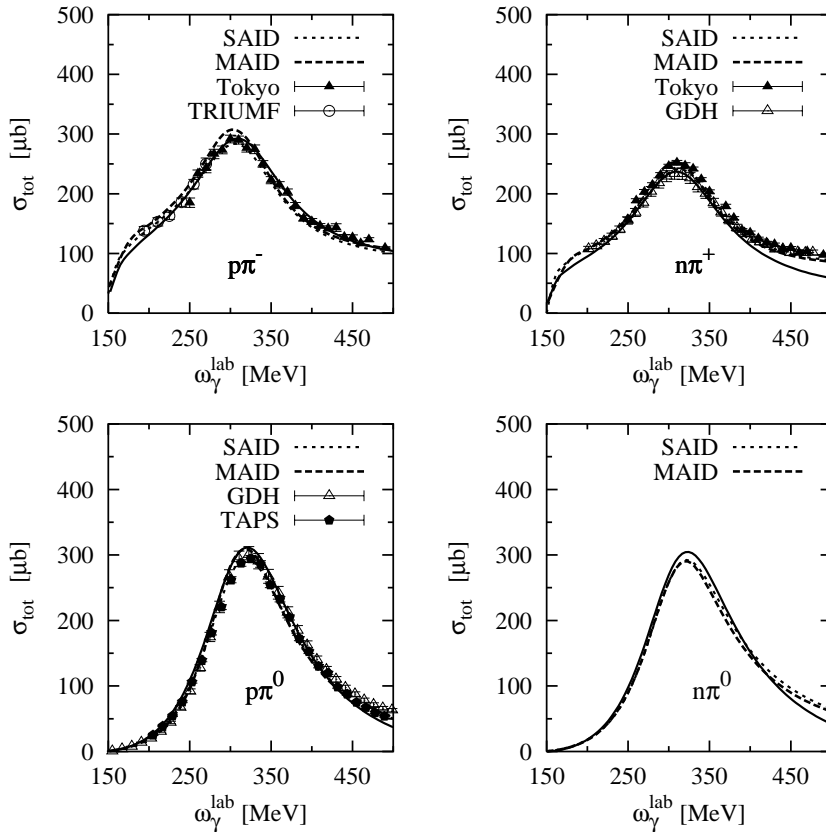


Figure 2.14: Total cross sections for pion photoproduction on the nucleon as a function of photon energy for the four physical reactions. The solid curve shows the result of our calculation, the dashed curve shows the results using the MAID program [17] and the dotted one shows the results of the VPI analysis of the SAID program [28]. The experimental data are from GDH [39], Tokyo [40], TRIUMF [41] and TAPS [42].

contribute to the neutral pion reactions. The agreement of our calculation with the experimental data from [42] and [39] in case of the  $\pi^0$  photoproduction on the proton is good and give a clear indication that the model which we used in our predictions can be applied directly to calculate the electromagnetic photoproduction of pions on the deuteron which we will study in the forthcoming chapters.

# Chapter 3

## Photoproduction of $\pi$ -Mesons on the Deuteron

In the previous chapter, we have constructed the elementary photoproduction operator on the free nucleon in a general frame of reference to use it as input in our calculations during the present chapter. This chapter is concerned with incoherent pion photoproduction on the deuteron which can be produced through the following three reactions

$$\gamma d \rightarrow pp\pi^-, \quad \gamma d \rightarrow nn\pi^+, \quad \gamma d \rightarrow pn\pi^0. \quad (3.1)$$

Let  $(\omega_\gamma, \vec{k})$ ,  $(E_{\vec{d}}, \vec{d})$ ,  $(\omega_{\vec{q}}, \vec{q})$ ,  $(E_{\vec{p}_1}, \vec{p}_1)$  and  $(E_{\vec{p}_2}, \vec{p}_2)$  be the four-momenta of the incoming photon, deuteron, the outgoing pion and two nucleons, respectively. The general expression for the unpolarized differential cross section of pion photoproduction reaction on the deuteron is given using the conventions of Bjorken and Drell [43] by

$$d\sigma = (2\pi)^{-5} \delta^4(k + d - p_1 - p_2 - q) \frac{1}{|\vec{v}_\gamma - \vec{v}_d|} \frac{1}{2} \frac{d^3 q}{2\omega_{\vec{q}}} \frac{d^3 p_1}{E_{\vec{p}_1}} \frac{d^3 p_2}{E_{\vec{p}_2}} \frac{M_N^2}{2\omega_\gamma 2E_{\vec{d}}} \times \frac{1}{6} \sum_{sm_s t, m_\gamma m_d} |\mathcal{M}_{sm_s, m_\gamma m_d}^{(t\mu)}|^2, \quad (3.2)$$

where  $m_\gamma$  is the photon polarization,  $m_d$  the spin projection of the deuteron,  $s$  the total spin of the two outgoing nucleons,  $m_s$  its spin projection,  $t$  the total isospin of the two outgoing nucleons,  $m_t$  ( $= -\mu$ ) its isospin projection and  $\vec{v}_\gamma$  and  $\vec{v}_d$  are the velocities of the photon and the deuteron, respectively.  $\mu$  denotes the pion charge. The states of all particles are covariantly normalized (see appendix A.2). The reaction amplitude is given by

$$\mathcal{M}_{sm_s, m_\gamma m_d}^{(t\mu)} = \langle \vec{p}_1 \vec{p}_2, sm_s, t, -\mu | \mathcal{M}(\vec{q}, \mu, \vec{k}, m_\gamma) | \vec{d}, m_d \rangle. \quad (3.3)$$

Choosing the  $z$ -axis in the direction of the incoming photon and isolating the azimuthal dependence of the direction of pion momentum, we obtain the following general form for the reaction matrix

$$\mathcal{M}_{sm_s, m_\gamma m_d}^{(t\mu)}(\theta_\pi, \phi_\pi) = \mathcal{O}_{sm_s, m_\gamma m_d}^{(t\mu)}(\theta_\pi) e^{i(m_\gamma + m_d)\phi_\pi}. \quad (3.4)$$

Using parity conservation one can show that the  $\mathcal{M}$ -matrix elements obey the following symmetry relation

$$\mathcal{O}_{s, -m_s, -m_\gamma, -m_d}^{(t\mu)} = (-)^{s+m_s+m_\gamma+m_d} \mathcal{O}_{s, m_s, m_\gamma, m_d}^{(t\mu)}. \quad (3.5)$$

This symmetry relation reduces the number of complex amplitudes from 24 to 12 independent ones. For their determination one needs 23 real observables since a overall phase remains arbitrary.

The unpolarized differential cross section in Eq. (3.2) is a product of two terms. The first term is a kinematical one describing the invariant phase space. The second one describes the dynamics of the process and is determined by the transition matrix element  $\mathcal{M}$ . In the following we discuss these two terms in more detail.

### 3.1 Kinematics

Calculations of total and differential cross sections are carried out in the rest frame of the deuteron (laboratory frame) which is shown diagrammatically in Fig. 3.1. In this frame the relative velocity of both particles in the initial state is unity in units of  $c$ . The coordinate system is chosen to have a right-hand orientation with  $z$ -axis along the momentum  $\vec{k}$  of the incoming photon and  $y$ -axis parallel to  $\vec{k} \times \vec{q}$ . The  $x$ - $z$ -plane is then given by the outgoing pion, i.e.  $\phi_\pi = 0$ , where  $\phi_\pi$  is azimuthal angle of the pion.

The four-momenta of the incoming photon and deuteron are given in the laboratory frame by  $k^\mu = (\omega_\gamma, \vec{k})$  and  $d^\mu = (M_d, \vec{0})$ , respectively, where  $M_d$  is the deuteron mass and  $\omega_\gamma$  is the photon energy in the laboratory frame. Energy-momentum conservation gives

$$\vec{k} = \vec{q} + \vec{p}_1 + \vec{p}_2 \quad (3.6)$$

and

$$\omega_\gamma + M_d = \omega_{\vec{q}} + E_{\vec{p}_1} + E_{\vec{p}_2} = E_{\gamma d}, \quad (3.7)$$

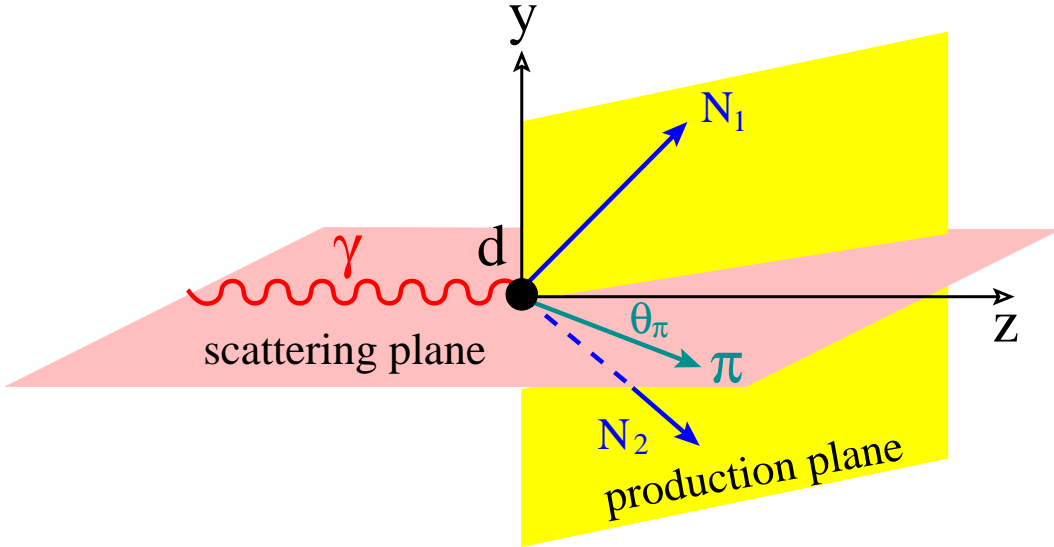


Figure 3.1: Kinematics in the laboratory frame for the reaction  $\gamma d \rightarrow \pi NN$ .

where  $E_{\gamma d}$  is the total energy of the system.

The invariant mass of the  $\gamma d$ -system is given by

$$\begin{aligned}
 W_{\gamma d} &= \sqrt{(k^\mu + d^\mu)(k_\mu + d_\mu)} \\
 &= \sqrt{(M_d + \omega_\gamma)^2 - \vec{k}^2} \\
 &= \sqrt{M_d^2 + 2M_d\omega_\gamma}.
 \end{aligned} \tag{3.8}$$

The final state is determined by the four momenta of the two outgoing nucleons and the outgoing pion. Energies of these particles are then fixed by

$$\begin{aligned}
 E_{\vec{p}_i} &= \sqrt{M_N^2 + \vec{p}_i^2}, \quad (i \in \{1, 2\}), \\
 \omega_{\vec{q}} &= \sqrt{m_\pi^2 + \vec{q}^2}.
 \end{aligned} \tag{3.9}$$

Finally, four-momentum conservation reduces the number of the independent variables to five, out of nine. In this work, the pion momentum  $q$ , its angles  $\theta_\pi$  and  $\phi_\pi$ , the polar angle  $\theta_{p_r}$  and the azimuthal angle  $\phi_{p_r}$  of the relative momentum  $\vec{p}_r$  of the two outgoing nucleons are selected as independent variables. We prefer this choice of variables, because in this case the kinematical factor, i.e. the phase space factor, does not have any singularities on the boundary of the available phase space, when  $p_r \rightarrow 0$  (see also [23]). This means in particular that with another selection of the

free kinematical variables singularities in the phase space, i.e. kinematical factor, at the boundary of the physical region can occur (see for example [44]).

The total and relative momenta of the final  $NN$ -system are given respectively by

$$\vec{P} = \vec{p}_1 + \vec{p}_2 \quad (3.10)$$

and

$$\vec{p}_r = \frac{1}{2} (\vec{p}_1 - \vec{p}_2) . \quad (3.11)$$

The inverted relations read

$$\vec{p}_1 = \frac{1}{2} \vec{P} + \vec{p}_r \quad (3.12)$$

$$\vec{p}_2 = \frac{1}{2} \vec{P} - \vec{p}_r . \quad (3.13)$$

The absolute value of the relative momentum  $\vec{p}_r$  is given by

$$p_r = \frac{1}{2} \sqrt{\frac{E_{NN}^2 (W_{NN}^2 - 4M_N^2)}{E_{NN}^2 - P^2 \cos^2 \theta_{Pp_r}}} , \quad (3.14)$$

where

$$\begin{aligned} E_{NN} &= \omega_\gamma + M_d - \omega_{\vec{q}} = E_{\vec{p}_1} + E_{\vec{p}_2} , \\ W_{NN}^2 &= E_{NN}^2 - P^2 \end{aligned} \quad (3.15)$$

and  $\theta_{Pp_r}$  is the angle between  $\vec{P}$  and  $\vec{p}_r$ . The absolute value of the total momentum  $P = |\vec{P}|$  is given from Eqs. (3.6) and (3.10) by

$$P = |\vec{k} - \vec{q}| . \quad (3.16)$$

The main features of the processes (3.1) will be investigated by considering the partially integrated differential cross sections  $d^3\sigma/(d\Omega_\pi dq)$  and  $d^2\sigma/d\Omega_\pi$ , which are obtained from the fully exclusive cross section

$$\frac{d^5\sigma}{d\Omega_{p_r} d\Omega_\pi dq} = \frac{\rho_s}{6} \sum_{sm_{st}, m_\gamma m_d} |\mathcal{M}_{sm_s, m_\gamma m_d}^{(t\mu)}|^2 \quad (3.17)$$

by appropriate integration. The phase space factor  $\rho_s$  depends on the selection of the five independent variables in Eq. (3.2). It is expressed in terms of relative and total momenta of the two final nucleons as follows

$$\rho_s = \frac{1}{(2\pi)^5} \frac{p_r^2 M_N^2}{|E_{\vec{p}_2}(p_r + \frac{1}{2}P \cos \theta_{Pp_r}) + E_{\vec{p}_1}(p_r - \frac{1}{2}P \cos \theta_{Pp_r})|} \frac{q^2}{16\omega_\gamma M_d \omega_{\vec{q}}} , \quad (3.18)$$

whereas  $q$  between 0 and  $q_{max}$ . Since the limit value of both the numerator and the denominator are zero when  $p_r \rightarrow 0$ , we can apply the L'Hospital's rule to obtain the exact limit value for the phase space as follows

$$\begin{aligned} \lim_{p_r \rightarrow 0} \rho_s &= \lim_{p_r \rightarrow 0} \frac{\frac{\partial}{\partial p_r} p_r^2}{\frac{\partial}{\partial p_r} |E_{\vec{p}_2}(p_r + \frac{1}{2}P \cos \theta_{Pp_r}) + E_{\vec{p}_1}(p_r - \frac{1}{2}P \cos \theta_{Pp_r})|} \\ &\quad \times \frac{1}{(2\pi)^5} \frac{M_N^2 q^2}{16\omega_\gamma M_d \omega_{\vec{q}}} \\ &= 0. \end{aligned} \quad (3.19)$$

The existence of this limit value ensures that the phase space factor has no singularities on the boundary of the physical region.

## 3.2 Two-Nucleon Wave Function

Using a covariant normalization (see appendix A.2) the deuteron wave function in the momentum space is given in the rest frame of the deuteron by

$$\Psi_{dm_d}(\vec{p}) = \frac{E_{\vec{p}}}{M_N} \sum_{m_s} \chi_{1m_s} \tilde{\Psi}_{m_d m_s}(\vec{p}), \quad (3.20)$$

where

$$\tilde{\Psi}_{m_d m_s}(\vec{p}) = (2\pi)^{\frac{3}{2}} \sqrt{2M_d} \sum_{\substack{L=0,2 \\ m_L}} i^L u_L(p) Y_{Lm_L}(\hat{p}) (Lm_L 1m_s | 1m_d). \quad (3.21)$$

For the radial wave functions  $u_L(p)$  we use the parametrization of the Bonn potential (full model) [45] (see appendix D)

$$u_0(p) = \sqrt{\frac{2}{\pi}} \sum_{i=1}^{n_u} \frac{C_i}{p^2 + m_i^2}, \quad (3.22)$$

$$u_2(p) = \sqrt{\frac{2}{\pi}} \sum_{i=1}^{n_w} \frac{D_i}{p^2 + m_i^2}. \quad (3.23)$$

In case of the impulse approximation (see section 3.3.1), we use for the  $NN$  final state a complete antisymmetric  $NN$  plane wave. For the total spin and isospin part of the two nucleon wave functions we use a coupled basis ( $|sm_s\rangle |tm_t\rangle$ ). The corresponding antisymmetric final  $NN$  wave function can formally be written as

$$|\vec{p}_1 \vec{p}_2, sm_s, tm_t\rangle = \frac{1}{\sqrt{2}} (|\vec{p}_1\rangle^{(1)} |\vec{p}_2\rangle^{(2)} - (-)^{s+t} |\vec{p}_2\rangle^{(1)} |\vec{p}_1\rangle^{(2)}) |sm_s\rangle |tm_t\rangle, \quad (3.24)$$

where  $|\vec{p}_i\rangle^{(j)}$  describes a state in which a nucleon "j" has the momentum  $\vec{p}_i$ . Only the  $t = 1$  channel contributes in the case of charged pions whereas for  $\pi^0$  production both  $t = 0$  and  $t = 1$  channels have to be taken into account.

### 3.3 Matrix Elements for $\gamma d \rightarrow \pi NN$

The transition matrix elements  $\mathcal{M}_{sm_s, m_\gamma m_d}^{(t\mu)}$  are calculated in the frame of time-ordered perturbation theory, using the elementary operator introduced in chapter 2 and including  $NN$  and  $\pi N$  rescattering in the final state. Scattering reactions are described in terms of probability amplitudes relating the initial and final asymptotic states of the combined system of projectile and target. In this section we consider the transition matrix element  $\mathcal{M}$  of Eq. (3.2) which describes the dynamics of the processes (3.1). These processes are diagrammatically shown in Fig. 3.2. There, all contributions of two-body currents are neglected. All possible rescattering diagrams are shown separately in Fig. 3.3. The  $\mathcal{M}$ -matrix has the general form

$$\mathcal{M} = \langle \pi NN; \vec{q} \vec{p}_1 \vec{p}_2, \alpha | \epsilon_\mu J^\mu(0) | \gamma d; \vec{k} \vec{d}, \beta \rangle, \quad (3.25)$$

where  $J^\mu(0)$  is the current operator,  $\alpha$  and  $\beta$  stand for the quantum numbers of the states asymptotically.

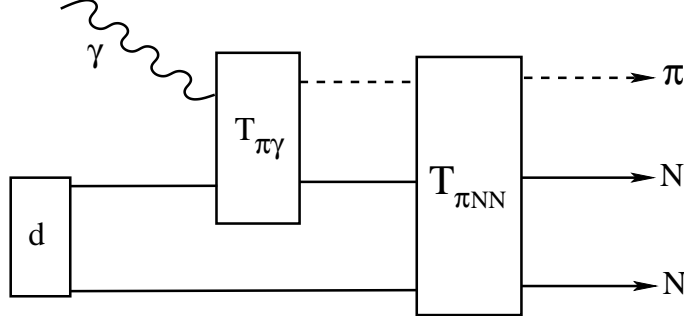


Figure 3.2: Diagrammatic representation of the  $\gamma d \rightarrow \pi NN$  amplitude including rescattering in the final state and neglecting all contributions of two-body currents.

We include in this work besides the pure impulse approximation (IA), the driving terms from  $NN$ - and  $\pi N$ -rescattering, so that the full transition matrix element reads

$$\mathcal{M}_{sm_s, m_\gamma m_d}^{(t\mu)} = \mathcal{M}_{sm_s, m_\gamma m_d}^{(t\mu) IA} + \mathcal{M}_{sm_s, m_\gamma m_d}^{(t\mu) NN} + \mathcal{M}_{sm_s, m_\gamma m_d}^{(t\mu) \pi N}, \quad (3.26)$$

in an obvious notation.

Now, we will consider successively all the three terms of Eq. (3.26), i.e., the impulse

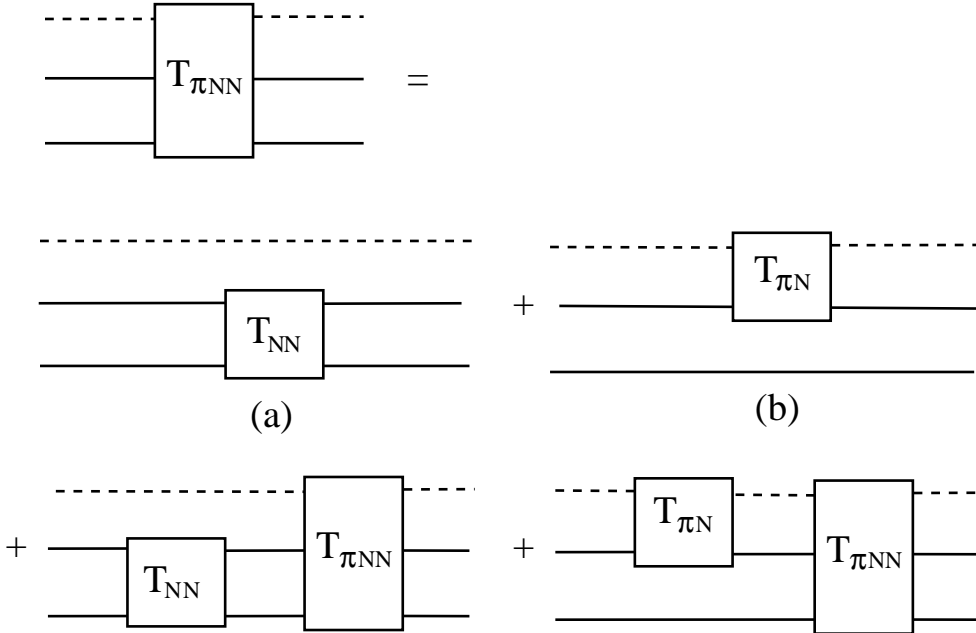


Figure 3.3: Diagrammatic representation of final state interactions of the reaction  $\gamma d \rightarrow \pi NN$ : (a) and (b) are "driving terms" from  $NN$  and  $\pi N$  rescattering in the final state, respectively.

approximation, the  $NN$  final state interaction and the  $\pi N$  rescattering in more detail.

### 3.3.1 The Impulse Approximation (IA)

In order to qualitatively explain the approximations concerning the rescattering terms which are of important interest in this work and discussed below, we would like to demonstrate here some features of the reaction amplitude keeping in (3.26) only the IA term. In case of the  $\gamma d \rightarrow \pi NN$  reaction, the impulse approximation leads to the so-called spectator nucleon model. The Feynman diagrams of this model are shown in Fig. 3.4. The corresponding transition matrix  $\mathcal{M}^{IA}$  is then given by

$$\mathcal{M}^{IA} = T_{\pi\gamma}^{(1)} \mathbb{1}^{(2)} + \mathbb{1}^{(1)} T_{\pi\gamma}^{(2)}, \quad (3.27)$$

where the upper index indicates on which of the nucleons the elementary production operator acts. The operator  $\mathcal{M}^{IA}$  contains contributions of pure single nucleon terms.

Using the initial and final states from section 3.2 and the operator of the pion photoproduction in the two-nucleon space from Eq. (3.27) we can write now the

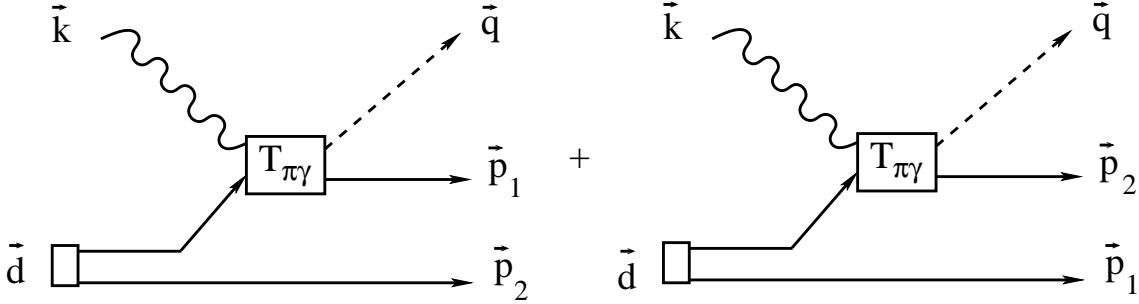


Figure 3.4: Feynman diagrams for the reaction  $\gamma d \rightarrow \pi NN$  in the impulse approximation.

$\mathcal{M}^{IA}$ -matrix element using a covariant normalization for all particles (see appendix A.2) as follows

$$\begin{aligned} \langle \vec{p}_1 \vec{p}_2, s m_s, t, -\mu | \mathcal{M}^{IA}(\vec{k}, m_\gamma, \vec{q}, \mu) | \vec{d}, m_d \rangle &= \frac{1}{2} \int \frac{d^3 p'_1}{(2\pi)^3} \int \frac{d^3 p'_2}{(2\pi)^3} \frac{M_N M_N}{E_{\vec{p}'_1} E_{\vec{p}'_2}} \\ &\times \sum_{m_{s'}} \langle \vec{p}_1 \vec{p}_2, s m_s, t, -\mu | \mathcal{M}^{IA}(\vec{k}, m_\gamma, \vec{q}, \mu) | \vec{p}'_1 \vec{p}'_2, 1 m_{s'}, 00 \rangle \\ &\times \langle \vec{p}'_1 \vec{p}'_2, 1 m_{s'}, 00 | \vec{d}, m_d \rangle. \end{aligned} \quad (3.28)$$

In the laboratory frame one finds for the matrix element (3.28) the following expression

$$\begin{aligned} \langle \vec{p}_1 \vec{p}_2, s m_s, t, -\mu | \mathcal{M}^{IA}(\vec{k}, m_\gamma, \vec{q}, \mu) | \vec{d} = 0, m_d, 00 \rangle &= \\ \frac{1}{\sqrt{2}} \sum_{m_{s'}} \langle s m_s, t, -\mu | &\left[ \left( \langle \vec{p}_1 | T_{\pi\gamma}^{(1)} | -\vec{p}_2 \rangle - (-)^{s+t} \langle \vec{p}_1 | T_{\pi\gamma}^{(2)} | -\vec{p}_2 \rangle \right) \tilde{\Psi}_{m_{s'}, m_d}(\vec{p}_2) \right. \\ &\left. + \left( \langle \vec{p}_2 | T_{\pi\gamma}^{(2)} | -\vec{p}_1 \rangle - (-)^{s+t} \langle \vec{p}_2 | T_{\pi\gamma}^{(1)} | -\vec{p}_1 \rangle \right) \tilde{\Psi}_{m_{s'}, m_d}(\vec{p}_1) \right] | 1 m_{s'}, 00 \rangle. \end{aligned} \quad (3.29)$$

Note that the upper index is maintained on  $T_{\pi\gamma}$ . The reason for that lies in the fact that the  $T_{\pi\gamma}$ -matrix contains spin and isospin operators, which still act on the spinors of the  $NN$  system. Using the symmetry properties

$$\langle s m_s | \mathbb{1}^{(1)} \sigma_\nu^{(2)} | s' m_{s'} \rangle = (-)^{s-s'} \langle s m_s | \sigma_\nu^{(1)} \mathbb{1}^{(2)} | s' m_{s'} \rangle, \quad (3.30)$$

which applies also likewise to the  $\tau$ -matrices, the matrix element of Eq. (3.29) is given by the following expression

$$\begin{aligned} \mathcal{M}_{s m_s, m_\gamma m_d}^{(t\mu) IA} &= \langle \vec{p}_1 \vec{p}_2, s m_s, t, -\mu | \mathcal{M}^{IA}(\vec{k}, m_\gamma, \vec{q}, \mu) | \vec{d} = 0, m_d, 00 \rangle \\ &= \sqrt{2} \sum_{m_{s'}} \langle s m_s, t, -\mu | \left( \langle \vec{p}_1 | T_{\pi\gamma}^{(1)} | -\vec{p}_2 \rangle \tilde{\Psi}_{m_{s'}, m_d}(\vec{p}_2) \right. \\ &\quad \left. - (-)^{s+t} \langle \vec{p}_2 | T_{\pi\gamma}^{(1)} | -\vec{p}_1 \rangle \tilde{\Psi}_{m_{s'}, m_d}(\vec{p}_1) \right) | 1 m_{s'}, 00 \rangle. \end{aligned} \quad (3.31)$$

The evaluation of the spin and isospin operators becomes very simple, because they act now on the nucleon "1" only. Using the Wigner-Eckart-theorem (see for example [46]) one finds

$$\langle sm_s | \sigma_\nu^{(1)} | 1m_{s'} \rangle = (-)^{s-1} 3\sqrt{2} (1\nu 1m_{s'} | sm_s) \begin{Bmatrix} \frac{1}{2} & 1 & \frac{1}{2} \\ 1 & \frac{1}{2} & s \end{Bmatrix}, \quad (3.32)$$

$$\langle tm_t | \tau_\mu^{\dagger(1)} | 00 \rangle = (-)^\mu \delta_{t,1} \delta_{m_t,-\mu}. \quad (3.33)$$

### 3.3.2 The $NN$ Final State Interaction

Now we will consider in addition  $NN$ -rescattering in the final state. The corresponding matrix element is given by the second term in Eq. (3.26). The Feynman diagram for this process is shown in Fig. 3.5 for the case when the production operator acts on nucleon "1". Note that the second diagram when the operator acts on nucleon "2" is also taken into account in the calculation.

The transition matrix element with  $NN$ -rescattering of the diagram in Fig. 3.5 is given by

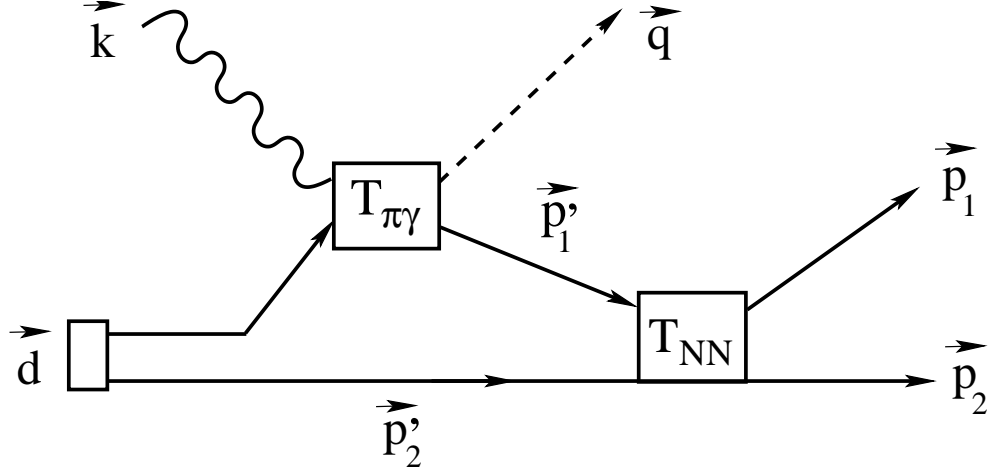


Figure 3.5: Feynman diagram for the reaction  $\gamma d \rightarrow \pi NN$  including  $NN$ -rescattering in the final state.

$$\begin{aligned} \mathcal{M}_{sm_s, m_\gamma m_d}^{(t\mu) NN} &= \langle \vec{q}, \vec{p}_1 \vec{p}_2; \mu, sm_s, t, -\mu | \mathcal{M}^{NN}(\vec{k}, m_\gamma) | \vec{d} = 0, m_d, 00 \rangle \\ &= \frac{1}{2(2\pi)^9} \sum_{s'm_{s'}t'\mu'} \iiint \frac{d^3 q'}{2\omega_{q'}} \frac{d^3 p'_1}{E_{p'_1}/M_N} \frac{d^3 p'_2}{E_{p'_2}/M_N} \end{aligned}$$

$$\begin{aligned}
& \times \langle \vec{q}, \vec{p}_1 \vec{p}_2; \mu, sm_s, t, -\mu | \mathcal{R}_{NN}(W_{NN}) | \vec{q}', \vec{p}'_1 \vec{p}'_2; \mu', s'm_{s'}, t', -\mu' \rangle \\
& \times \mathcal{G}_{0NN}^{\pi NN}(E_{\gamma d}, \vec{q}, \vec{p}'_1, \vec{p}'_2) \\
& \times \langle \vec{q}', \vec{p}'_1 \vec{p}'_2; \mu', s'm_{s'}, t', -\mu' | \mathcal{M}^{IA}(\vec{k}, m_\gamma) | \vec{d} = 0, m_d, 00 \rangle. \quad (3.34)
\end{aligned}$$

Here  $\mathcal{R}_{NN}$  denotes the half-off-shell  $NN$ -scattering matrix,  $\mathcal{G}_{0NN}^{\pi NN}(E_{\gamma d}, \vec{q}, \vec{p}'_1, \vec{p}'_2)$  is the free  $\pi NN$  propagator and  $\mathcal{M}^{IA}$ -matrix is given in Eq. (3.31).

### 3.3.2.1 The Half-Off-Shell $NN$ -Scattering Matrix

The  $NN$  dynamics in the final state is determined by the half-off-shell  $NN$ -scattering amplitude  $\mathcal{R}_{NN}$ . In the presence of a spectator meson it is given by introducing the relative and total momenta  $\vec{p}_r$  and  $\vec{P}$ , respectively, of the two outgoing nucleons (see Eqs. (3.10) and (3.11)) and using the basis states

$$\langle p_r \theta_r \phi_r | \vec{p}_r, sm_s, tm_t \rangle = \sum_{JM_J \ell m_\ell} (sm_s \ell m_\ell | JM_J) u_{\ell J}^{st}(p_r) Y_{\ell m_\ell}(\hat{p}_r) |\ell s JM_J \rangle |tm_t \rangle \quad (3.35)$$

by

$$\begin{aligned}
\langle \vec{q}, \vec{p}_1 \vec{p}_2; \mu, sm_s, t, -\mu | \mathcal{R}_{NN}(W_{NN}) | \vec{q}', \vec{p}'_1 \vec{p}'_2; \mu', s'm_{s'}, t', -\mu' \rangle &= 2(2\pi)^9 \delta_{\mu' \mu} \delta_{s' s} \delta_{t' t} \\
&\times \omega_{\vec{q}} \delta^3(\vec{q}' - \vec{q}) \delta^3(\vec{P}' - \vec{P}) \sqrt{\frac{E_{\vec{p}_1} E_{\vec{p}_2} E_{\vec{p}'_1} E_{\vec{p}'_2}}{M_N^4}} D_{m_s m_{s'}}^{st\mu}(W_{NN}, \vec{p}_r, \vec{p}'_r), \quad (3.36)
\end{aligned}$$

with

$$\begin{aligned}
\mathcal{D}_{m_s m_{s'}}^{st\mu}(W_{NN}, \vec{p}_r, \vec{p}'_r) &= \langle \vec{p}_r, sm_s, t - \mu | \mathcal{R}_{NN}(W_{NN}) | \vec{p}'_r, sm_{s'}, t - \mu \rangle \\
&= \sum_{J \ell \ell'} \mathcal{F}_{\ell \ell' m_s m_{s'}}^{J s}( \hat{p}_r, \hat{p}'_r ) \mathcal{T}_{\ell \ell'}^{J s t \mu}(W_{NN}, p_r, p'_r), \quad (3.37)
\end{aligned}$$

where  $\ell$  is the orbital angular momentum and  $J$  is the total angular momentum of the two-nucleon system. The initial and final relative momenta of the two nucleons in the  $NN$ -subsystem are given, respectively, by

$$\begin{aligned}
\vec{p}'_r &= \frac{1}{2}(\vec{p}'_1 - \vec{p}'_2), \\
\vec{p}_r &= \frac{1}{2}(\vec{p}_1 - \vec{p}_2). \quad (3.38)
\end{aligned}$$

where  $\vec{p}'_1 = \vec{p}'_r + \frac{1}{2}(\vec{k} - \vec{q})$  and  $\vec{p}'_2 = -\vec{p}'_r + \frac{1}{2}(\vec{k} - \vec{q})$  with the integration variable  $\vec{p}'_r$ . The function  $\mathcal{F}_{\ell \ell' m_s m_{s'}}^{J s}( \hat{p}_r, \hat{p}'_r )$  is given by

$$\mathcal{F}_{\ell \ell' \ell m_s m_{s'}}^{J s}( \hat{p}_r, \hat{p}'_r ) = \sum_{M_J m_\ell m_{\ell'}} (\ell m_\ell sm_s | JM_J) (\ell' m_{\ell'} sm_{s'} | JM_J) Y_{\ell m_\ell}^*(\hat{p}_r) Y_{\ell' m_{\ell'}}(\hat{p}'_r). \quad (3.39)$$

The half-off-shell partial wave amplitudes  $\mathcal{T}_{\ell\ell'}^{Jst\mu}(W_{NN}, p_r, p'_r)$  were found for partial waves with total angular momentum  $J \leq 3$ , which are important in the energy region under consideration, by numerical solution of the Lippmann-Schwinger (LS) equation [47]. In appendix F we give a detailed solution of the LS equation for a given  $NN$  potential model. In the calculations presented here, these amplitudes are obtained from the separable representation of the Paris  $NN$  potential [48, 49], which reproduces its on-shell as well as off-shell properties.

### 3.3.2.2 The $\pi NN$ Propagator

The free  $\pi NN$  propagator is given by

$$\mathcal{G}_{0NN}^{\pi NN}(E_{\gamma d}, \vec{q}, \vec{p}'_1, \vec{p}'_2) = \frac{1}{E_{\gamma d} - \omega_{\pi}(\vec{q}) - E_{N_1}(\vec{p}'_1) - E_{N_2}(\vec{p}'_2) + i\epsilon}. \quad (3.40)$$

In the nonrelativistic limit it is given by

$$\mathcal{G}_{0NN}^{\pi NN}(E_{\gamma d}, \vec{q}, \vec{p}'_1, \vec{p}'_2) = \frac{M_N}{\tilde{p}'^2 - p_r'^2 + i\epsilon}, \quad (3.41)$$

where  $\tilde{p}'$  is given by

$$\tilde{p}'^2 = M_N \left( E_{\gamma d} - \omega_{\pi}(\vec{q}) - 2M_N - \frac{(\vec{k} - \vec{q})^2}{4M_N} \right). \quad (3.42)$$

The magnitude of the relative on-shell momentum of the two nucleons is given by

$$p_0 = \sqrt{M_N(W_{NN} - 2M_N)}. \quad (3.43)$$

Collecting the various pieces and substituting Eqs. (3.36) and (3.41) in Eq. (3.34), we obtain the following expression for the transition matrix element with  $NN$  rescattering

$$\begin{aligned} \mathcal{M}_{sm_s, m_{\gamma} m_d}^{(t\mu) NN}(\vec{k}, \vec{q}, \vec{p}_1, \vec{p}_2) &= \sum_{m_{s'}} \int d^3 \vec{p}'_r \sqrt{\frac{E_{\vec{p}_1} E_{\vec{p}_2}}{E_{\vec{p}'_1} E_{\vec{p}'_2}}} \mathcal{D}_{m_s m_{s'}}^{st\mu}(W_{NN}, \vec{p}_r, \vec{p}'_r) \\ &\times \frac{M_N}{\tilde{p}'^2 - p_r'^2 + i\epsilon} \mathcal{M}_{sm_{s'}, m_{\gamma} m_d}^{(t\mu) IA}(\vec{k}, \vec{q}, \vec{p}'_1, \vec{p}'_2), \end{aligned} \quad (3.44)$$

where  $\mathcal{D}_{m_s m_{s'}}^{st\mu}(W_{NN}, \vec{p}_r, \vec{p}'_r)$  is given by Eq. (3.37). The three dimensional integral over  $\vec{p}'_r$  is carried out numerically.

### 3.3.3 The $\pi N$ Final State Interaction

In addition to the  $NN$  final state interaction we consider also in this work the  $\pi N$ -rescattering in the final state. The corresponding matrix element in this case is given by the third term in Eq. (3.26). The Feynman diagram for this process is shown in Fig. 3.6 for the case when the production operator acts only on nucleon "1". The second diagram when the operator acts on nucleon "2" is also taken into account in the calculation.

The transition matrix element with  $\pi N$ -rescattering in the final state (see Fig. 3.6) is given by

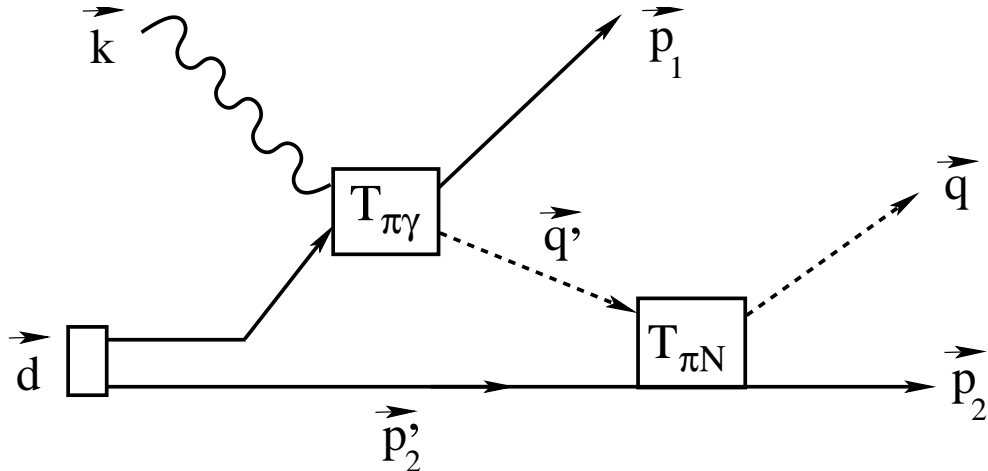


Figure 3.6: Feynman diagram for the reaction  $\gamma d \rightarrow \pi NN$  including  $\pi N$ -rescattering in the final state.

$$\begin{aligned}
 M_{sm_s, m_\gamma m_d}^{(t\mu) \pi N} &= \langle \vec{q}, \vec{p}_1 \vec{p}_2'; \mu, sm_s, t, -\mu | \mathcal{M}^{\pi N}(\vec{k}, m_\gamma) | \vec{d} = 0, m_d, 00 \rangle \\
 &= \frac{1}{2(2\pi)^9} \sum_{s'm_{s'}, t'\mu'} \iiint \frac{d^3 q'}{2\omega_{q'}} \frac{d^3 p_1'}{E_{p_1'} / M_N} \frac{d^3 p_2'}{E_{p_2'} / M_N} \\
 &\quad \times \{ \langle \vec{q}, \vec{p}_1 \vec{p}_2'; \mu, sm_s, t, -\mu | \mathcal{R}_{\pi N}(W_{\pi N}(\vec{p}_2')) | \vec{q}', \vec{p}_1' \vec{p}_2'; \mu', s'm_{s'}, t', -\mu' \rangle \\
 &\quad - (-)^{s+t} (\vec{p}_1 \leftrightarrow \vec{p}_2) \} \mathcal{G}_{0\pi N}^{\pi NN}(E_{\gamma d}, \vec{q}', \vec{p}_1, \vec{p}_2') \\
 &\quad \times \langle \vec{q}', \vec{p}_1' \vec{p}_2'; \mu', s'm_{s'}, t', -\mu' | \mathcal{M}^{IA}(\vec{k}, m_\gamma) | \vec{d} = 0, m_d, 00 \rangle, \quad (3.45)
 \end{aligned}$$

where  $\mathcal{R}_{\pi N}$  denotes the half-off-shell  $\pi N$ -scattering matrix at the invariant mass

$$W_{\pi N}(\vec{p}_2) = \sqrt{(E_{\vec{p}_2} + \omega_{\vec{q}})^2 - (\vec{p}_2 + \vec{q})^2} \quad (3.46)$$

of the  $\pi N$  subsystem,  $\mathcal{G}_{0\pi N}^{\pi NN}(E_{\gamma d}, \vec{q}', \vec{p}_1, \vec{p}_2')$  is the free  $\pi NN$  propagator (see Eq. (3.40)) and  $\mathcal{M}^{IA}$ -matrix is given in Eq. (3.31).

### 3.3.3.1 The Half-Off-Shell $\pi N$ -Scattering Matrix

Using the coupled basis states

$$\begin{aligned} |\vec{q}, \vec{p}_1 \vec{p}_2; \mu, sm_s, t, -\mu\rangle &= \sum_{\substack{m_{s_1} m_{t_1} \\ m_{s_2} m_{t_2}}} \left( \frac{1}{2} m_{s_1} \frac{1}{2} m_{s_2} \mid sm_s \right) \left( \frac{1}{2} m_{t_1} \frac{1}{2} m_{t_2} \mid t - \mu \right) \\ &\times |\vec{q}, \vec{p}_1, \vec{p}_2; 1\mu, \frac{1}{2}m_{s_1}, \frac{1}{2}m_{t_1}, \frac{1}{2}m_{s_2}, \frac{1}{2}m_{t_2}\rangle, \end{aligned} \quad (3.47)$$

the half-off-shell  $\pi N$ -scattering amplitude  $\mathcal{R}_{\pi N}$  is given in the presence of a spectator nucleon by

$$\begin{aligned} \langle \vec{q}, \vec{p}_1 \vec{p}_2; \mu, sm_s, t, -\mu | \mathcal{R}_{\pi N}(W_{\pi N}(\vec{p}_2)) | \vec{q}', \vec{p}'_1 \vec{p}'_2; \mu', s'm_{s'}, t', -\mu' \rangle &= (2\pi)^3 \frac{E_{\vec{p}_1}}{M_N} \\ &\times \delta^3(\vec{p}'_1 - \vec{p}_1) \sum_{\substack{m_{s_2} m_{t_2} m_{s'_2} m_{t'_2}}} \mathcal{A}_{t\mu, t'\mu'}^{sm_s s' m_{s'}}(m_{s_2}, m_{t_2}, m_{s'_2}, m_{t'_2}) \\ &\times \langle \vec{q}, \vec{p}_2; 1\mu, \frac{1}{2}m_{s_2}, \frac{1}{2}m_{t_2} | \mathcal{R}_{\pi N}(W_{\pi N}(\vec{p}_2)) | \vec{q}', \vec{p}'_2; 1\mu', \frac{1}{2}m_{s'_2}, \frac{1}{2}m_{t'_2} \rangle, \end{aligned} \quad (3.48)$$

where  $m_{s_2}$  ( $m_{s'_2}$ ) and  $m_{t_2}$  ( $m_{t'_2}$ ) are the spin and isospin projections of the final (initial) nucleon which is interacting with the pion in the  $\pi N$  subsystem, respectively. The function  $\mathcal{A}$  is given by

$$\begin{aligned} \mathcal{A}_{t\mu, t'\mu'}^{sm_s s' m_{s'}}(m_{s_2}, m_{t_2}, m_{s'_2}, m_{t'_2}) &= \sum_{\substack{m_{s_1} m_{t_1}}} \delta_{m_{s'_1} m_{s_1}} \delta_{m_{t'_1} m_{t_1}} \\ &\times \left( \frac{1}{2} m_{s_1} \frac{1}{2} m_{s_2} \mid sm_s \right) \left( \frac{1}{2} m_{t_1} \frac{1}{2} m_{t_2} \mid t - \mu \right) \\ &\times \left( \frac{1}{2} m_{s'_1} \frac{1}{2} m_{s'_2} \mid s'm_{s'} \right) \left( \frac{1}{2} m_{t'_1} \frac{1}{2} m_{t'_2} \mid t' - \mu' \right), \end{aligned} \quad (3.49)$$

where  $m_{s_1}$  and  $m_{t_1}$  are the spin and isospin projections of the spectator nucleon, respectively.

Coupling the pion and nucleon isospins into the total isospin  $\tilde{t}$  of the pion-nucleon pair according to

$$|\vec{q}, \vec{p}_2; 1\mu, \frac{1}{2}m_{s_2}, \frac{1}{2}m_{t_2}\rangle = \sum_{\tilde{t} \tilde{m}_t} (1\mu \frac{1}{2}m_{t_2} \mid \tilde{t} \tilde{m}_t) |\vec{q}, \vec{p}_2; \tilde{t} \tilde{m}_t, \frac{1}{2}m_{s_2}, \frac{1}{2}m_{t_2}\rangle \quad (3.50)$$

and introducing the relative and total momenta of the final (initial) pion-nucleon subsystem which are given, respectively, by

$$\tilde{\vec{p}}_r = \frac{M_N \vec{q} - m_\pi \vec{p}_2}{M_N + m_\pi} \quad \left( \tilde{\vec{p}}'_r = \frac{M_N \vec{q}' - m_\pi \vec{p}'_2}{M_N + m_\pi} \right) \quad (3.51)$$

and

$$\tilde{\vec{P}} = \vec{q} + \vec{p}_2 \quad \left( \tilde{\vec{P}}' = \vec{q}' + \vec{p}'_2 \right) \quad (3.52)$$

we can re-write Eq. (3.48) in the form

$$\begin{aligned} \langle \vec{q}, \vec{p}_1 \vec{p}_2; \mu, s m_s, t, -\mu | \mathcal{R}_{\pi N}(W_{\pi N}(\vec{p}_2)) | \vec{q}', \vec{p}'_1 \vec{p}'_2; \mu', s' m_{s'}, t', -\mu' \rangle &= 2(2\pi)^9 \frac{E_{\vec{p}_1}}{M_N} \\ &\times \sqrt{\frac{E_{\vec{p}_2} E_{\vec{p}'_2}}{M_N^2}} \sqrt{\omega_{\vec{q}} \omega_{\vec{q}'}} \delta^3(\vec{p}_1 - \vec{p}'_1) \delta^3(\tilde{\vec{P}} - \tilde{\vec{P}}') \\ &\times \sum_{m_{s_2} m_{t_2} m_{s'_2} m_{t'_2}} \mathcal{A}_{t\mu, t'\mu'}^{s m_s s' m_{s'}}(m_{s_2}, m_{t_2}, m_{s'_2}, m_{t'_2}) \\ &\times \sum_{\tilde{t} \tilde{m}_t \tilde{t}' \tilde{m}_{t'}} \mathcal{B}_{\mu\mu' \tilde{t}\tilde{t}'}^{\tilde{m}_t \tilde{m}_{t'}}(m_{t_2}, m_{t'_2}) \\ &\times \langle \tilde{\vec{p}}_r, \frac{1}{2} m_{s_2}, \tilde{t} \tilde{m}_t | \tilde{\mathcal{R}}_{\pi N}(W_{\pi N}(\vec{p}_2)) | \tilde{\vec{p}}'_r, \frac{1}{2} m_{s'_2}, \tilde{t}' \tilde{m}_{t'} \rangle. \end{aligned} \quad (3.53)$$

The function  $\mathcal{B}$  is given by

$$\mathcal{B}_{\mu\mu' \tilde{t}\tilde{t}'}^{\tilde{m}_t \tilde{m}_{t'}}(m_{t_2}, m_{t'_2}) = (1\mu \frac{1}{2} m_{t_2} | \tilde{t} \tilde{m}_t) (1\mu' \frac{1}{2} m_{t'_2} | \tilde{t}' \tilde{m}_{t'}). \quad (3.54)$$

Using the partial wave expansion

$$\begin{aligned} \langle \tilde{\vec{p}}_r \theta \phi | \tilde{\vec{p}}_r, \frac{1}{2} m_{s_2}, \tilde{t} \tilde{m}_t \rangle &= \sum_{\tilde{J} \tilde{M}_J \tilde{\ell} \tilde{m}_\ell} \left( \frac{1}{2} m_{s_2} \tilde{\ell} \tilde{m}_\ell | \tilde{J} \tilde{M}_J \right) \tilde{u}_{\tilde{\ell} \tilde{J}}^{\tilde{t}}(\tilde{p}_r) \\ &\times Y_{\tilde{\ell} \tilde{m}_\ell}(\tilde{\vec{p}}_r) | \tilde{\ell} \frac{1}{2} \tilde{J} \tilde{M}_J \rangle | \tilde{t} \tilde{m}_t \rangle, \end{aligned} \quad (3.55)$$

where  $\tilde{\ell}$ ,  $\tilde{J}$  and  $\tilde{M}_J$  denote the relative orbital angular momentum, the total angular momentum and its  $z$ -axis projection of the  $\pi N$  system, respectively, we obtain

$$\begin{aligned} \langle \tilde{\vec{p}}_r, \frac{1}{2} m_{s_2}, \tilde{t} \tilde{m}_t | \tilde{\mathcal{R}}_{\pi N}(W_{\pi N}(\vec{p}_2)) | \tilde{\vec{p}}'_r, \frac{1}{2} m_{s'_2}, \tilde{t}' \tilde{m}_{t'} \rangle &= \mathcal{Q}_{\tilde{m}_t \tilde{m}_{t'}}^{\tilde{t} \tilde{t}'}(W_{\pi N}(\vec{p}_2), \tilde{\vec{p}}_r, \tilde{\vec{p}}'_r) \\ &= \sum_{\tilde{J} \tilde{M}_J \tilde{\ell} \tilde{m}_\ell} \delta_{\tilde{t} \tilde{t}'} \delta_{\tilde{m}_{t'} \tilde{m}_t} \delta_{\tilde{\ell} \tilde{\ell}} \delta_{\tilde{m}_{t'} \tilde{m}_\ell} \delta_{\tilde{J}' \tilde{J}} \delta_{\tilde{M}_{J'} \tilde{M}_J} \left( \frac{1}{2} m_{s_2} \tilde{\ell} \tilde{m}_\ell | \tilde{J} \tilde{M}_J \right) \\ &\times \left( \frac{1}{2} m_{s'_2} \tilde{\ell}' \tilde{m}_{t'} | \tilde{J}' \tilde{M}_{J'} \right) Y_{\tilde{\ell} \tilde{m}_\ell}^*(\tilde{\vec{p}}_r) Y_{\tilde{\ell}' \tilde{m}_{t'}}(\tilde{\vec{p}}'_r) \tilde{\mathcal{R}}_{\pi N}^{\tilde{J} \tilde{\ell} \tilde{t}}(W_{\pi N}(\vec{p}_2), \tilde{\vec{p}}_r, \tilde{\vec{p}}'_r). \end{aligned} \quad (3.56)$$

Inserting Eq. (3.56) in (3.53), we obtain the final form for the half-off-shell  $\pi N$ -scattering amplitude. In the calculations presented here, the half-off-shell partial wave amplitudes  $\tilde{\mathcal{R}}_{\pi N}^{J \tilde{\ell} \tilde{t}}(W_{\pi N}(\vec{p}_2), \tilde{\vec{p}}_r, \tilde{\vec{p}}'_r)$  were obtained for all  $S$ -,  $P$ - and  $D$ -waves

channels by solving the Lippmann-Schwinger equation [47] for a separable energy-dependent  $\pi N$  potential built in Ref. [15]. This potential describes precisely the on-shell as well as the off-shell properties of the  $\pi N$  scattering amplitude. More details about this potential is given in appendix F.

Collecting the various pieces, we obtain the following expression for the amplitude (3.45) with  $\pi N$ -rescattering in the final state

$$\begin{aligned}
M_{sm_s, m_\gamma m_d}^{(t\mu) \pi N}(\vec{k}, \vec{q}, \vec{p}_1, \vec{p}_2) &= \frac{1}{2} \sum_{s'm_s, t'\mu'} \int d^3 \vec{p} \sqrt{\frac{\omega_{\vec{q}}}{\omega_{\vec{q}'} \sqrt{\frac{E_{\vec{p}_2}}{E_{\vec{p}'_2}}}}} \\
&\times \sum_{m_{s_2} m_{t_2} m_{s'_2} m_{t'_2}} \mathcal{A}_{t\mu, t'\mu'}^{sm_s s' m_{s'}}(m_{s_2}, m_{t_2}, m_{s'_2}, m_{t'_2}) \\
&\times \left[ \sum_{\tilde{t}\tilde{m}_t \tilde{t}'\tilde{m}_{t'}} \mathcal{B}_{\mu\mu' \tilde{t}\tilde{t}'}^{\tilde{m}_t \tilde{m}_{t'}}(m_{t_2}, m_{t'_2}) \right. \\
&\times \left\{ \mathcal{Q}_{\tilde{m}_t \tilde{m}_{t'}}^{\tilde{t}\tilde{t}'}(W_{\pi N}(\vec{p}_2), \tilde{\vec{p}}_r, \tilde{\vec{p}}'_r) \mathcal{G}_{0\pi N}^{\pi NN}(E_{\gamma d}, \vec{q}'(\vec{p}), \vec{p}_1, \vec{p}'_2(\vec{p})) \right. \\
&\left. \left. \times \mathcal{M}_{s'm_s, m_\gamma m_d}^{(t'\mu') IA}(\vec{k}, \vec{q}'(\vec{p}), \vec{p}_1, \vec{p}'_2(\vec{p})) - (-)^{s+t}(\vec{p}_1 \leftrightarrow \vec{p}_2) \right\} \right], \tag{3.57}
\end{aligned}$$

where  $\tilde{\vec{p}}'_r(\vec{p})$  and  $\tilde{\vec{p}}_r$  are given in Eq. (3.51) and

$$\begin{aligned}
\vec{q}'(\vec{p}) &= \vec{p} - \tilde{\vec{p}}_1 \quad \text{with} \quad \tilde{\vec{p}}_1 = \vec{p}_1 - \vec{k} \\
\vec{p}'_2(\vec{p}) &= -\vec{p}.
\end{aligned} \tag{3.58}$$

Similarly to the case of  $NN$  scattering, the three dimensional integral over  $\vec{p}$  is carried out numerically.



# Chapter 4

## Results and Discussion

In this chapter we will present and discuss our results for pion photoproduction on the deuteron in the  $\Delta(1232)$  resonance region including  $NN$  and  $\pi N$  rescattering in the final state. We will discuss the important observables that have been measured experimentally, such as the total and differential cross sections. Since several experiments to test the Gerasimov-Drell-Hearn (GDH) sum rule both on the proton and on the neutron are now in preparation or planned at different laboratories around the world (MAMI, ELSA, LEGS, GRAAL and TJNAF), the theoretical investigation of the spin asymmetry and the corresponding GDH integral are nowadays a very interesting subject of research. This sum rule is derived under very general assumptions (Lorentz and gauge invariance, causality, relativity and unitarity). This makes its verification to be an important check of our understanding of the hadronic spin structure. The inclusion of final state interaction effects may play an important role on the spin asymmetry and the corresponding GDH sum rule for the deuteron. Therefore, we will also discuss in this chapter the influence of rescattering effects on the spin asymmetry and the GDH sum rule for the deuteron and, for comparison, for the nucleon.

The discussion in this chapter is divided into three parts. In the first part, we present our results for the total cross section of the processes (3.1) in comparison with experimental data and other theoretical predictions. In the second part, we discuss the semi-exclusive differential cross section  $d^2\sigma/d\Omega_\pi$ . We also compare our results for the differential cross section with experimental data and other theories. In the third part, we study the influence of  $NN$  and  $\pi N$  rescattering on the spin asymmetry and the corresponding GDH sum rule for the deuteron. We would like to mention that the results presented here are calculated using the deuteron wave function of the Bonn potential (full model) [45] (see section 3.2).

To calculate the semi-exclusive differential cross section  $d^2\sigma/d\Omega_\pi$ , the fully exclusive

differential cross section  $d^5\sigma/(d\Omega_\pi dq_\pi d\Omega_{p_r})$  (see Eq. (3.17)) was integrated over the pion momentum  $q_\pi$  and the polar angle  $\theta_{p_r}$  and the azimuthal angle  $\phi_{p_r}$  of the relative momentum  $\vec{p}_r$  of the two outgoing nucleons. The total cross section was calculated by integrating Eq. (3.17) over all the remaining independent variables, i.e., the pion momentum  $q_\pi$ , its angles  $\theta_\pi$  and  $\phi_\pi$ , the polar angle  $\theta_{p_r}$  and the azimuthal angle  $\phi_{p_r}$  of the relative momentum of the two outgoing nucleons. These integrations are carried out numerically. The number of integration points was being increased until the accuracy of calculated observables becomes good to 1%.

## 4.1 Total Cross Section

We start the discussion with presenting our results for the total cross sections in Fig. 4.1 including  $NN$  and  $\pi N$  final state interaction effects.

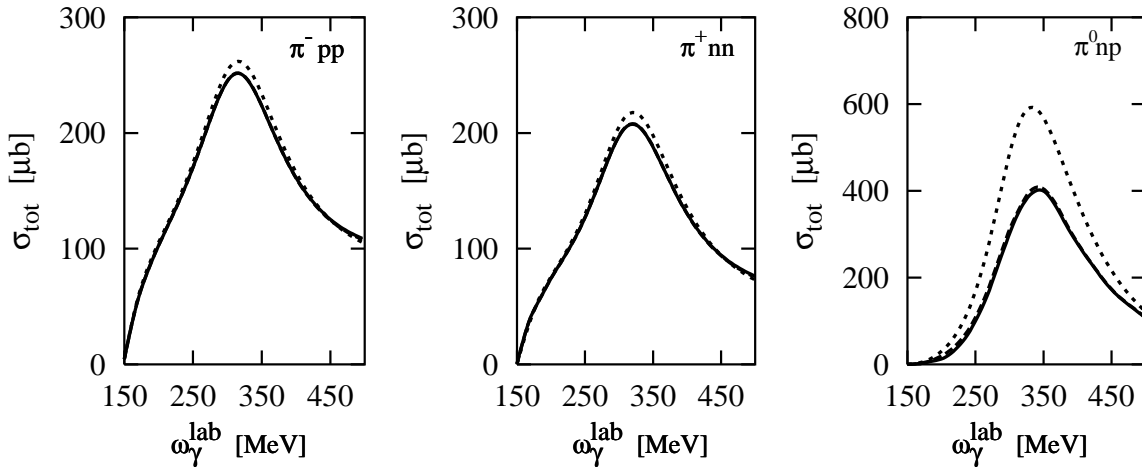


Figure 4.1: Total cross sections for  $\gamma d \rightarrow \pi NN$  reaction obtained within the impulse approximation (dotted curves) in comparison with the calculation including  $NN$  final state interaction (dashed curves) and the calculation with additional  $\pi N$  rescattering (solid curves). The left, middle and right panels represent the total cross section for  $\gamma d \rightarrow \pi^- pp$ ,  $\pi^+ nn$  and  $\pi^0 np$ , respectively.

Fig. 4.1 shows that the differences between the full and the spectator model calculations clearly demonstrate the importance of rescattering effects, in particular for the  $\pi^0$  channel. One can see that final state interactions lead to a strong reduction of the total cross section. In the case of charged pion photoproduction reactions, the final state interaction effects are small in comparison with the case of neutral pion photoproduction reaction. The difference between the solid and dashed curves in Fig.

4.1 shows that the  $\pi N$  rescattering changes the final results only by a few percent. A possible explanation for this smallness comes from the fact that the scattering length of the most important  $S$ -wave  $\pi N$ -scattering is about two orders smaller than the one of  $NN$ -scattering. In the energy range of the  $\Delta(1232)$  resonance, one finds the strongest manifestation of rescattering effects. In the case of  $\pi^-$  and  $\pi^+$  channels, one sees that the  $NN$  and  $\pi N$  rescattering effects reduce the total cross sections for both channels in the energy range of the  $\Delta(1232)$  resonance by about 5%. For lower and higher energies, the influence of rescattering effects changes the results for total cross sections of the charged pion channels with a few percent. With respect to  $\pi^0$  channel, we see from the right panel of Fig. 4.1 that, the influence of rescattering effects is much more significant than the case of charged pion channels. It leads to a strong reduction of the total cross section by about 35% in the energy range of the  $\Delta(1232)$  resonance.

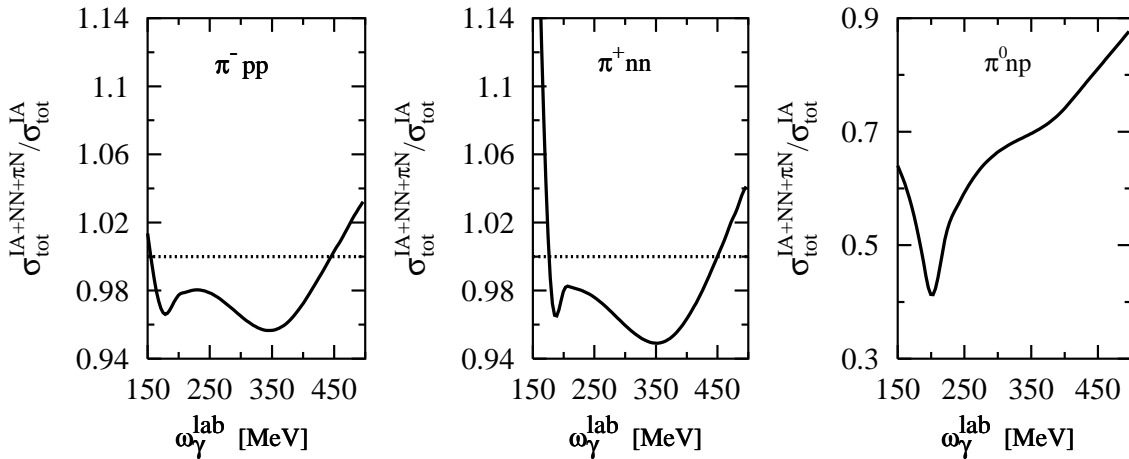


Figure 4.2: The ratio  $\sigma_{tot}^{IA+NN+\pi N}/\sigma_{tot}^{IA}$  as a function of the photon energy in the laboratory frame. The left, middle and right panels represent the ratio for  $\gamma d \rightarrow \pi^- pp$ ,  $\pi^+ nn$  and  $\pi^0 np$ , respectively.

In order to show in greater detail the relative influence of rescattering effects on the total cross sections, we show in Figs. 4.2 and 4.3 the ratios  $\sigma_{tot}^{IA+NN+\pi N}/\sigma_{tot}^{IA}$  and  $\sigma_{tot}^{IA+NN+\pi N}/\sigma_{tot}^{IA+NN}$ , respectively, as a function of the photon energy in the laboratory frame. Here  $\sigma_{tot}^{IA}$  denotes the total cross section in the impulse approximation,  $\sigma_{tot}^{IA+NN}$  denotes the total cross section including  $NN$  rescattering and  $\sigma_{tot}^{IA+NN+\pi N}$  denotes the total cross section with additional  $\pi N$  rescattering (see section 3.3).

Fig. 4.2 shows the combined effect of  $NN$  and  $\pi N$  rescattering as a function of the photon energy. This emphasize the important role of final state interactions for the total cross sections, especially for  $\pi^0$  photoproduction on the deuteron. It

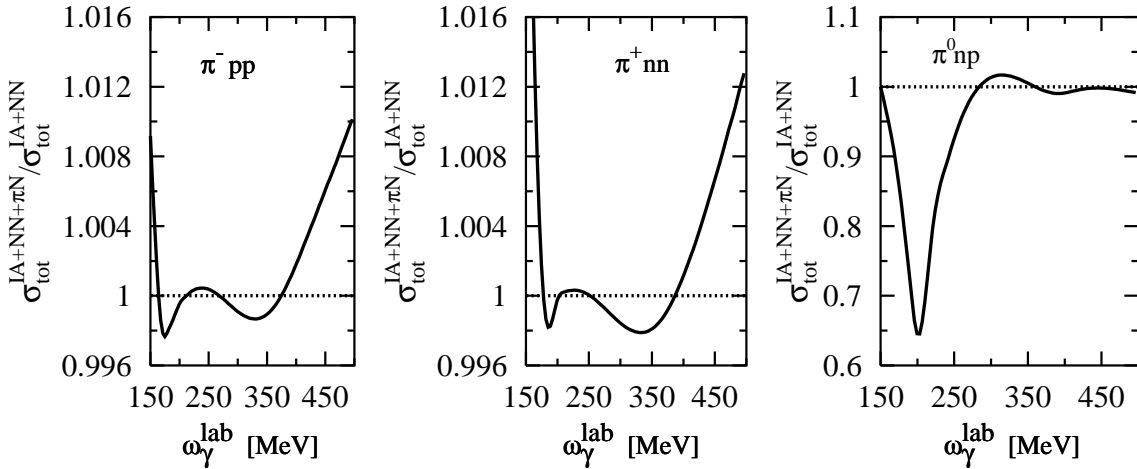


Figure 4.3: The ratio  $\sigma_{tot}^{IA+NN+\pi N}/\sigma_{tot}^{IA+NN}$  as a function of the photon energy. The left, middle and right panels represent the ratio for  $\gamma d \rightarrow \pi^- pp$ ,  $\pi^+ nn$  and  $\pi^0 np$ , respectively.

is obvious that for charged pion channels the ratio has a similar shape, but in the case of  $\pi^0$  production, a totally different shape is observed. At energies near to the pion threshold, the effect of rescattering increases the total cross section for  $\pi^+$  production than for  $\pi^-$  production. For  $\pi^+$  production we found that at 150 MeV the ratio is 1.32, while it reads 1.01 for  $\pi^-$  production at the same energy. For  $\pi^0$  production, the situation is completely different since final state interactions lead to a strong reduction which amounts to about 60% at 200 MeV. This demonstrates that rescattering effects play a very important role, in particular, in the case of  $\pi^0$  photoproduction.

As next we show the relative effect of  $\pi N$  rescattering in Fig. 4.3. In general, we obtain a similar shape as in the case of  $\sigma_{tot}^{IA+NN+\pi N}/\sigma_{tot}^{IA}$  (see Fig. 4.2), especially that the peaks have approximately the same energy. Fig. 4.3 shows that the influence of  $\pi N$  rescattering in the region of the  $\Delta$  resonance is much less important than  $NN$  rescattering. For energies near to the pion threshold, we see that the effect of  $\pi N$  rescattering increases the total cross sections for charged pion channels. This increment is noticeable in the case of  $\pi^+$  production since the ratio reads 1.033 at 150 MeV. Furthermore, we see that the effect of  $\pi N$  rescattering in the case of  $\pi^0$  production leads to a strong reduction for the total cross section, in particular at 200 MeV. A very big effect of the  $\pi N$  rescattering in the threshold region was also found in Refs. [14, 50, 51, 52]. As already mentioned in [52], that the charged pion channels are also of importance in the threshold region, because a big  $\pi^\pm N$  rescattering effect is certainly possible.

### 4.1.1 Comparison with Experimental Data

Here we compare our results for the total cross sections of the reaction  $\gamma d \rightarrow \pi NN$  including  $NN$  and  $\pi N$  rescattering in the final state with experimental data. In our comparison with experiment we concentrate our discussion on  $\pi^-$  and  $\pi^0$  photo-production on the deuteron, since data for  $\pi^+$  production in the  $\Delta(1232)$  resonance region are not available. In the case of  $\pi^-$  production we compare our results with the experimental data from Refs. [21, 53, 54]. For  $\pi^0$  production we compare our results with the experimental data from [22].

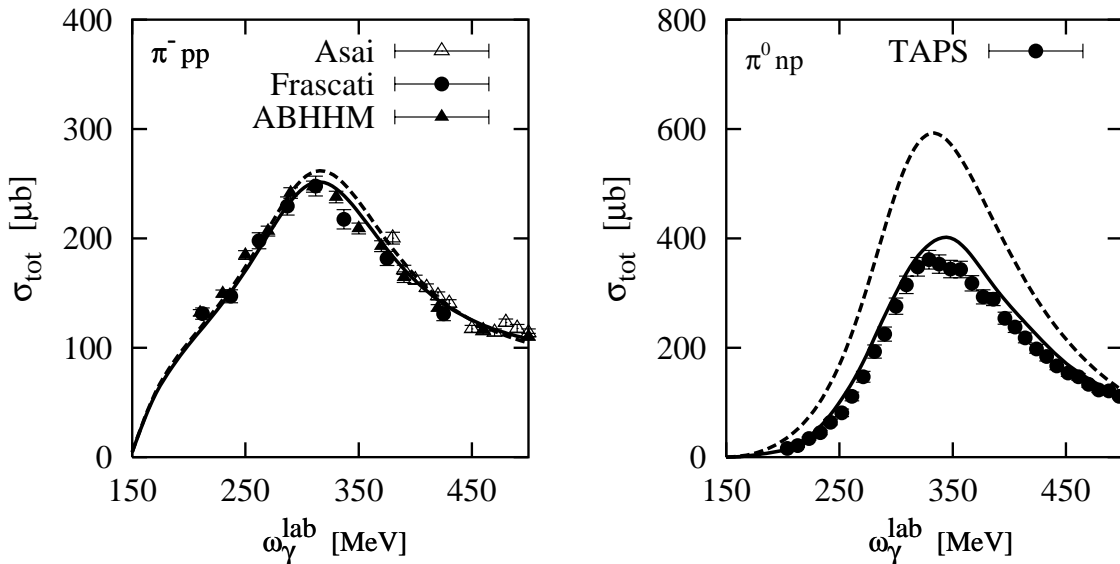


Figure 4.4: Total cross sections for  $\pi^-$  (left panel) and  $\pi^0$  (right panel) photoproduction on the deuteron. Solid curves show our results with  $NN$  and  $\pi N$  rescattering in the final state and dashed curves show the results in the impulse approximation. The experimental data are from [21] (ABHHM), [53] (Frascati) and [54] (Asai) in case of  $\pi^-$  production and from [22] (TAPS) in case of  $\pi^0$  production.

Fig. 4.4 shows our results for the total cross sections for  $\pi^-$  and  $\pi^0$  photoproduction on the deuteron compared with experimental data. One readily notes, that the spectator approach can not describe the experimental data in the  $\Delta(1232)$  resonance region (see also [23]), especially in the case of  $\pi^0$  production. Note, that the contribution of final state interactions in the case of  $\pi^0$  production is much larger than that for  $\pi^-$  production. Furthermore, final state interaction effects lead to a strong reduction of total cross section. The inclusion of such effects improve the agreement between experimental data and theoretical predictions. Indeed, a quite significant contribution from  $NN$  rescattering is found. Only in the center of the peak for  $\pi^0$

production our model overestimates the measured total cross section by about 6%. Moreover, we found that the  $\pi N$  rescattering changes the final results only by a few percent. As mentioned before, this smallness can be explained by the fact that the most important  $S$ -wave  $\pi N$  scattering length is about two orders smaller than the one for  $NN$  scattering.

These results clearly show that the rescattering effects are significant and reduce the total cross section in the  $\Delta(1232)$  resonance region. This means, in particular with respect to a test of theoretical models for pion production amplitudes on the neutron, that one needs a reliable description of the rescattering process. Compared to experimental data, one readily finds that the sizable discrepancies without rescattering are largely reduced and that a reasonable agreement with the data is achieved.

#### 4.1.2 Comparison with other Theoretical Predictions

Pion photoproduction on the deuteron in the impulse approximation has been studied by Schmidt *et al.* [23] neglecting all kinds of final state interactions and other two-body operators. Since data for  $\pi^+$  and  $\pi^0$  photoproduction on the deuteron were absent at the time of these calculations, the authors had no possibility to compare their predictions with experimental data for these channels. A comparison with experimental data was possible only for  $\pi^-$  production, where they found a slight overestimation of the data. They reported that the reason for that is an overestimation of the elementary reaction on the neutron. They mentioned also that the differences between their theoretical predictions and the experimental data show very clearly that the calculation of pion photoproduction on nuclei in the nucleon spectator model can only be considered as a first step towards a more realistic description of this process. As noted in [12, 24, 25, 52] the effect of  $NN$  rescattering is important in the incoherent pion photoproduction on the deuteron, especially for small pion angles.

Laget [12, 13, 20] and Blomqvist and Laget [11] have investigated pion photoproduction on the deuteron with the inclusion of pion rescattering and  $NN$  final state interaction within a diagrammatic ansatz. They used the elementary photoproduction operator of Blomqvist and Laget [11] as input in their calculations. At the time of these calculations, a comparison with experimental data was possible only for  $\pi^-$  production since data for  $\pi^+$  and  $\pi^0$  production in the  $\Delta(1232)$  resonance region were not available. The agreement of their predictions including final state interactions with the experimental data of the cross sections of the reaction  $\gamma d \rightarrow \pi^- pp$  is quite good. They found that the final state interaction effects are small for the charged pion photoproduction reactions in comparison with the case of the neutral

channel. As mentioned in [22], these predictions are significantly above the data for  $\pi^0$  photoproduction on the deuteron. A possible reason for this may be that they used the Blomqvist and Laget parametrization [11] of the elementary photoproduction amplitude. This amplitude is constructed using different  $\Delta$  parametrizations for neutral and charged pion photoproduction. It gives a satisfactory fit to the amplitude for charged pion photoproduction, but it is not able to describe the neutral pion photoproduction from the proton. An attempt to remedy this defect in [55] led to a  $\pi^0$  photoproduction amplitude which is not very suitable for the use in nuclear calculations.

Levchuk *et al.* [24] studied quasifree  $\pi^0$  photoproduction from the neutron via the  $d(\gamma, \pi^0)np$  reaction using the elementary photoproduction operator of Blomqvist and Laget [11]. The contributions from the pole diagrams as well as one-loop diagrams both with  $np$  and  $\pi N$  rescattering were taken into account. They wanted to explore the possibility of measuring the  $E_{1+}/M_{1+}$  ratio via photoproduction from the quasifree neutron. The isospin  $I = 3/2$  component of this ratio characterizes the relative strength of the recently much discussed (see e.g. [26, 27]) quadrupole  $E2$ -excitation of the  $\Delta$  resonance. The idea was that the  $n(\gamma, \pi^0)n$  reaction would be very useful for the isospin separation of the multipoles. In agreement with the results from the Laget model [12], Levchuk *et al.* find that the largest effects disturbing the extraction of the multipoles for quasifree neutrons arise from the  $np$  final state interaction. They predict that these effects lead to a strong reduction of the cross section at pion forward angles, but are much less important for backward angles. They found also that the correction due to  $np$  rescattering decreases with increasing pion angle and becomes to be less than 8% at  $\theta_\pi \geq 90^\circ$ . Furthermore, they pointed out that the contribution of the proton pole diagram and the one of  $\pi N$  rescattering are negligible. The experimental data from [22] for the  $d(\gamma, \pi^0)np$  reaction qualitatively support this prediction since the disagreement with the spectator approach is most severe at pion forward angles but less pronounced at backward angles. However, a comparison of the data to the Laget model including final state interactions shows some unexplained reduction of the cross section at backward angles.

Recently and during the calculations of this thesis work, Levchuk *et al.* [25] studied the inclusive reaction  $d(\gamma, \pi)NN$  in the  $\Delta$  resonance region. This calculation is based on the use of the diagrammatic approach. Pole diagrams and one-loop diagrams with  $NN$  and  $\pi N$  rescattering in the final state are considered. The authors in [25] pointed out that the main difference between their calculation and the one of Ref. [12] is that a more realistic version of the elementary pion photoproduction operator is used. It is taken in on-shell form and calculated using the SAID [28] and MAID [17] multipole analyses. This operator is constructed in the  $\gamma N$  c. m. frame. Therefore, it has to be transformed to an arbitrary frame of reference to be used as input

in calculations on light nuclei. This may be done by a Lorentz boost of all four momenta on which the elementary amplitude depends. Their predictions for total and differential cross sections including final state interactions show good agreement with the experimental data.

Now, we compare our results for the total cross section of the processes (3.1) with the theoretical predictions from [25] as shown in Fig. 4.5.

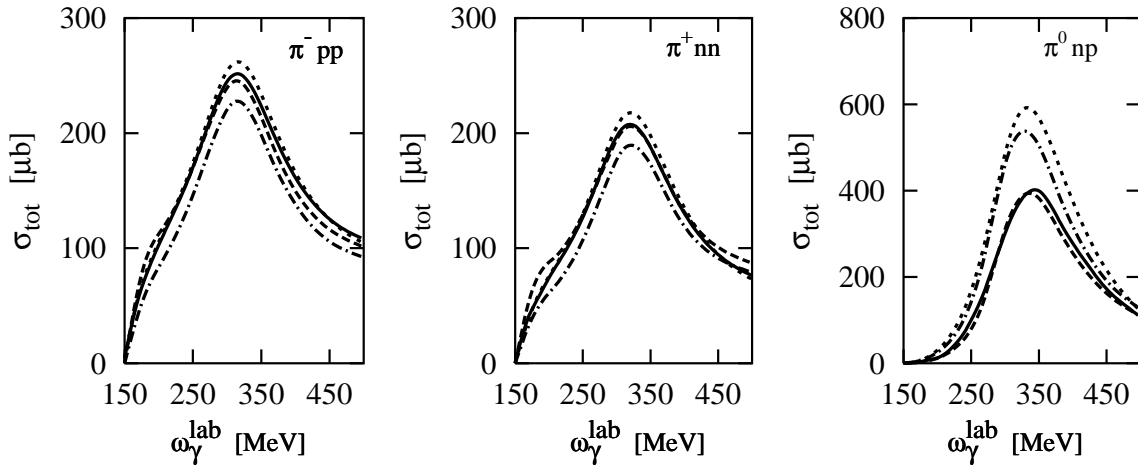


Figure 4.5: Total cross sections for pion photoproduction on the deuteron obtained within the impulse approximation (dotted curves) in comparison with the calculation when  $NN$  and  $\pi N$  final state interactions are taken into account (solid curves). The results of Levchuk *et al.* [25] as shown by the dash-dotted curves for the impulse approximation and by the dashed curves with  $NN$ - and  $\pi N$ -rescattering.

In the impulse approximation, Fig. 4.5 shows that our results for charged pion photoproduction (dotted curves) are higher than the results including rescattering effects (solid curves). This means that rescattering effects lead to a reduction of the total cross sections in our case. In the same figure, we see from the difference between the dash-dotted and dashed curves that the theoretical predictions from [25] display the opposite situation. In the next section we will give an explanation for this opposite situation in some detail. In the case of  $\pi^0$  photoproduction, rescattering effects lead in both cases to a strong reduction of the total cross section.

Including final state interactions we found small discrepancies between our calculations which are given by the solid curves in Fig. 4.5 and the predictions of Ref. [25] which are given by the dashed curves in the same figure. A reason for that may be the use of different pion photoproduction operators. As mentioned in section 3.3.2 that we used in our calculation the separable representation of the Paris  $NN$

potential [48, 49] to solve the Lippmann-Schwinger equation for the  $NN$  scattering. In [25], the authors used another type of  $NN$  potentials which is the Bonn OBE potential model (OBEPR) [45]. This choice of different  $NN$  potential models may also be a reason for the small discrepancies between both theoretical predictions. In the case of  $\pi N$  scattering, the separable energy-dependent  $\pi N$  potential built in [15] is used in both theoretical predictions.

## 4.2 Differential Cross Section

In this section we discuss our results for the differential cross sections and compare with experimental data and other theoretical predictions. We begin with presenting our results in Fig. 4.6.

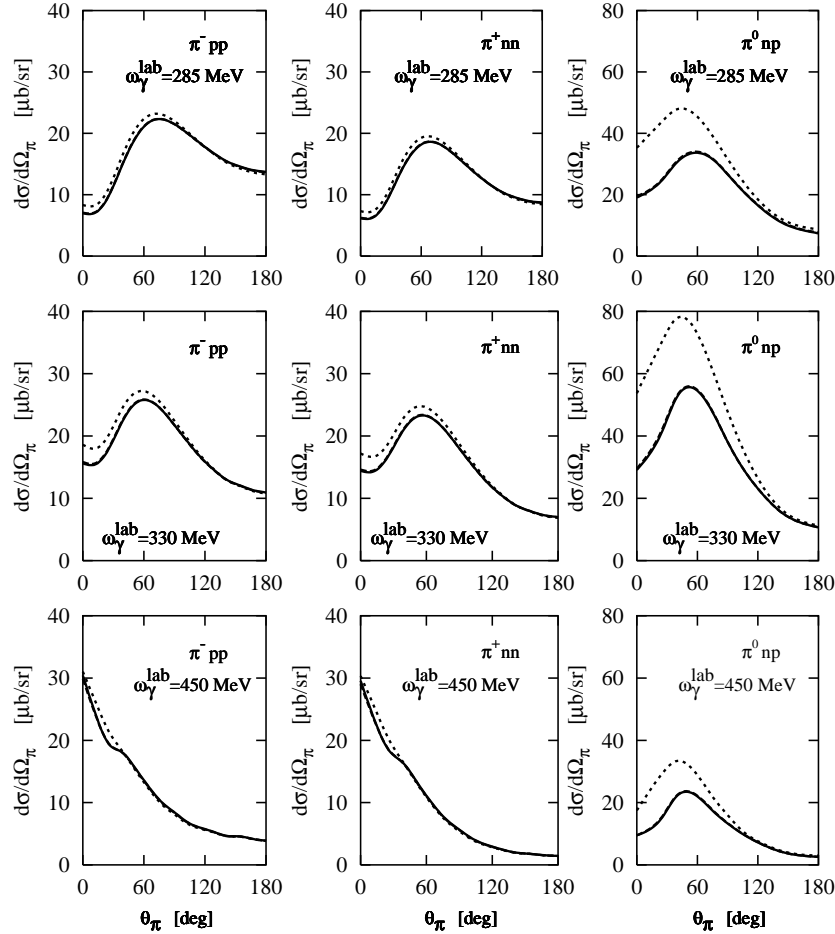


Figure 4.6: Differential cross sections for pion photoproduction on the deuteron within the impulse approximation (dotted curves) in comparison with the calculation including  $NN$  final state interaction (dashed curves) and the calculation with additional  $\pi N$  rescattering (solid curves). The left, middle and right panels represent the differential cross section for  $\gamma d \rightarrow \pi^- pp$ ,  $\pi^+ nn$  and  $\pi^0 np$ , respectively.

As in the case of total cross section in the previous section, Fig. 4.6 shows that the difference between the full and the spectator model calculations clearly demonstrate the importance of rescattering effects. One sees also that  $\pi N$  rescattering changes

the final results for the differential cross sections only by a few percent. Furthermore, for charged pion channels, one can see that the effect of final state interactions becomes small for low and high energies, but it becomes maximal at energies near to the  $\Delta(1232)$  resonance. In the case of  $\pi^0$  channel, it is obvious that the effect of rescattering is important for all energies, in particular for forward pion angles. In the case of both charged and neutral pions, we see that rescattering effect is quite small for backward pion angles. Looking at the right and middle panels in Fig. 4.6, one can see that at  $\theta_\pi = 0$ , the differential cross section increases with increasing photon energy. This increase comes mainly from the Born terms. We found that more than 70% from the values of the differential cross section at  $\theta_\pi = 0$  comes from the Born terms and less than 30% comes from the contribution of the  $\Delta(1232)$  resonance (see Fig. 4.7).

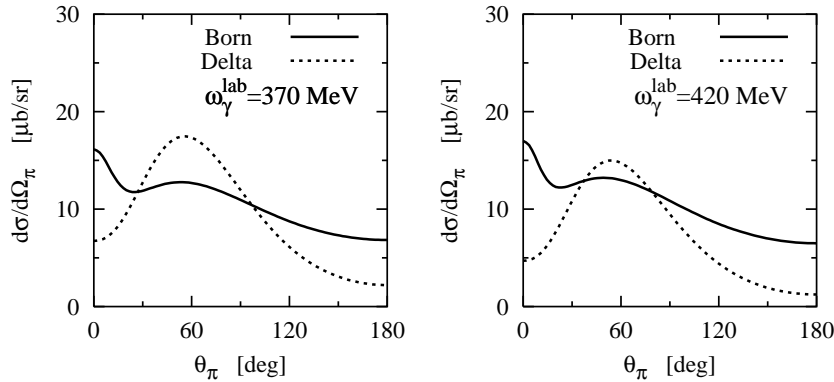


Figure 4.7: Differential cross section for  $\pi^-$  photoproduction on the deuteron in the impulse approximation at different photon energies. The solid curve shows the results using only the Born terms and the dotted one shows the contribution of the  $\Delta(1232)$  resonance.

In order to show in more detail the relative importance of final state interactions on the differential cross sections, we show in Figs. 4.8 and 4.9 the ratios  $d\sigma^{IA+NN+\pi N}/d\sigma^{IA}$  and  $d\sigma^{IA+NN+\pi N}/d\sigma^{IA+NN}$ , respectively, as a function of the pion angle in the laboratory frame.

Fig. 4.8 shows the relative effect of both  $NN$  and  $\pi N$  final state interactions by the ratio  $d\sigma^{IA+NN+\pi N}/d\sigma^{IA}$  as a function of the pion angle. As mentioned in the previous section, we see that the ratio has a similar shape for charged pion channels. It is also obvious that rescattering effects are important for forward pions and much less important for backward pions. In the case of  $\pi^0$  production, we see that the influence of final state interaction effects on the differential cross section is significant. Rescattering effects lead to a strong reduction of the differential cross sections, in

particular for small pion angles. The contribution decreases quickly when the pion angle increases and becomes very small for backward pion angles.

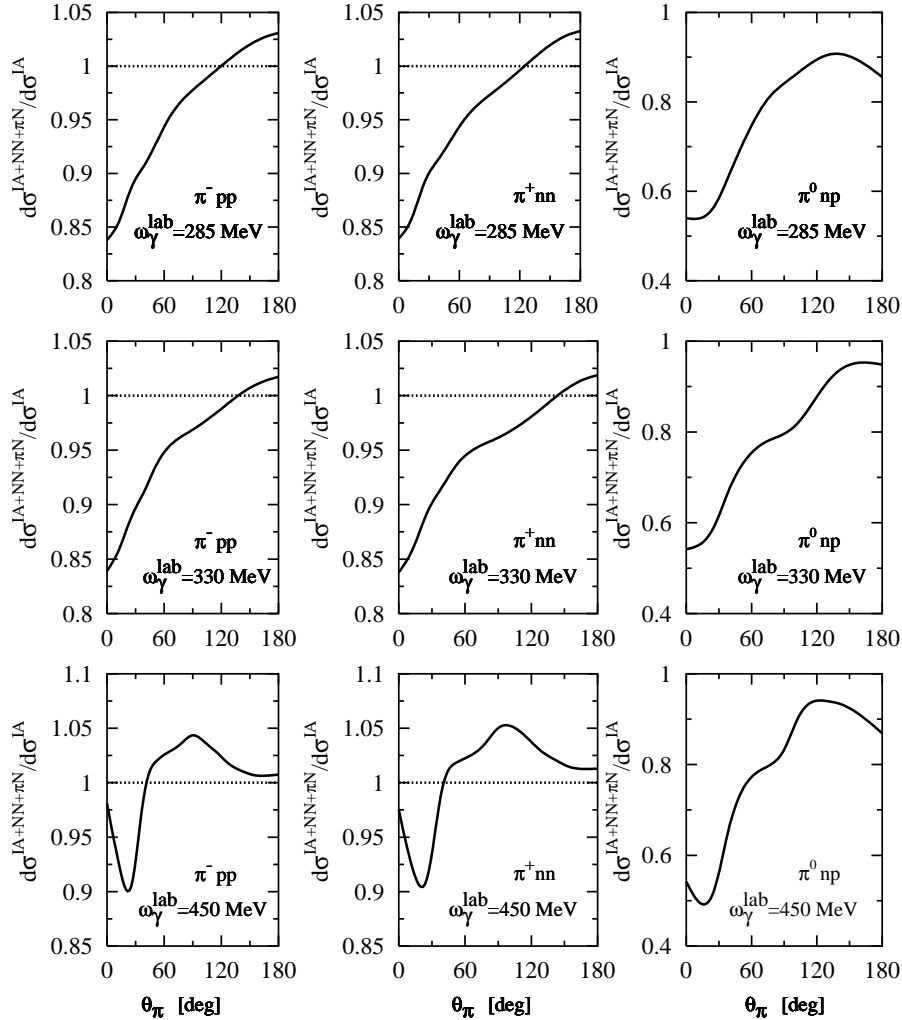


Figure 4.8: The ratio  $d\sigma^{IA+NN+\pi N}/d\sigma^{IA}$  as a function of the pion angle in the laboratory frame at different photon energies. The left, middle and right panels represent the ratio for the  $\gamma d \rightarrow \pi^- pp$ ,  $\pi^+ nn$  and  $\pi^0 np$ , respectively.

Now, we would like to clarify the relative effect of  $\pi N$  rescattering in Fig. 4.9 by the ratio  $d\sigma^{IA+NN+\pi N}/d\sigma^{IA+NN}$ . Here one can also see that we obtain a similar shape for the charged pion channels, but a totally different shape for the  $\pi^0$  channel is seen. The effect of  $\pi N$  rescattering is seen much less important than  $NN$  rescattering. This effect is less than 1% for charged pion channels and less than 5% for neutral

channel. In the energy range of the  $\Delta(1232)$  resonance, we find that this effect is maximal at pion forward angles.

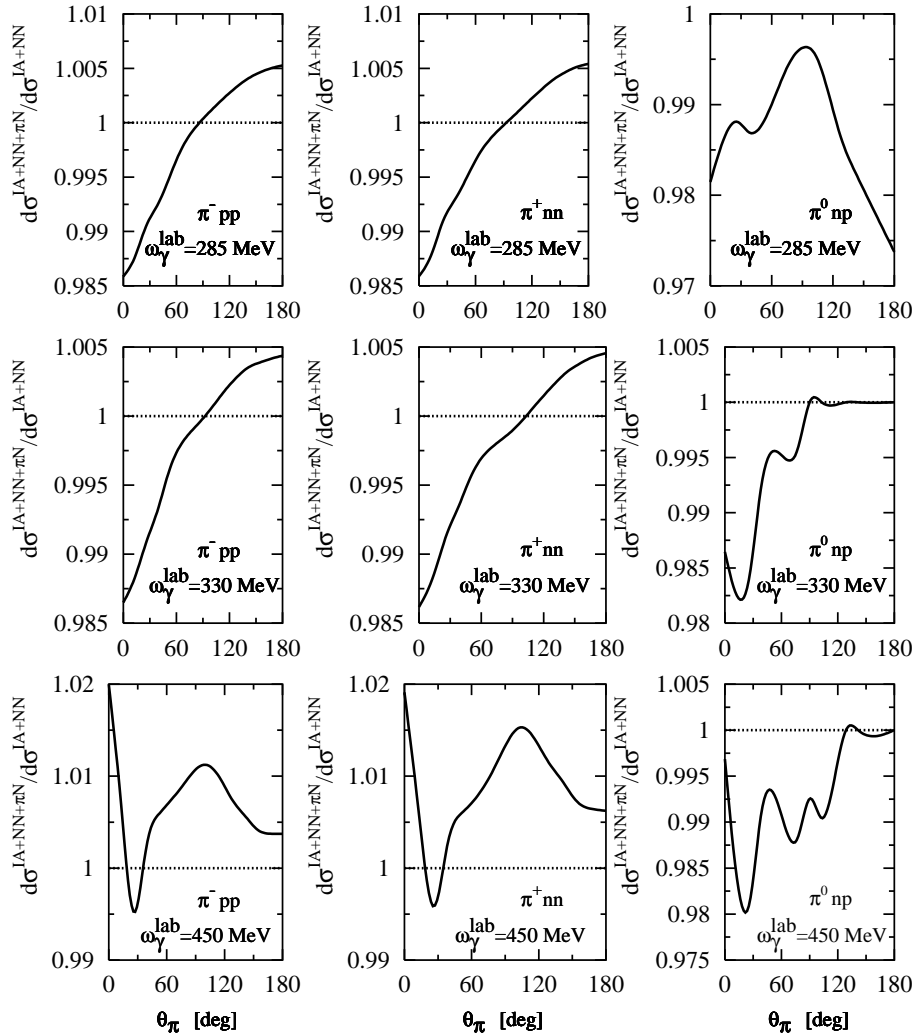


Figure 4.9: The ratio  $d\sigma^{IA+NN+\pi N}/d\sigma^{IA+NN}$  as a function of the pion angle at different photon energies. The left, middle and right panels represent the ratio for the  $\gamma d \rightarrow \pi^- pp$ ,  $\pi^+ nn$  and  $\pi^0 np$ , respectively.

#### 4.2.1 Comparison with Experimental Data

Here we compare our results for the differential cross sections with the experimental data from [21] for  $\pi^-$  production and from [22] for  $\pi^0$  production. This comparison is shown in Fig. 4.10. As mentioned in the previous section, there are no data

available for  $\pi^+$  production on the deuteron in the  $\Delta(1232)$  region so that we can not compare our predictions with experimental data for this channel. Therefore, we concentrate our discussion on  $\pi^-$  and  $\pi^0$  production. The effect of final state interactions in the case of charged pion channels is expected to be quite different in comparison with the neutral channel.

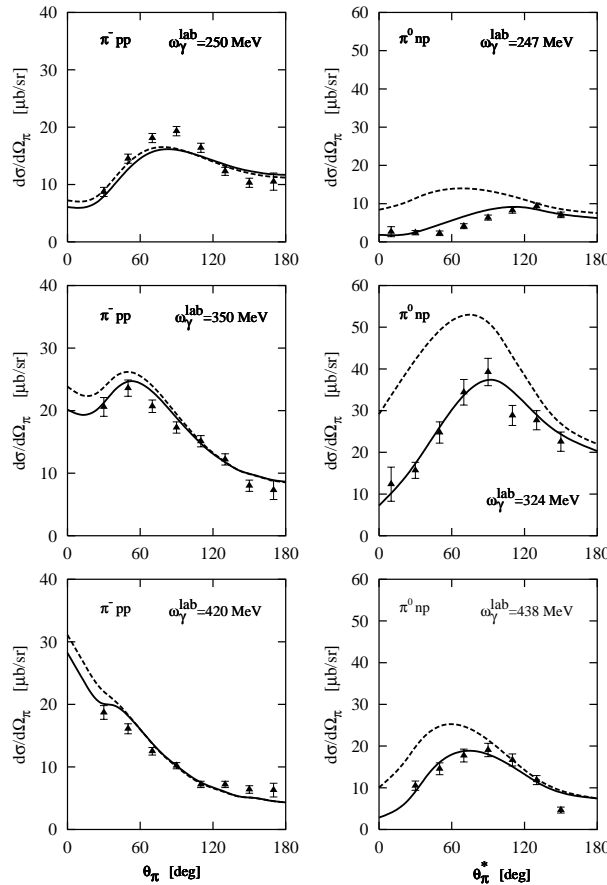


Figure 4.10: Differential cross sections for  $\pi^-$  (left panels) and  $\pi^0$  (right panels) photoproduction on the deuteron. Solid curves show our results include  $NN$  and  $\pi N$  rescattering and dashed curves show the results in the impulse approximation. The experimental data are from [21] for  $\pi^-$  production and from [22] for  $\pi^0$  production.

In Ref. [22] the differential cross sections for the reaction  $d(\gamma, \pi^0)np$  are given in the so-called  $\gamma N$  c. m. frame. Therefore, in order to compare our results for the differential cross sections of the reaction  $d(\gamma, \pi^0)np$  with the experimental data from [22] we need to transform the differential cross sections from the rest frame of the deuteron to the  $\gamma N$  c. m. frame. The Jacoby determinant which we need for this

purpose is given in appendix E. The pion angle in the  $\gamma N$  c. m. frame is denoted by  $\theta_\pi^*$ .

Fig. 4.10 shows that the spectator approach can not describe the experimental data for differential cross sections. One sees also that the effect of final state interactions leads to a strong reduction of the differential cross sections, especially for forward pion angles but it is much less important for backward angles. The inclusion of such effects improves the agreement between experimental data and our calculations. After including final state interactions we obtain in general a good agreement with the experimental data for differential cross sections. Small discrepancies are found only at backward pion angles. We see that the agreement with the experimental data of the reaction  $\gamma d \rightarrow \pi^- pp$  measured in a bubble chamber experiment [21], is quite good. The comparison with the TAPS data [22] for the reaction  $\gamma d \rightarrow \pi^0 np$  yields a quite reasonable description of the experimental differential cross section, in particular in the energy range of the  $\Delta(1232)$  resonance. The effect of final state interactions is found to be smaller for charged pion channels than in the case of neutral channel.

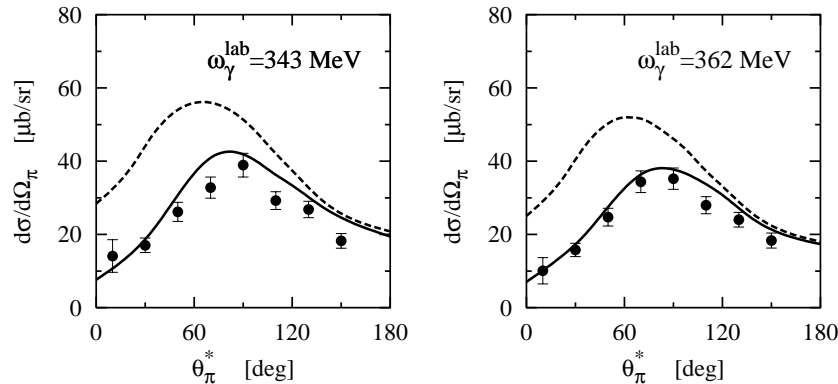


Figure 4.11: Differential cross section for  $\pi^0$  photoproduction on the deuteron as a function of pion angle in the  $\gamma N$  c. m. frame. Solid curves show our results include  $NN$  and  $\pi N$  rescattering and dashed curves show the results in the impulse approximation. The experimental data are from [22].

As shown in Fig. 4.4 that our predictions for the total cross section overestimate the experimental data for  $\pi^0$  photoproduction in the energy region between 340–360 MeV by about 6%. In order to see how good is the agreement with the experimental data for the differential cross section at this energy region, we predict in Fig. 4.11 a comparison between our results and the experimental data from TAPS [22]. It is noticeable that our predictions overestimate the experimental differential cross section at this energy, is particular at backward pion angles.

### 4.2.2 Comparison with other Theoretical Predictions

In this section we compare our results for the differential cross sections with the theoretical predictions of Levchuk *et al.* [25]. As in [25], the pion angle is given in the  $\gamma N$  c. m. frame in the case of  $\pi^0$  channel.

It is worthwhile first to point out that, in the impulse approximation Fig. 4.12 shows the following interesting features. Without final state interactions we found a big difference between our calculation and the prediction from [25] for charged pion channels at pion forward angles (see the difference between the dotted and the dash-dotted curves in Fig. 4.12). Therefore, we checked in this work where this big difference comes from.

First, we assume that the authors in Ref. [25] used a wrong  $NN$  antisymmetrization. That is why we examine using a wrong  $NN$  antisymmetrization procedure in our work. We found that if we use a wrong  $NN$  antisymmetrization for the  $s = 0$  channel, i.e.,

$$|\vec{p}_1 \vec{p}_2, sm_s, tm_t\rangle = \frac{1}{\sqrt{2}} (|\vec{p}_1\rangle^{(1)} |\vec{p}_2\rangle^{(2)} + (-)^{s+t} |\vec{p}_2\rangle^{(1)} |\vec{p}_1\rangle^{(2)}) |sm_s\rangle |tm_t\rangle, \quad (4.1)$$

and a correct one for  $s = 1$  channel, i.e.,

$$|\vec{p}_1 \vec{p}_2, sm_s, tm_t\rangle = \frac{1}{\sqrt{2}} (|\vec{p}_1\rangle^{(1)} |\vec{p}_2\rangle^{(2)} - (-)^{s+t} |\vec{p}_2\rangle^{(1)} |\vec{p}_1\rangle^{(2)}) |sm_s\rangle |tm_t\rangle, \quad (4.2)$$

we obtain results as shown in Fig. 4.13 (dotted curves) with the same energy shape as that of Levchuk *et al.* [25] (dashed curves). This probably means that, they did not use the correct  $NN$  antisymmetrization in their calculations.

Moreover, since we use a coupled basis state for the  $NN$  antisymmetrization in our calculations, we also checked the use of an uncoupled, i.e., helicity basis which was used in [25]. We found that both approaches give the same results. This confirms the  $NN$  antisymmetrization which we use and one can only suspect that the difference to the results of Ref. [25] may originate from an error in the antisymmetrization.

To investigate the influence of  $\pi N \rightarrow KY$  rescattering in kaon photoproduction on the deuteron, the authors in [56] used the same procedures as in Levchuk *et al.* [25] to calculate pion photoproduction on the deuteron in the impulse approximation. They obtained results as shown in Fig. 4.14 (dashed curves). It is obvious that their results using the elementary production operator from MAID [17] analysis are in good agreement with our results (solid curves) using the elementary production operator presented in chapter 2. It is also clear that in both cases the differential cross section has a high value at  $\theta_\pi = 0$  and not as in the case of Ref. [25]. This suggests that the model in Ref. [25] has a kind of error.

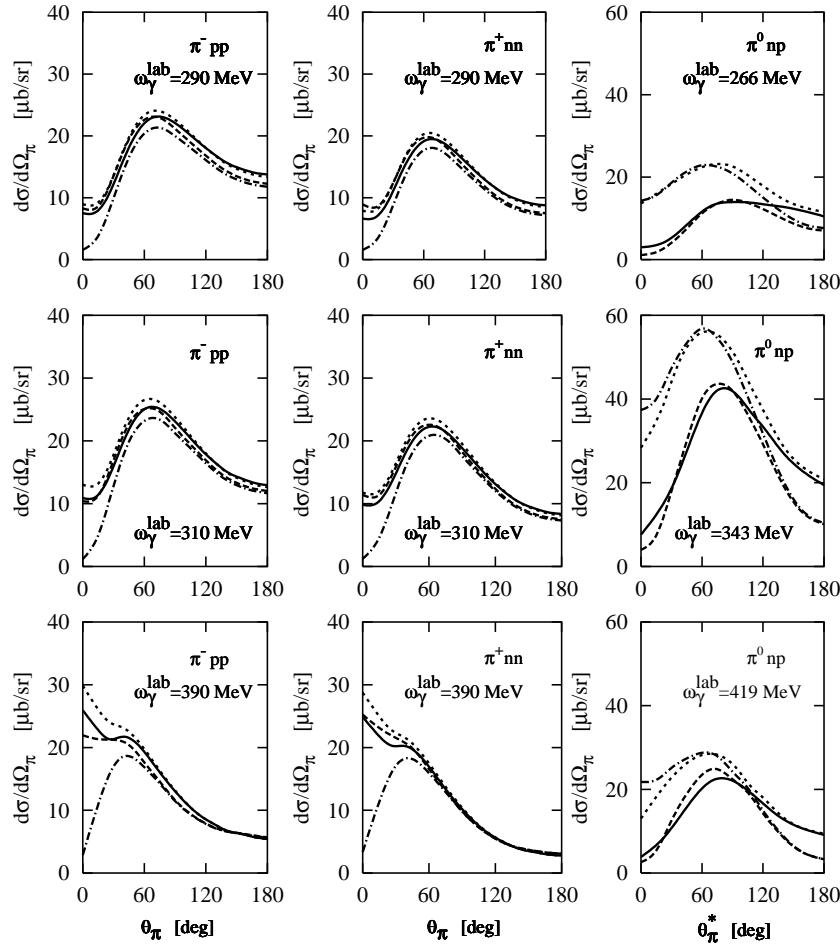


Figure 4.12: Differential cross sections for pion photoproduction on the deuteron in comparison with the results from [25] at different photon energies. Full curves show our results when rescattering effects are included and dotted curves show our results in the impulse approximation. Dashed and dash-dotted curves show the results from [25] with and without rescattering effects, respectively.

After including final state interaction effects, Fig. 4.12 shows that the agreement of our results (solid curves) and the theoretical predictions from [25] (dashed curves) is good. A small discrepancy between both calculations is observed. A reason for that may be due to the use of different pion photoproduction operators.

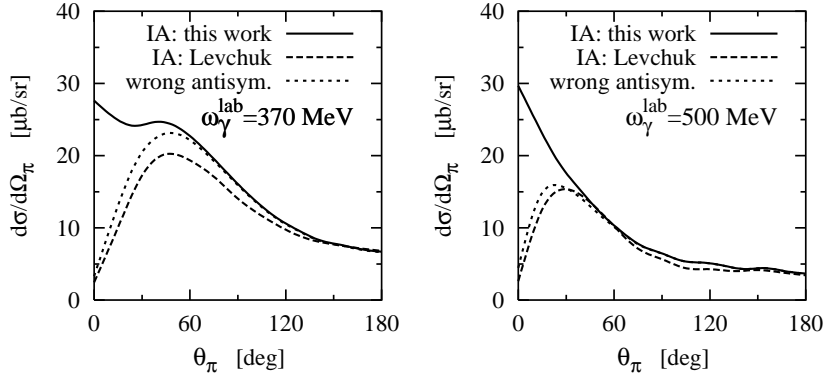


Figure 4.13: Differential cross section for  $\pi^-$  photoproduction on the deuteron in the impulse approximation. The full curve shows the results of our calculation and the dashed one shows the results from [25]. The dotted curve shows our results with a wrong  $NN$  antisymmetrization for  $s = 0$  channel, as given in Eq. (4.1).

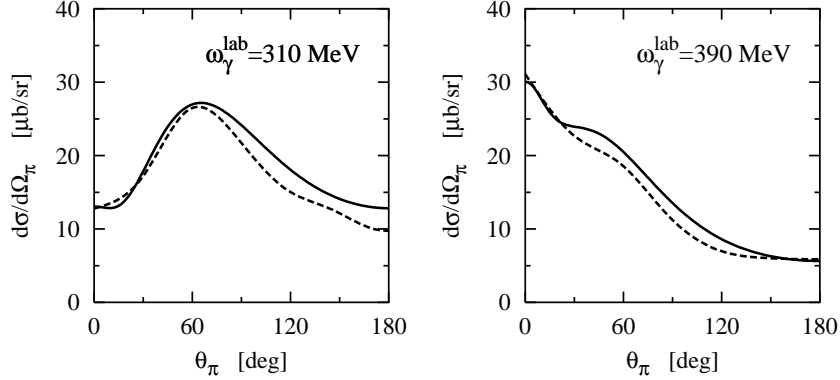


Figure 4.14: Differential cross section for  $\pi^-$  photoproduction on the deuteron in the impulse approximation. The full curve shows our results using the elementary production operator of chapter 2 and the dashed one shows the results from [56] using the elementary reaction amplitude from MAID [17] analysis.

### 4.3 Spin Asymmetry and Gerasimov-Drell-Hearn Sum Rule

Recently, several experiments to test the GDH sum rule both on the proton and on the neutron are now in preparation or planned at different laboratories around the world (MAMI, ELSA, LEGS, GRAAL and TJNAF). This makes the study of polarization observables nowadays of great interest in the field of intermediate energy nuclear physics. The spin asymmetry of the total photoabsorption cross section, entering into the Gerasimov-Drell-Hearn (GDH) sum rule [57, 58], is of particular interest. Therefore, we evaluate in this section the contribution of incoherent single pion photoproduction including  $NN$  and  $\pi N$  rescattering to the spin asymmetry and the corresponding GDH sum rule for the deuteron using the model developed in chapter 3.

The verification of the GDH sum rule is an important issue, which enables a check of some fundamental physical principles related to the spin of the nucleon. The GDH sum rule connects the anomalous magnetic moment of a particle with the energy weighted integral from threshold up to infinity over the spin asymmetry of the total photoabsorption cross section, i.e., the difference of the total photoabsorption cross sections for circularly polarized photons on a target with spin parallel and antiparallel to the spin of the photon (see Fig. 4.15). In detail it reads for a particle of mass  $M$ , charge  $eQ$ , anomalous magnetic moment  $\kappa$  and spin  $S$

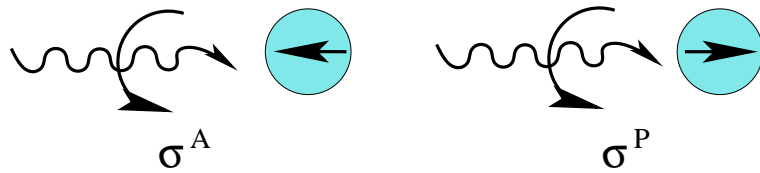


Figure 4.15: Illustration of the relative spin orientation of the incoming photon and the target nuclei in the GDH sum rule.

$$I^{GDH}(\infty) = 4\pi^2 \kappa^2 \frac{e^2}{M^2} S = \int_0^\infty \frac{dk}{k} (\sigma^P(k) - \sigma^A(k)), \quad (4.3)$$

where  $\sigma^{P/A}(k)$  denote the total absorption cross sections for circularly polarized photons on a target with spin parallel and antiparallel to the photon spin, respectively, and the anomalous magnetic moment is defined by the total magnetic moment operator of the particle

$$\vec{M} = (Q + \kappa) \frac{e}{M} \vec{S}. \quad (4.4)$$

This sum rule gives a very interesting relation between a magnetic ground-state property of a particle and an integral property of its whole excitation spectrum. In other words, this sum rule shows that the existence of a nonvanishing anomalous magnetic moment points directly to an internal dynamic structure of the particle. Furthermore, because the left-hand side of Eq. (4.3) is positive, it tells us that the integrated, energy-weighted total absorption cross section of a circularly polarized photon on a particle with its spin parallel to the photon spin is bigger than the one on a target with its spin antiparallel, if the particle possesses a nonvanishing anomalous magnetic moment.

Since proton and neutron have large anomalous magnetic moments ( $\kappa_p = 1.79$  and  $\kappa_n = -1.91$ ), one finds correspondingly large GDH sum rule predictions for them, i.e.,  $I_p^{GDH}(\infty) = 204.8 \mu b$  for the proton and  $I_n^{GDH}(\infty) = 233.2 \mu b$  for the neutron. Applying the GDH sum rule to the deuteron, one finds a very interesting feature. The deuteron has isospin zero, ruling out the contribution of the large nucleon isovector anomalous magnetic moments to its magnetic moment. Therefore, one expects a very small anomalous magnetic moment for the deuteron. In fact, the experimental value is  $\kappa_d = -0.143$  resulting in a GDH prediction of  $I_d^{GDH}(\infty) = 0.65 \mu b$ , which is more than two orders of magnitude smaller than the nucleon values.

In recent years, Arenhövel *et al.* [59] have evaluated explicitly the GDH sum rule for the deuteron by integrating the difference of the two total photoabsorption cross sections with photon and deuteron spins parallel and antiparallel up to a photon energy of 550 MeV. There, three contributions are included: (i) the photodisintegration channel  $\gamma d \rightarrow np$ , (ii) the coherent pion photoproduction  $\gamma d \rightarrow \pi^0 d$  and (iii) the incoherent single pion photoproduction  $\gamma d \rightarrow \pi NN$ . In their calculation of the  $\gamma d \rightarrow \pi NN$  contributions to the GDH integral, the authors restricted themselves to the impulse approximation using the spectator nucleon approach of Schmidt *et al.* [23]. For the total GDH value from explicit integration up to 550 MeV, they found a negative value  $I_d^{GDH}(550 \text{ MeV}) = -183 \mu b$ . However, some uncertainty lies in the contribution of the incoherent single pion production channel because final state interactions and other two-body operators are not included in the spectator nucleon model of Ref. [23]. As discussed previously, final state interactions in incoherent single pion photoproduction on the deuteron play an important role on the differential and total cross sections. Therefore, the influence of rescattering effects on the spin asymmetry and the corresponding GDH sum rule has to be investigated.

In this work, the influence of  $NN$  and  $\pi N$  rescattering effects in incoherent single pion photoproduction to the spin asymmetry and the GDH sum rule for the deuteron is investigated. We evaluated explicitly the GDH sum rule for the deuteron by

integrating the difference of the two total photoabsorption cross sections with photon and deuteron spins parallel and antiparallel up to a photon energy of 550 MeV. The upper integration limit of 550 MeV is chosen, because we consider only single pion production. The contributions which arise from coherent pion photoproduction and photodisintegration channels are given in Ref. [59] to which we refer for more details.

Our results for the spin asymmetry are collected in Fig. 4.16 for the individual contributions from the different charge states of the pion. Fig. 4.16 shows our results for the total photoabsorption cross sections for circularly polarized photons on a target with spin parallel  $\sigma^P$  (upper part) and antiparallel  $\sigma^A$  (middle part) to the photon spin. In the lower part of Fig. 4.16 the difference of the cross sections  $\sigma^P - \sigma^A$  for incoherent pion photoproduction on the deuteron including final state interactions is shown. For comparison, we also show our results on the free nucleon by the dash-dotted curves in Fig. 4.16 using the elementary production amplitude constructed in chapter 2. One notes qualitatively a similar behaviour for the spin asymmetry although the maxima and minima are smaller and also slightly shifted towards higher energies for the deuteron. The bottom panels in Fig. 4.16 show also that final state interactions lead to a strong reduction of the spin asymmetry in the energy region of the  $\Delta(1232)$  resonance. This reduction becomes more than 35% for  $\pi^0$  photoproduction and becomes more than 15% for charged pion channels. It is also obvious that  $\sigma^P$  is much greater than  $\sigma^A$ , in particular in the case of  $\pi^0$  production.

The results for the GDH sum rule are depicted in Fig. 4.17 and Table 4.1 for the individual contributions from the different charge states of the pion. Their total sum to the GDH sum rule is shown in Fig. 4.18. Our results on the free nucleon are also shown for comparison (see the dash-dotted curves in Figs. 4.17 and 4.18). It is obvious that a large positive contribution to the GDH sum rule comes from the  $\pi^0$  production channel whereas the charged pions give a negative but - in absolute size - smaller contribution to the GDH value. Up to an energy of 550 MeV one finds for the total contribution of the incoherent pion production channels a value  $I_{\gamma d \rightarrow NN\pi}^{GDH}(550 \text{ MeV}) = 87 \mu\text{b}$ .

A very interesting and important result is the large negative contribution from the  $\pi^\pm$  channels and the large positive contribution comes from the  $\pi^0$  channel to the GDH value. Hopefully, this low energy feature of the GDH sum rule could be checked experimentally in the near future. At the same time, precise data on  $\sigma^P - \sigma^A$  from a direct measurement is urgently needed.

Last but not least, we would like to conclude that the results presented here for the spin asymmetry and the GDH sum rule can be used as a basis for the simulation

Table 4.1: Contributions of incoherent single pion photoproduction to the GDH integral for the deuteron integrated up to 550 MeV in  $\mu\text{b}$ .

reaction	$I_{IA}^{GDH}$	$I_{IA+NN}^{GDH}$	$I_{IA+NN+\pi N}^{GDH}$
$\gamma d \rightarrow pp\pi^-$	-73	-87	-88
$\gamma d \rightarrow nn\pi^+$	-27	-39	-41
$\gamma d \rightarrow np\pi^0$	287	220	216
$\gamma d \rightarrow \pi NN$	187	94	87

of the behaviour of polarization observables and for an optimal planning of new polarization experiments of the reaction  $\gamma d \rightarrow \pi NN$ .

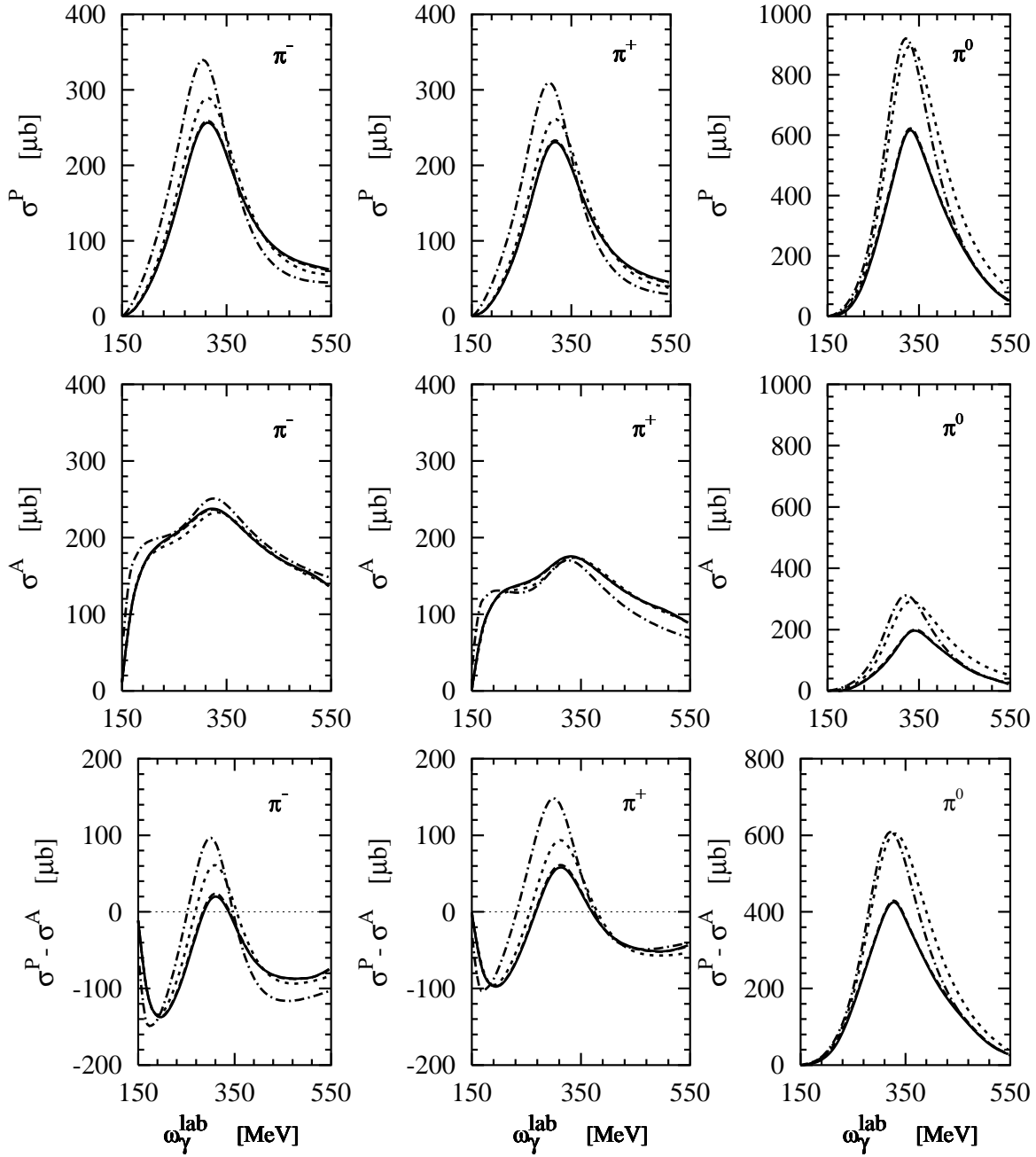


Figure 4.16: Total absorption cross sections for circularly polarized photons on a target with spin parallel  $\sigma^P$  (upper part) and antiparallel  $\sigma^A$  (middle part) to the photon spin. Lower part shows the difference of the cross sections. Dotted curves show the results in the impulse approximation, dashed curves show the results including  $NN$  rescattering and solid curves show the results with additional  $\pi N$  rescattering. The dash-dotted curves show the results for  $\pi^-$  on the neutron (left panels),  $\pi^+$  on the proton (middle panels) and  $\pi^0$  on both the proton and the neutron (right panels).

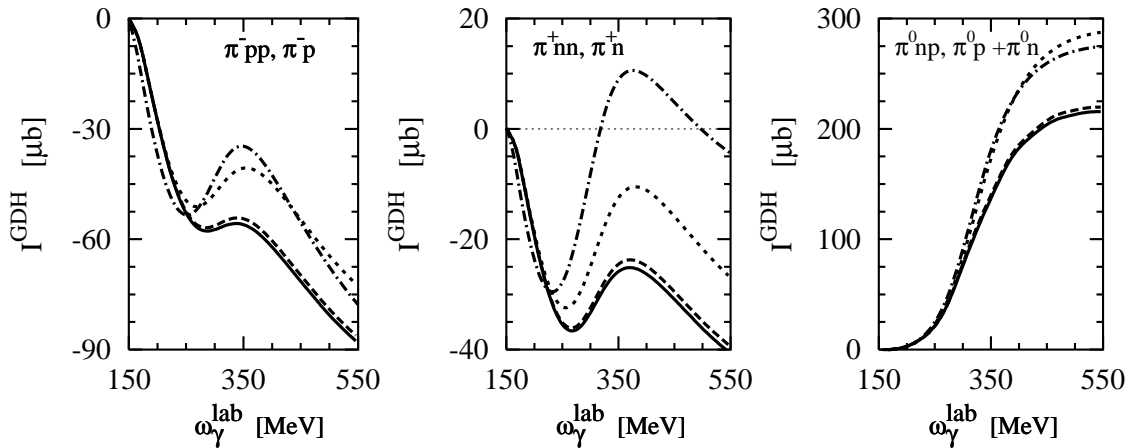


Figure 4.17: The Gerasimov-Drell-Hearn integral (see Eq. (4.3)) as a function of the upper limit of integration for the different channels of incoherent single pion photoproduction on the deuteron and the nucleon. Notation of the curves as in Fig. 4.16.

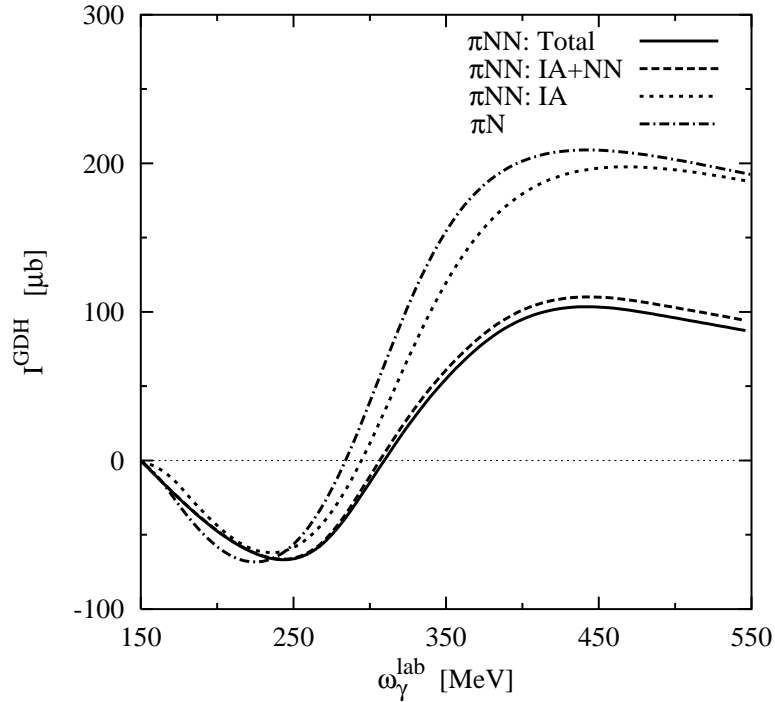


Figure 4.18: Summation of the contributions of the three channels of incoherent single pion photoproduction to the GDH sum rule for the deuteron and the nucleon as function of the upper integration energy. See caption of Fig. 4.16 for meaning of the curves.

# Chapter 5

## Summary and Outlook

### 5.1 Summary

The subject of this work was the investigation of the influence of final state interaction effects in incoherent single pion photoproduction on the deuteron in the  $\Delta(1232)$  resonance region. The transition matrix elements are calculated in the frame of time-ordered perturbation theory, using an elementary production operator, which yields a good agreement with experimental data, and including final state interaction effects.

For the elementary  $\gamma N \rightarrow \pi N$  photoproduction amplitude we used the effective Lagrangian model of Schmidt *et al.* [23]. This amplitude contains besides the standard pseudovector Born terms the resonance contribution from the  $\Delta(1232)$  excitation. The Born terms of the elementary production amplitude are determined in pseudovector  $\pi N$  coupling and supplied with a form factor. The  $\Delta(1232)$  resonance is considered in both the  $s$ - and  $u$ -channel. The parameters of the  $\Delta$  resonance and the cut-off of the form factors are fixed on the leading photoproduction multipole amplitudes. We found a good agreement between our results for total and differential cross sections and experimental data.

This elementary production operator is then used to study pion photoproduction on the deuteron. In addition to the impulse approximation, where all kind of final state interactions and other two-body operators are neglected, we have included as presumably dominant final state interaction effects two-body interactions in the  $NN$ - and  $\pi N$ -subsystems. As models for the interaction of the  $NN$ - and  $\pi N$ -subsystems we used separable interactions which are fitted to the phase shift data for  $NN$  and  $\pi N$  scattering. For  $NN$  scattering we have included all partial waves with total angular momentum  $J \leq 3$  by numerical solution of the Lippmann-Schwinger equation [47] with the separable representation of the Paris  $NN$  potential [48, 49].

In the case of  $\pi N$  rescattering we have considered the  $S$ -,  $P$ - and  $D$ -waves by solving the Lippmann-Schwinger equation for a separable energy-dependent  $\pi N$  potential from [15].

For the total cross section we found that the influence of  $NN$  and  $\pi N$  rescattering effects on the total cross section is significant. These effects reduce the total cross sections for the charged pion photoproduction reactions in the  $\Delta(1232)$  resonance region by about 5%. In the case of  $\pi^0$  photoproduction reaction, rescattering is much more important, reducing the total cross section by about 35% on the maximum. Furthermore, it was found that  $\pi N$  rescattering is much less important compared to  $NN$  rescattering. In comparison with experimental data, we found that the inclusion of  $NN$  and  $\pi N$  rescattering effects leads to an improved agreement between experimental data and theoretical predictions. Only in the maximum of  $\pi^0$  production our model overestimates the measured total cross section by about 6%. In comparison with the theoretical predictions from [25], we found that for charged pion production the inclusion of rescattering effects leads to a reduction of the total cross sections in contrast to the theoretical predictions from [25]. This different behaviour may have its origin in the difference already for the impulse approximation for which [25] predicts a 14% lower total cross section. In the case of  $\pi^0$  channel, also in [25] a strong reduction by rescattering has been found. After including final state interactions we found, however, only small differences between our calculations and the predictions from [25].

In the case of the differential cross section one may draw the following conclusions. The inclusion of  $NN$  and  $\pi N$  final state interactions reduces the differential cross sections for the charged pion channels mainly at pion forward angles by about 15%. The reduction is much stronger for the  $\pi^0$  channel by about 40% at pion forward angles. At pion backward angles the influence is much less important. As already noted for the total cross section, the  $\pi N$  rescattering changes the final results only by a few percent. In comparison with experiment, after including final state interactions we have obtained a satisfactory agreement with the experimental data. Small discrepancies were found only at backward pion angles. In comparison with the theoretical predictions from [25], without final state interactions we found a big difference between both calculations for the differential cross sections for charged pion channels at pion forward angles. After including rescattering effects we have obtained a good agreement with the theoretical predictions from [25].

Finally, we have evaluated in this work the contribution of incoherent single pion photoproduction to the spin asymmetry of the total photoabsorption cross section. We found that the inclusion of final state interactions leads to a strong reduction of the spin asymmetry in the energy region of the  $\Delta(1232)$  resonance. This reduction

amounts to about 35% for  $\pi^0$  photoproduction and about 15% for charged pion channels. The corresponding GDH integral was also evaluated up to 550 MeV. We found that a large positive contribution to the GDH sum rule comes from the  $\pi^0$  production channel whereas the charged pions give a negative but - in absolute size - smaller contribution to the GDH value. Up to an energy of 550 MeV we have obtained for the total contribution of the incoherent pion production channels a value  $I_{\gamma d \rightarrow NN\pi}^{GDH}(550 \text{ MeV}) = 87 \mu\text{b}$ .

## 5.2 Future Extensions

The studies we have discussed here will serve as the basis for further investigations including the dynamics of the  $\pi NN$  system in a more complete way. Undoubtedly, there is still a lot of work to be done both experimentally and theoretically. Indeed, many challenging and interesting lessons have yet to be learned before a deep understanding of the incoherent pion photoproduction process on the deuteron will emerge. In first instance, this work could be continued by the further refinement of the elementary production operator. Modifying the elementary pion photoproduction operator on the free nucleon above the two pion threshold with, for example, the inclusion of the  $\omega$  and  $\rho$  meson exchange in the  $t$ -channel and contributions at higher energies may improve our results for the spin asymmetry and the corresponding GDH sum rule for the deuteron. Our goal is to have an operator that can describe the elementary process on the free nucleon reasonably well over a larger energy region and that is suitable for applications to nuclear systems.

In view of the importance of the first order rescattering it is natural to ask about the role of higher order rescattering terms. Answering this question points to the necessity of a three-body approach, where the final state interaction is included to all orders. This may result in a better agreement between experimental data and theoretical predictions for  $\pi^0$  photoproduction. Furthermore, the inclusion of such rescattering terms may be important in studying polarization observables. Studying these observables will give us much more detailed information and thus will provide much more stringent tests for theoretical models. In fact we plan to embark on such a study in the near future.

In the long run, one would need also to extend the formalism to the threshold region for which the elementary production operator has to be improved. This process is of great interest since experimental data for the reaction  $d(\gamma, \pi^0 n)p$  have been measured recently in Mainz (MAMI/TAPS) and Saskatoon (SAL) [60]. Moreover, the formalism should be extended to investigate coherent and incoherent electroproduction of pions on the deuteron including final state interaction effects in both the

threshold and the  $\Delta(1232)$  resonance regions in order to analyze recent results from MAMI [61].

## Appendices

---



# Appendix A

## General Notations and Conventions

### A.1 Dirac Algebra

Throughout this work we adopt the natural system of units where  $\hbar = c = 1$ ; conversion factor:  $\hbar c = 197.32696$  MeV.fm<sup>1</sup>. We also follow the convention of Bjorken and Drell [43], where the contravariant space-time four-vector is defined as

$$x^\mu \equiv (x^0, x^1, x^2, x^3) \equiv (t, \vec{x}) \equiv (t, x, y, z), \quad (\text{A.1})$$

and the covariant space-time four-vector is given by

$$\begin{aligned} x_\mu &\equiv (x_0, x_1, x_2, x_3) \equiv (t, -\vec{x}) \equiv (t, -x, -y, -z) \\ &= g_{\mu\nu} x^\nu, \end{aligned} \quad (\text{A.2})$$

with the transformation matrix

$$g_{\mu\nu} = \begin{pmatrix} 1 & 0 & 0 & 0 \\ 0 & -1 & 0 & 0 \\ 0 & 0 & -1 & 0 \\ 0 & 0 & 0 & -1 \end{pmatrix}. \quad (\text{A.3})$$

Likewise the contravariant four-momentum is

$$p^\mu \equiv (p^0, p^1, p^2, p^3) \equiv (E_p, \vec{p}), \quad (\text{A.4})$$

and the scalar product between two four-momenta is given by

$$p \cdot q \equiv p^\mu q_\mu \equiv E_p E_q - \vec{p} \cdot \vec{q}. \quad (\text{A.5})$$

---

<sup>1</sup>In the calculations of this work we use units of MeV for energies, masses and momenta.

The Dirac matrices are

$$\gamma^\mu \equiv (\gamma^0, \vec{\gamma}), \quad (\text{A.6})$$

with the matrix representation

$$\gamma^0 = \begin{pmatrix} \mathbb{1} & 0 \\ 0 & -\mathbb{1} \end{pmatrix}, \quad \vec{\gamma} = \begin{pmatrix} 0 & \vec{\sigma} \\ -\vec{\sigma} & 0 \end{pmatrix}, \quad (\text{A.7})$$

where  $\gamma_0$  is hermitian and  $\gamma_1, \gamma_2$  and  $\gamma_3$  are anti-hermitian. The Pauli matrices  $\vec{\sigma} = (\sigma^1, \sigma^2, \sigma^3)$  are denoted by

$$\sigma^1 = \begin{pmatrix} 0 & 1 \\ 1 & 0 \end{pmatrix}, \quad \sigma^2 = \begin{pmatrix} 0 & -i \\ i & 0 \end{pmatrix}, \quad \sigma^3 = \begin{pmatrix} 1 & 0 \\ 0 & -1 \end{pmatrix}. \quad (\text{A.8})$$

These matrices satisfy the anticommutation relations

$$\{\sigma^i, \sigma^j\} \equiv \sigma^i \sigma^j + \sigma^j \sigma^i = 2\delta_{ij}, \quad (\text{A.9})$$

as well as the commutation relations

$$[\sigma^i, \sigma^j] \equiv \sigma^i \sigma^j - \sigma^j \sigma^i = 2i\epsilon_{ijk}\sigma^k, \quad (\text{A.10})$$

where  $\epsilon_{ijk}$  represents the antisymmetric Levi-Civita tensor in  $R^3$ .

The Dirac matrices  $\gamma$  satisfy the anticommutation relations

$$\{\gamma^\mu, \gamma^\nu\} \equiv \gamma^\mu \gamma^\nu + \gamma^\nu \gamma^\mu = 2g^{\mu\nu}. \quad (\text{A.11})$$

Important combinations of  $\gamma$  matrices are the antisymmetric combination

$$\sigma^{\mu\nu} = \frac{i}{2} [\gamma^\mu, \gamma^\nu] \quad (\text{A.12})$$

with components

$$\sigma^{ij} = \epsilon_{ijk} \begin{pmatrix} \sigma^k & 0 \\ 0 & \sigma^k \end{pmatrix} \quad \text{and} \quad \sigma^{0i} = i \begin{pmatrix} 0 & \sigma^i \\ \sigma^i & 0 \end{pmatrix}. \quad (\text{A.13})$$

Other useful combinations are

$$\gamma^5 \equiv i\gamma^0\gamma^1\gamma^2\gamma^3 = \gamma_5 = \frac{1}{24}i\epsilon_{\mu\nu\rho\sigma}\gamma^\mu\gamma^\nu\gamma^\rho\gamma^\sigma = \begin{pmatrix} 0 & \mathbb{1} \\ \mathbb{1} & 0 \end{pmatrix}, \quad (\text{A.14})$$

$$i\epsilon_{\mu\nu\rho\sigma}\gamma^\mu = \gamma_5(-\gamma_\nu\gamma_\rho\gamma_\sigma + g_{\nu\rho}\gamma_\sigma + g_{\rho\sigma}\gamma_\nu - g_{\nu\sigma}\gamma_\rho), \quad (\text{A.15})$$

$$\gamma_5\sigma^{\mu\nu} = \frac{1}{2}i\epsilon^{\mu\nu\rho\sigma}\sigma_{\rho\sigma}, \quad (\text{A.16})$$

$$\gamma_5\gamma_\sigma = -\gamma_\sigma\gamma_5 = \frac{1}{6}i\epsilon_{\mu\nu\rho\sigma}\gamma^\mu\gamma^\nu\gamma^\rho. \quad (\text{A.17})$$

The antisymmetric Levi-Civita tensor is defined by

$$\epsilon_{\mu\nu\rho\sigma} = \begin{cases} +1 & \text{for an even permutation (e.g. 0, 1, 2, 3)} \\ -1 & \text{for an odd permutation} \\ 0 & \text{if two or more indices are the same} \end{cases} . \quad (\text{A.18})$$

The scalar product between  $\gamma$  matrices and a four-momentum is written as

$$\gamma^\mu p_\mu = \gamma^0 p^0 - \vec{\gamma} \cdot \vec{p} \equiv \not{p} . \quad (\text{A.19})$$

The positive-energy four-component free Dirac spinor has the form

$$u(p, s) = \left( \frac{E_p + m}{2m} \right)^{\frac{1}{2}} \begin{pmatrix} \chi_s \\ \vec{\sigma} \cdot \vec{p} \\ \hline E_p + m \chi_s \end{pmatrix} , \quad (\text{A.20})$$

and the negative-energy four-component Dirac spinor (antiparticle spinor) has the form

$$v(p, s) = \left( \frac{E_p + m}{2m} \right)^{\frac{1}{2}} \begin{pmatrix} -\vec{\sigma} \cdot \vec{p} \\ \hline E_p + m \chi_s \\ \chi_s \end{pmatrix} , \quad (\text{A.21})$$

where  $E_p = \sqrt{m^2 + p^2}$ . They are normalized as

$$\bar{u}(p, s)u(p, s) = 1 , \quad (\text{A.22})$$

$$\bar{v}(p, s)v(p, s) = -1 , \quad (\text{A.23})$$

where  $\chi_s$  are the two-component Pauli spinors with  $\chi_{+\frac{1}{2}} = \begin{pmatrix} 1 \\ 0 \end{pmatrix}$  and  $\chi_{-\frac{1}{2}} = \begin{pmatrix} 0 \\ 1 \end{pmatrix}$ , and the Dirac adjoint spinors are defined as

$$\bar{u}(p, s) = u^\dagger \gamma^0 , \quad (\text{A.24})$$

$$\bar{v}(p, s) = v^\dagger \gamma^0 . \quad (\text{A.25})$$

Using Dirac spinors  $u$  and  $v$ , the Dirac equations may be written as

$$(\not{p} - m)u(p, s) = 0 , \quad (\text{A.26})$$

$$(\not{p} + m)v(p, s) = 0 , \quad (\text{A.27})$$

which in terms of the adjoint spinors become

$$\bar{u}(p, s)(\not{p} - m) = 0 , \quad (\text{A.28})$$

$$\bar{v}(p, s)(\not{p} + m) = 0 . \quad (\text{A.29})$$

## A.2 Normalization of States

The general form of the state which describes the single particle  $X \in \{N, \Delta, \pi, \gamma\}$  with momentum  $\vec{p}$  and quantum numbers<sup>2</sup>  $a$  is  $|X; \vec{p}a\rangle$ . It is also possible to use the form  $|\vec{p}; a\rangle$  when we know the type of the used particle. In case of more than one particle, the state has the form  $|X_1, X_2; \vec{p}_1 a_1, \vec{p}_2 a_2\rangle$ .

For all the involved particles a covariantly normalized state is used in this work. The fermions are normalized as

$$\langle N; \vec{p}_2 | N; \vec{p}_1 \rangle = (2\pi)^3 \delta^3(\vec{p}_2 - \vec{p}_1) \frac{E_p}{M_N}. \quad (\text{A.30})$$

The normalized states for bosons are given by

$$\langle \pi; \vec{q}_2 | \pi; \vec{q}_1 \rangle = (2\pi)^3 \delta^3(\vec{q}_2 - \vec{q}_1) 2\omega_q, \quad \omega_q = \sqrt{m_\pi^2 + \vec{q}^2} \quad (\text{A.31})$$

$$\langle d; \vec{p}_2 | d; \vec{p}_1 \rangle = (2\pi)^3 \delta^3(\vec{p}_2 - \vec{p}_1) 2E_d, \quad E_d = \sqrt{M_d^2 + \vec{p}^2} \quad (\text{A.32})$$

$$\langle \gamma; \vec{k}_2 | \gamma; \vec{k}_1 \rangle = (2\pi)^3 \delta^3(\vec{k}_2 - \vec{k}_1) 2\omega_\gamma, \quad \omega_\gamma = |\vec{k}| = k. \quad (\text{A.33})$$

The completeness relation for fermions then reads

$$\mathbb{1} = \int \frac{d^3p}{(2\pi)^3} \frac{M_N}{E_p} |\vec{p}\rangle \langle \vec{p}| \quad (\text{A.34})$$

and for bosons reads

$$\mathbb{1} = \int \frac{d^3q}{(2\pi)^3} \frac{1}{2\omega} |\vec{q}\rangle \langle \vec{q}|. \quad (\text{A.35})$$

## A.3 Spherical Basis

For the construction of the physical pions from the pion field  $\vec{\Phi}$  and for the evaluation of the spin and isospin operators,  $\vec{\sigma}$  and  $\vec{\tau}$ , their representation in spherical basis is used. The basis vectors are given by

$$\begin{aligned} \hat{e}_\mu &= -\frac{\mu}{\sqrt{2}} (\hat{e}_x + i\mu \hat{e}_y), & \text{for } \mu = \pm 1 \\ \hat{e}_0 &= \hat{e}_z. \end{aligned} \quad (\text{A.36})$$

The spherical components of a given vector are determined by writing the scalar product

$$a_\mu = \vec{a} \cdot \hat{e}_\mu. \quad (\text{A.37})$$

<sup>2</sup>These quantum numbers indicate about spin, isospin, spin projection etc.

If the spherical components of two vectors are given, then the scalar product of these two vectors in spherical basis is given by

$$\vec{a} \cdot \vec{b} = \sum_{\mu} a_{\mu} (-)^{\mu} b_{-\mu} \quad (\text{A.38})$$

and the vector product is given by

$$(\vec{a} \times \vec{b})_{\mu} = -i\sqrt{2} \sum_{\mu_a \mu_b} (1\mu_a 1\mu_b | 1\mu) a_{\mu_a} b_{\mu_b} . \quad (\text{A.39})$$



## Appendix B

# Useful Formulas for the Elementary Process

In this appendix we give the useful formulas for the pion photoproduction reaction on the free nucleon. This process is schematically sketched in Fig. 2.1. Many of the formulas given here have been published elsewhere; our aim has been to collect all of the kinematic equations needed in this work.

### B.1 Kinematics and Relevant Formulas

The kinematics of pion photoproduction reaction on the free nucleon,  $\gamma N \rightarrow \pi N$ , are characterized by the four-momentum vectors  $k = (\omega_\gamma, \vec{k})$  for the incident photon,  $p_1 = (E_1, \vec{p}_1)$  for the initial nucleon,  $p_2 = (E_2, \vec{p}_2)$  for the final nucleon and  $q = (\omega_q, \vec{q})$  for the produced pion. Then the kinematical equations (energy-momentum conservations) are given by

$$\begin{aligned} \vec{p}_1 + \vec{k} &= \vec{p}_2 + \vec{q}, \\ p_1^2 &= p_2^2 = M_N^2, \\ q^2 &= m_\pi^2, \end{aligned} \tag{B.1}$$

where  $M_N$  is the nucleon mass and  $m_\pi$  is the pion mass.

The usual Mandelstam kinematical variables are given by

$$\begin{aligned} s &= (p_2 + q)^2 = (p_1 + k)^2, \\ t &= (k - q)^2 = (p_2 - p_1)^2, \\ u &= (p_2 - k)^2 = (p_1 - q)^2, \end{aligned} \tag{B.2}$$

and they satisfy

$$s + t + u = 2M_N^2 + m_\pi^2. \quad (\text{B.3})$$

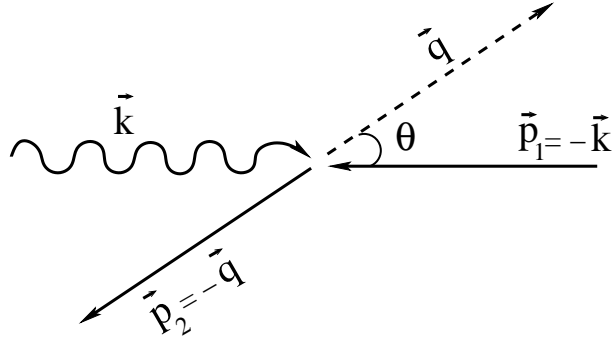


Figure B.1: Kinematics in the  $\pi N$  c.m. frame for the reaction  $\gamma N \rightarrow \pi N$ .

In the  $\pi N$  c.m. frame which given graphically in Fig. B.1 let  $W$  be the total energy of the system. Then

$$\begin{aligned} s &= W^2, \\ t &= 2\vec{k} \cdot \vec{q} - 2\omega_\gamma \omega_{\vec{q}} + m_\pi^2, \\ u &= -2\vec{k} \cdot \vec{q} - 2\omega_\gamma E_2 + M_N^2, \end{aligned} \quad (\text{B.4})$$

where  $\vec{p}_1 = -\vec{k}$  and  $\vec{p}_2 = -\vec{q}$  in the c.m. frame. The scattering angle  $\theta$  is given by

$$\cos \theta = \frac{(\vec{k} \cdot \vec{q})}{(|\vec{q}| |\vec{k}|)} = x. \quad (\text{B.5})$$

In the following, we will use the following notation to denote the 3-momentum in the system

$$k = |\vec{k}|, \quad \hat{k} = \frac{\vec{k}}{k}; \quad q = |\vec{q}|, \quad \hat{q} = \frac{\vec{q}}{q}. \quad (\text{B.6})$$

The invariant mass of the  $\pi N$  subsystem is given using the relativistic energy-momentum relations by

$$\begin{aligned} W^2 &= \left( \sqrt{M_N^2 + \vec{p}_2^2} + \sqrt{m_\pi^2 + \vec{q}^2} \right)^2 - (\vec{p}_2 + \vec{q})^2 \\ &= \left( \sqrt{M_N^2 + q^2} + \sqrt{m_\pi^2 + q^2} \right)^2 \\ &= M_N^2 + 2M_N \omega_\gamma^{lab}. \end{aligned} \quad (\text{B.7})$$

The various energies and momenta in the  $\pi N$  c.m. frame are given in terms of the invariant mass of the  $\pi N$  subsystem,  $W$ , by

$$k = \frac{W^2 - M_N^2}{2W} = \omega_\gamma, \quad (\text{B.8})$$

$$q = \frac{1}{2W} \sqrt{(W^2 - M_N^2 + m_\pi^2)^2 - 4m_\pi^2 W^2}, \quad (\text{B.9})$$

$$\omega_{\vec{q}} = \frac{W^2 - M_N^2 + m_\pi^2}{2W}, \quad (\text{B.10})$$

$$E_1 = \frac{W^2 + M_N^2}{2W}, \quad (\text{B.11})$$

$$E_2 = \frac{W^2 + M_N^2 - m_\pi^2}{2W}. \quad (\text{B.12})$$

## B.2 Multipole Decomposition of Amplitudes

The on-shell  $T_{fi}$ -matrix element is expanded in the c.m. frame to four independent amplitudes as follows [3]

$$\begin{aligned} \langle \vec{q}\mu | T_{fi}(W) | \vec{k}\epsilon \rangle &= \frac{4\pi W}{M_N} \left[ i(\vec{\sigma} \cdot \vec{\epsilon}) F_1 + (\vec{\sigma} \cdot \hat{\vec{q}}) \vec{\sigma} \cdot (\hat{\vec{k}} \times \vec{\epsilon}) F_2 + i(\vec{\sigma} \cdot \hat{\vec{k}}) (\hat{\vec{q}} \cdot \vec{\epsilon}) F_3 \right. \\ &\quad \left. + i(\vec{\sigma} \cdot \hat{\vec{q}}) (\hat{\vec{q}} \cdot \vec{\epsilon}) F_4 \right], \end{aligned} \quad (\text{B.13})$$

where  $F_i = F_i(W, x)$  with  $x = \hat{\vec{q}} \cdot \hat{\vec{k}}$  are the well known CGLN-amplitudes.  $\hat{\vec{k}}$  and  $\hat{\vec{q}}$  are momentum unit vectors of the photon and meson, respectively. The isospin decomposition of the CGLN-amplitudes has the form

$$F_i = F_i^{(-)} \frac{[\tau_\mu^+, \tau_0]}{2} + F_i^{(+)} \frac{\{\tau_\mu^+, \tau_0\}}{2} + F_i^{(0)} \tau_\mu^+ \quad (i = 1, 2, 3, 4), \quad (\text{B.14})$$

with the following commutator and the anti-commutator relations

$$\begin{aligned} [\tau_\mu^+, \tau_0] &= 2\mu\tau_\mu^+ = (-)^\mu 2\mu\tau_{-\mu}, \\ \{\tau_\mu^+, \tau_0\} &= (-)^\mu \{\tau_{-\mu}, \tau_0\} = 2\delta_{\mu,0}, \end{aligned} \quad (\text{B.15})$$

where  $\tau_\mu$  and  $\tau_3$  are the nucleon isospin matrices which act on the isospinor of the nucleon.

With this convention the amplitudes of the pion photoproduction process for the four physical channels consist as follows [62]

$$\begin{aligned}\langle n\pi^+ | F_i | \gamma p \rangle &= -\sqrt{2} [F_i^{(0)} + F_i^{(-)}], \\ \langle p\pi^- | F_i | \gamma n \rangle &= \sqrt{2} [F_i^{(0)} - F_i^{(-)}], \\ \langle p\pi^0 | F_i | \gamma p \rangle &= F_i^{(+)} + F_i^{(0)}, \\ \langle n\pi^0 | F_i | \gamma n \rangle &= F_i^{(+)} - F_i^{(0)}.\end{aligned}\tag{B.16}$$

The amplitudes  $F_i^{(3/2)}$  and  $F_i^{(1/2)}$  referring to the final  $\pi N$  isospin states with isospin  $\frac{3}{2}$  and  $\frac{1}{2}$ , respectively, are defined by

$$\begin{aligned}F_i^{(3/2)} &= F_i^{(+)} - F_i^{(-)} \quad (I = \frac{3}{2}), \\ F_i^{(1/2)} &= F_i^{(+)} + 2F_i^{(-)} \quad (I = \frac{1}{2}).\end{aligned}\tag{B.17}$$

The isoscalar amplitudes  $F_i^{(0)}$  leads only to a  $\pi N$  states with isospin  $\frac{1}{2}$ . In terms of these, one can define the neutron and the proton multipole amplitudes with total isospin  $I = \frac{1}{2}$  as follow

$$\begin{aligned}F_{i,n}^{(1/2)} &= F_i^{(0)} - \frac{1}{3}F_i^{(1/2)}, \\ F_{i,p}^{(1/2)} &= F_i^{(0)} + \frac{1}{3}F_i^{(1/2)},\end{aligned}\tag{B.18}$$

where the subscript  $p$  ( $n$ ) denotes a proton (neutron) target. The four charge channels in turn are given by

$$\begin{aligned}F_i(\gamma p \rightarrow n\pi^+) &= \sqrt{2} [F_{i,p}^{(1/2)} - \frac{1}{3}F_i^{(3/2)}], \\ F_i(\gamma n \rightarrow p\pi^-) &= \sqrt{2} [F_{i,n}^{(1/2)} + \frac{1}{3}F_i^{(3/2)}], \\ F_i(\gamma p \rightarrow p\pi^0) &= F_{i,p}^{(1/2)} + \frac{2}{3}F_i^{(3/2)}, \\ F_i(\gamma n \rightarrow n\pi^0) &= -F_{i,n}^{(1/2)} + \frac{2}{3}F_i^{(3/2)},\end{aligned}\tag{B.19}$$

where the isospin  $I = \frac{3}{2}$  multipole amplitudes,  $F_i^{(3/2)}$ , are the same for both protons and neutrons.

The partial wave decomposition of  $T_{fi}$  defines the multipole amplitudes  $A_{\ell\pm}(W)$ ,

where  $\ell_{\pm}$  is the  $\pi N$ -orbital angular momentum  $\ell$  and total angular momentum  $(\ell \pm \frac{1}{2})$  as well as  $A = E$  ( $A = M$ ) may characterize an electrical (magnetic) transition. The '+', '-' determine whether the nucleon spin  $\frac{1}{2}$  must be added to or subtracted from the orbital momentum to give the total final state momentum. One finds the following relations between the multipole and CGLN-amplitudes [7, 63]

$$\begin{aligned}
E_{\ell+} &= \frac{1}{2\ell+2} \int_{-1}^{+1} dx \left[ P_{\ell}(x)F_1 - P_{\ell+1}(x)F_2 + \frac{\ell}{2\ell+1}(P_{\ell-1}(x) - P_{\ell+1}(x))F_3 \right. \\
&\quad \left. + \frac{\ell+1}{2\ell+3}(P_{\ell}(x) - P_{\ell+2}(x))F_4 \right], \\
E_{\ell-} &= \frac{1}{2\ell} \int_{-1}^{+1} dx \left[ P_{\ell}(x)F_1 - P_{\ell-1}(x)F_2 + \frac{\ell+1}{2\ell+1}(P_{\ell+1}(x) - P_{\ell-1}(x))F_3 \right. \\
&\quad \left. + \frac{\ell}{2\ell-1}(P_{\ell}(x) - P_{\ell-2}(x))F_4 \right], \\
M_{\ell+} &= \frac{1}{2\ell+2} \int_{-1}^{+1} dx \left[ P_{\ell}(x)F_1 - P_{\ell+1}(x)F_2 + \frac{1}{2\ell+1}(P_{\ell+1}(x) - P_{\ell-1}(x))F_3 \right], \\
M_{\ell-} &= \frac{1}{2\ell} \int_{-1}^{+1} dx \left[ -P_{\ell}(x)F_1 + P_{\ell-1}(x)F_2 + \frac{1}{2\ell+1}(P_{\ell-1}(x) - P_{\ell+1}(x))F_3 \right].
\end{aligned} \tag{B.20}$$

Here the  $P_{\ell}(x)$  are Legendre polynomials of the first kind.

The partial wave decomposition of the CGLN-amplitudes into multipole amplitudes  $E_{\ell\pm}$ ,  $M_{\ell\pm}$  corresponding to good parity and angular momentum states is very convenient for the description of the resonance excitation process:

$$\begin{aligned}
F_1 &= \sum_{\ell=0}^{\infty} \{(\ell M_{\ell+} + E_{\ell+})P'_{\ell+1} + [(\ell+1)M_{\ell-} + E_{\ell-}]P'_{\ell-1}\}, \\
F_2 &= \sum_{\ell=0}^{\infty} [(\ell+1)M_{\ell+} + \ell M_{\ell-}]P'_{\ell}, \\
F_3 &= \sum_{\ell=0}^{\infty} [(E_{\ell+} - M_{\ell+})P''_{\ell+1} + (E_{\ell-} + M_{\ell-})P''_{\ell-1}], \\
F_4 &= \sum_{\ell=0}^{\infty} (M_{\ell+} - E_{\ell+} - M_{\ell-} - E_{\ell-})P''_{\ell},
\end{aligned} \tag{B.21}$$

where the  $P'_{\ell}$  and  $P''_{\ell}$  are the derivatives of Legendre polynomials.



# Appendix C

## Field Operators

This appendix is concerned with the field operators for nucleon, pion and photon. For more information about field operators and the derivation of commutator and anti-commutator relations we refer to [64]. Quantized nucleon, pion and photon fields are used in the determination of the vertices in chapter 2. The field operator of the nucleon has the form

$$\Psi(\vec{x}) = \sum_{m_s, m_t} \int \frac{d^3 p}{(2\pi)^3} \frac{M_N}{E_{\vec{p}}} (b(\vec{p}, m_s, m_t) u(\vec{p}, m_s) e^{i\vec{p}\cdot\vec{x}} + d^\dagger(\vec{p}, m_s, m_t) v(\vec{p}, m_s) e^{-i\vec{p}\cdot\vec{x}}) \quad (\text{C.1})$$

or

$$\bar{\Psi}(\vec{x}) = \sum_{m_s, m_t} \int \frac{d^3 p}{(2\pi)^3} \frac{M_N}{E_{\vec{p}}} (b^\dagger(\vec{p}, m_s, m_t) \bar{u}(\vec{p}, m_s) e^{-i\vec{p}\cdot\vec{x}} + d(\vec{p}, m_s, m_t) \bar{v}(\vec{p}, m_s) e^{i\vec{p}\cdot\vec{x}}) , \quad (\text{C.2})$$

with the following anti-commutator relations for the creation and annihilation operators, respectively

$$\{b(\vec{p}_1, m_s, m_t), b^\dagger(\vec{p}_2, m_{s'}, m_{t'})\} = (2\pi)^3 \delta^3(\vec{p}_2 - \vec{p}_1) \delta_{m_s, m_{s'}} \delta_{m_t, m_{t'}} \frac{E_{\vec{p}_1}}{M_N} \quad (\text{C.3})$$

$$\{d(\vec{p}_1, m_s, m_t), d^\dagger(\vec{p}_2, m_{s'}, m_{t'})\} = (2\pi)^3 \delta^3(\vec{p}_2 - \vec{p}_1) \delta_{m_s, m_{s'}} \delta_{m_t, m_{t'}} \frac{E_{\vec{p}_1}}{M_N} . \quad (\text{C.4})$$

The pion field is given by

$$\Phi_\mu = \int \frac{d^3 q}{(2\pi)^3} \frac{1}{2\omega_{\vec{q}}} (a_{-\mu}(\vec{q}) e^{i\vec{q}\cdot\vec{x}} + a_\mu^\dagger(\vec{q}) e^{-i\vec{q}\cdot\vec{x}}) \quad (\text{C.5})$$

with the commutator relation

$$[a_\mu(\vec{q}_1), a_{\mu'}^\dagger(\vec{q}_2)] = (2\pi)^3 \delta^3(\vec{q}_2 - \vec{q}_1) \delta_{\mu,\mu'} 2\omega_{\vec{q}} \quad (\text{C.6})$$

The photon field in Coulomb gauge  $\vec{k} \cdot \vec{\epsilon} = 0$  is given by

$$\vec{A}(\vec{x}) = \sum_{m_\gamma} \int \frac{d^3k}{(2\pi)^3} \frac{\vec{\epsilon}_{m_\gamma}}{2\omega_\gamma} \left( a_{m_\gamma}(\vec{k}) e^{i\vec{k} \cdot \vec{x}} + a_{m_\gamma}^\dagger(\vec{k}) e^{-i\vec{k} \cdot \vec{x}} \right), \quad (\text{C.7})$$

with the commutator relation

$$[a_{m_\gamma}(\vec{k}_1), a_{m'_\gamma}^\dagger(\vec{k}_2)] = (2\pi)^3 \delta^3(\vec{k}_2 - \vec{k}_1) \delta_{m_\gamma, m'_\gamma} 2\omega_\gamma. \quad (\text{C.8})$$

The effect of creation and annihilation operators on the vacuum state is given by

$$b^\dagger(\vec{p}, m_s, m_t) |0\rangle = |N; \vec{p} m_s m_t\rangle, \quad b(\vec{p}, m_s, m_t) |0\rangle = 0, \quad (\text{C.9})$$

$$a_\mu^\dagger(\vec{q}) |0\rangle = |\pi; \vec{q} \mu\rangle, \quad a_\mu(\vec{q}) |0\rangle = 0, \quad (\text{C.10})$$

$$a_{m_\gamma}^\dagger(\vec{k}) |0\rangle = |\gamma; \vec{k} m_\gamma\rangle, \quad a_{m_\gamma}(\vec{k}) |0\rangle = 0. \quad (\text{C.11})$$

## Appendix D

# Parametrization of the Deuteron Wave Functions

For practical purposes it is more convenient to work with an analytical parametrization of the  $S$ - and  $D$ -waves in momentum space,  $u_0(p)$  and  $u_2(p)$ , respectively, rather than with the discrete sets  $u_0(p_i)$  and  $u_2(p_i)$ . The ansatz for the analytic version of the momentum space wave functions of the non-relativistic version OBEP of the Bonn OBE-potential [45] is

$$u_0(p) = \sqrt{\frac{2}{\pi}} \sum_{i=1}^{n_u} \frac{C_i}{p^2 + m_i^2}, \quad (\text{D.1})$$

$$u_2(p) = \sqrt{\frac{2}{\pi}} \sum_{i=1}^{n_w} \frac{D_i}{p^2 + m_i^2}, \quad (\text{D.2})$$

with the normalization

$$\int_0^\infty dp \, p^2 \{u_0^2(p) + u_2^2(p)\} = 1. \quad (\text{D.3})$$

In Table D.1 we list the coefficients  $C_i$  and  $D_i$  of the parametrized deuteron wave functions  $u_0(p)$  and  $u_2(p)$  of the Bonn OBE-potential. In order to make the  $u_0(p)$  and  $u_2(p)$  fulfill the necessary boundary conditions, the last value of  $C_i$  and the last three values of  $D_i$  must be calculated through the following relations [45]

$$C_{n_u} = - \sum_{i=1}^{n_u-1} C_i,$$

$$D_{n_w-2} = \frac{m_{n_w-2}^2}{(m_{n_w}^2 - m_{n_w-2}^2)(m_{n_w-1}^2 - m_{n_w-2}^2)}$$

Table D.1: Coefficients of the parametrized deuteron wave functions for the Bonn OBE-potential (full model) [45]. The last  $C_i$  and the last three  $D_i$  are to be computed from Eq. (D.4) ( $n_u = n_w = 11$ ).

$C_i$ (fm $^{-1/2}$ )	$D_i$ (fm $^{-1/2}$ )
0.90457337 +00	0.24133026 -01
-0.35058661 +00	-0.64430531 +00
-0.17635927 +00	0.51093352 +00
-0.10418261 +02	-0.54419065 +01
0.45089439 +02	0.15872034 +02
-0.14861947 +03	-0.14742981 +02
0.31779642 +03	0.44956539 +01
-0.37496518 +03	-0.71152863 -01
0.22560032 +03	see Eq. (D.4)
-0.54858290 +02	see Eq. (D.4)
see Eq. (D.4)	see Eq. (D.4)

$$\times \left( -m_{n_w-1}^2 m_{n_w}^2 \sum_{i=1}^{n_w-3} \frac{D_i}{m_i^2} + (m_{n_w-1}^2 + m_{n_w}^2) \sum_{i=1}^{n_w-3} D_i - \sum_{i=1}^{n_w-3} D_i m_i^2 \right), \quad (D.4)$$

and two other relations obtained by circular permutation of  $(n_w - 2)$ ,  $(n_w - 1)$  and  $n_w$ . The masses  $m_i$  are chosen to be

$$m_i = \alpha + (i-1)m_0,$$

with  $\alpha = \sqrt{E_b M_N} = 0.231609$  fm $^{-1}$ , where  $E_b$  is the deuteron binding energy, and  $m_0 = 0.9$  fm $^{-1}$ . This choice ensures the correct asymptotic behaviour. In analogy with Ref. [45] we use  $n_u = n_w = 11$ .

## Appendix E

# Transformation of Differential Cross Section

In Ref. [22] the differential cross sections for the reaction  $d(\gamma, \pi^0)np$  are given in the so-called photon-nucleon center-of-mass frame<sup>1</sup>. This frame corresponds to an assumption that both nucleons in the deuteron have the same momenta  $-\frac{\vec{k}}{2}$  in the  $\gamma d$  c. m. frame. This means that both nucleons in the deuteron are at rest in the laboratory frame of the deuteron.

In order to compare our theoretical predictions for differential cross sections of the reaction  $d(\gamma, \pi^0)np$  with the experimental data from Ref. [22] we need therefore to transform the differential cross sections from the  $\gamma d$  rest frame to the c. m. frame of the incident photon and a nucleon at rest. Therefore, we give in this appendix the Jacoby determinant which we need for this purpose.

Since the azimuthal angle remains unchanged by the transformation between the laboratory and the c. m. systems, we have [65]

$$\frac{d\sigma}{d\Omega^{cm}} = \frac{d\sigma}{d\Omega^{lab}} \frac{\partial Z}{\partial Z^*}, \quad (\text{E.1})$$

where  $Z^* (= \cos \theta_\pi^*)$  and  $Z (= \cos \theta_\pi^{lab})$  are the pion angle in the c.m. and the  $\gamma d$  laboratory frame, respectively. The derivative of  $Z$  with respect to  $Z^*$  gives direct the requested Jacoby determinant.

Using the Mandelstam variable  $t$  from Eq. (B.4) one can express  $Z$  through  $Z^*$  as follows

$$Z = \frac{Z^* \omega_\gamma^* q_\pi^* - E_\pi^* \omega_\gamma^* + E_\pi^{lab} \omega_\gamma^{lab}}{\omega_\gamma^{lab} q_\pi^{lab}}. \quad (\text{E.2})$$

---

<sup>1</sup>Throughout this appendix parameters in this frame are labelled by (\*).

which gives the following expression for the Jacoby determinant

$$\frac{\partial Z}{\partial Z^*} = \frac{\omega_\gamma^* q_\pi^*}{\omega_\gamma^{lab}} \left[ \left( \frac{E_\pi^{lab}}{q_\pi^{lab}} Z - 1 \right) \frac{\partial E_\pi^{lab}}{\partial Z} + q_\pi^{lab} \right]^{-1}, \quad (\text{E.3})$$

where  $\omega_\gamma^*$ ,  $q_\pi^*$  and  $E_\pi^*$  are the photon energy (Eq. B.8), pion momentum (Eq. B.9) and pion energy (Eq. B.10) in the c.m. frame, respectively; and  $\omega_\gamma^{lab}$ ,  $q_\pi^{lab}$  and  $E_\pi^{lab}$  are the photon energy, pion momentum and pion energy in the laboratory frame, respectively.

Using the Mandelstam variable  $u$  from Eq. (B.4), one can express the pion energy in the laboratory frame as follows

$$E_\pi^{lab} = \frac{E_N^* E_\pi^* + \omega_\gamma^* q_\pi^* Z^*}{M_N}, \quad (\text{E.4})$$

where  $E_N^* = \sqrt{M_N^2 + \omega_\gamma^{*2}}$  is the nucleon energy in the c.m. frame. Using the well known formulae for momentum and energies from appendix B.1 (see also [44]) the pion energy in the laboratory frame is then given by

$$E_\pi^{lab} = \frac{\mathcal{A}\mathcal{B} + \omega_\gamma^{lab} Z\mathcal{C}}{\mathcal{A}^2 - \omega_\gamma^{lab2} Z^2}, \quad (\text{E.5})$$

where

$$\mathcal{A} = (M_N + \omega_\gamma^{lab}), \quad (\text{E.6})$$

$$\mathcal{B} = (M_N \omega_\gamma^{lab} + \frac{1}{2} m_\pi^2), \quad (\text{E.7})$$

and

$$\mathcal{C} = \sqrt{\mathcal{B}^2 + \omega_\gamma^{lab2} m_\pi^2 Z^2 - m_\pi^2 \mathcal{A}^2}. \quad (\text{E.8})$$

# Appendix F

## Two-Body Subsystems

In this appendix we give some details of the  $NN$  and  $\pi N$  potential models which we use to study the  $NN$  and  $\pi N$  interaction in the  $NN$  and  $\pi N$  subsystems. In the calculations of this work we solve the three dimensional integral equation of Lippmann-Schwinger [47] to calculate the  $\mathcal{T}$ -matrix elements of the two-body scattering and then show how phase shifts are obtained.

The use of separable potentials in the two-body interaction has greatly stimulated the theoretical investigation of the three-body problem in the last three decades. Most of the important properties of the three-body system are already well described by the simplest type of separable models. These separable models are most widely used in case of the  $\pi NN$  system (see for example [66] and references therein). For the  $NN$  and  $\pi N$  interactions in the  $NN$ - and  $\pi N$ -subsystems we use a specific class of separable potentials [15, 48, 49] which historically have played and still play a major role in the development of few-body physics and also fit the phase shift data for both  $NN$ - and  $\pi N$ -scattering. The formalism to obtain the full two-body  $\mathcal{T}$ -matrix and the scattering phase shifts is given in this appendix in more detail. Momentum space separable potentials for  $NN$ - and  $\pi N$ -interactions are also given.

### F.1 The $NN$ Subsystem

#### F.1.1 $NN$ Scattering Equation

In this section we discuss how the  $\mathcal{T}$ -matrix for  $NN$ -scattering which we use as input in our predictions in chapter 3 is calculated. Two-nucleon scattering is described by the Lippmann-Schwinger equation which given graphically in Fig. F.1.

In partial wave decomposition, represented by the orbital angular momentum  $\ell$ , total angular momentum  $J$ , spin  $s$  and isospin  $t$ , the  $\mathcal{T}$ -matrix of the two-nucleon

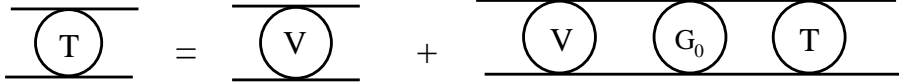


Figure F.1: The graphical diagram of the Lippmann-Schwinger equation for  $NN$  interaction.

scattering may be written as

$$\langle \ell' J' s' t' | \mathcal{T}(p', p; E) | \ell J s t \rangle = \delta_{J' J} \delta_{s' s} \delta_{t' t} \mathcal{T}_{\ell \ell'}^{Jst}(p', p; E), \quad (\text{F.1})$$

where  $\vec{p}$  and  $\vec{p}'$  are the relative three-momenta of the two interacting nucleons in the initial and final state, respectively; and  $p \equiv |\vec{p}|$  and  $p' \equiv |\vec{p}'|$ .  $E$  denotes the energy of the two interacting nucleons in the c. m. frame and is given by  $E = \frac{p_0^2}{M_N}$ , where  $p_0$  is the magnitude of the initial relative momentum (c. m. on-shell momentum) which is related to the laboratory energy by

$$T_{lab} = \frac{2p_0^2}{M_N}. \quad (\text{F.2})$$

For a given  $NN$  potential  $V$ , the  $\mathcal{T}$ -matrix is obtained from the Lippmann-Schwinger equation [47] which in partial wave decomposition reads<sup>1</sup>

$$\mathcal{T}_\ell(p', p; E) = V_\ell(p', p) + \int_0^\infty dk k^2 V_\ell(p', k) \frac{M_N}{M_N E - k^2 + i\epsilon} \mathcal{T}_\ell(k, p; E) \quad (\text{F.3})$$

for single channels. For the coupled channels it reads

$$\begin{aligned} \mathcal{T}_{\ell\ell'}(p', p; E) &= V_{\ell\ell'}(p', p) \\ &+ \sum_{\ell''} \int_0^\infty dk k^2 V_{\ell\ell''}(p', k) \frac{M_N}{M_N E - k^2 + i\epsilon} \mathcal{T}_{\ell''\ell'}(k, p; E), \end{aligned} \quad (\text{F.4})$$

where  $\vec{k}$  is the relative three-momenta of the two interacting nucleons in the intermediate state and  $k \equiv |\vec{k}|$ .

Using the identity

$$\frac{1}{x - x_0 + i\epsilon} = \mathcal{P} \frac{1}{x - x_0} - i\pi \delta(x - x_0), \quad (\text{F.5})$$

where  $\mathcal{P}$  denotes the principle value integral, one gets the  $\mathcal{T}$ -matrix elements in partial wave decomposition

$$\begin{aligned} \mathcal{T}_\ell(p', p; E) &= V_\ell(p', p) + \mathcal{P} \int_0^\infty dk k^2 V_\ell(p', k) \frac{M_N}{p_0^2 - k^2} \mathcal{T}_\ell(k, p; E) \\ &- \frac{1}{2} i\pi M_N p_0 V_\ell(p', p_0) \mathcal{T}_\ell(p_0, p; E) \end{aligned} \quad (\text{F.6})$$

<sup>1</sup>We drop the indices  $Jst$  for simplicity.

for single channels and

$$\begin{aligned} \mathcal{T}_{\ell\ell'}(p', p; E) &= V_{\ell\ell'}(p', p) + \sum_{\ell''=J\pm 1} \mathcal{P} \int_0^\infty dk k^2 V_{\ell\ell''}(p', k) \frac{M_N}{p_0^2 - k^2} \mathcal{T}_{\ell''\ell'}(k, p; E) \\ &\quad - \frac{1}{2} i\pi M_N p_0 V_{\ell\ell'}(p', p_0) \mathcal{T}_{\ell\ell'}(p_0, p; E) \end{aligned} \quad (\text{F.7})$$

for coupled channels. These one-dimensional integral equations, Eqs. (F.6) and (F.7), can be solved numerically by means of a matrix inversion algorithm.

Let us first consider the partial wave one-dimensional integral equation for uncoupled channels given by Eq. (F.6). The integral should now be approximated by a  $n$ -point integration routine

$$\int_0^\infty dk F(k) = \sum_{i=1}^n F(k_i) w_i, \quad (\text{F.8})$$

where  $k_i$  and  $w_i$  are the Gaussian integration points and weights, respectively. Since the original Gauss points,  $\mathcal{K}_i$  (with weights  $\mathcal{W}_i$ ) are in the interval  $(-1, +1)$ , we have to map them to the interval  $(0, \infty)$ , the range of our integration. For this purpose we use the mapping

$$k_i = B \tan \left\{ \frac{\pi}{4} (\mathcal{K}_i + 1) \right\}, \quad (\text{F.9})$$

with the new weights

$$w_i = B \frac{\pi}{4} \left\{ \frac{\mathcal{W}_i}{\cos^2[\frac{\pi}{4}(\mathcal{K}_i + 1)]} \right\}, \quad (\text{F.10})$$

where  $B = 400$  MeV is used. For the Gauss integral we use  $n = 16$  mesh points.

To solve Eqs. (F.6) and (F.7), the principle value integration has to be replaced by a smooth integrand, which can be achieved by adding a term of measure zero

$$\begin{aligned} \mathcal{T}_\ell(p', p; E) &= V_\ell(p', p) + \int_0^\infty dk \frac{M_N}{p_0^2 - k^2} \left\{ k^2 V_\ell(p', k) \mathcal{T}_\ell(k, p; E) \right. \\ &\quad \left. - p_0^2 V_\ell(p', p_0) \mathcal{T}_\ell(p_0, p; E) \right\} - \frac{1}{2} i\pi M_N p_0 V_\ell(p', p_0) \mathcal{T}_\ell(p_0, p; E). \end{aligned} \quad (\text{F.11})$$

All of the  $n$  integration points,  $k_1, k_2, \dots, k_n$ , are required to be unequal to  $p_0$ . If we call  $p_0$  the  $(n+1)$  point ( $p_0 = p_{n+1}$ ), then for  $p = p_0$  Eq. (F.11) can be rewritten as

$$\begin{aligned} V_\ell(p_i, p_{n+1}) &= \mathcal{T}_\ell(p_i, p_{n+1}; E) - \sum_{k=1}^n \frac{M_N w_k}{p_{n+1}^2 - p_k^2} \left\{ p_k^2 V_\ell(p_i, p_k) \mathcal{T}_\ell(p_k, p_{n+1}; E) \right. \\ &\quad \left. - p_{n+1}^2 V_\ell(p_i, p_{n+1}) \mathcal{T}_\ell(p_{n+1}, p_{n+1}; E) \right\} \\ &\quad + \frac{1}{2} i\pi M_N p_{n+1} V_\ell(p_i, p_{n+1}) \mathcal{T}_\ell(p_{n+1}, p_{n+1}; E). \end{aligned} \quad (\text{F.12})$$

Thus, the scattering equation can be written in matrix form as

$$V_\ell(p_i, p_{n+1}) = \sum_{j=1}^{n+1} A_\ell(p_i, p_j) \mathcal{T}_\ell(p_j, p_{n+1}; E), \quad (\text{F.13})$$

where the dimensionless  $A_\ell(p_i, p_j)$  matrix is given by

$$\begin{aligned} A_\ell(p_i, p_j) = & \delta_{ij} - \frac{M_N w_j p_j^2}{p_{n+1}^2 - p_j^2} V_\ell(p_i, p_j) \\ & + \left\{ \left( \sum_{k=1}^n \frac{w_k}{p_{n+1}^2 - p_k^2} \right) p_{n+1} + \frac{i\pi}{2} \right\} M_N p_{n+1} V_\ell(p_i, p_{n+1}) \delta_{n+1, j}. \end{aligned} \quad (\text{F.14})$$

Choosing the momentum grid such that  $p_j \neq p_{n+1} \forall j \leq n$ , the matrix  $A(p_i, p_j)$  is nonsingular and can be inverted to obtain the on-shell or half-off-shell  $\mathcal{T}$ -matrix<sup>2</sup>

$$\mathcal{T}_\ell(p_i, p_{n+1}; E) = \sum_{j=1}^{n+1} \{A_\ell(p_i, p_j)\}^{-1} V_\ell(p_j, p_{n+1}). \quad (\text{F.15})$$

The extension to coupled channels is straightforward. One simply combines the points to form a larger  $(2n+2) \times (2n+2)$  dimensional matrix

$$V(p_i, p_j) = \sum_{m=1}^{2n+2} A(p_i, p_m) \mathcal{T}_\ell(p_m, p_j; E). \quad (\text{F.16})$$

Here the  $i, j$  and  $m$  labels include both the points  $k_1, k_2, \dots, k_{n+1}$  and the  $\ell$ -value. For example, for  $\ell = J - 1$  we take the  $1 \leq i \leq (n+1)$  points as  $k_1, k_2, \dots, k_{n+1}$ . For  $\ell = J + 1$ , the label  $i$  ranges as  $(n+2) \leq i \leq (2n+2)$  with identical  $k$ -values,  $k_1, k_2, \dots, k_{n+1} \equiv k_{n+2}, k_{n+3}, \dots, k_{2n+2}$ .

So far, we have never mentioned the total isospin of the two-nucleon system,  $t$  (which is either 0 or 1). The reason for this is simply that  $t$  is not an independent quantum number. That is, owing to the antisymmetry of the two-fermion state, the quantum numbers  $\ell, s$ , and  $t$  have to fulfill the condition

$$(-1)^{\ell+s+t} = -1. \quad (\text{F.17})$$

Thus, for a given  $\ell$  and  $s$ , the total isospin  $t$  of the two-nucleon state is fixed.

---

<sup>2</sup>For the matrix  $T(a, b; E)$  we mean by "on-shell" that we are considering elastic scattering. This means that the matrix is "on-shell" when  $E_a = E_b = E$ , where  $E$  is the non-relativistic kinetic energy. If  $E_a \neq E_b = E$  then the matrix is "half-off-shell" and it is "full-off-shell" if  $E_a \neq E_b \neq E$ .

### F.1.2 Separable $NN$ Potential Model

Now we outline the model which we use to study the  $NN$  interaction in the  $NN$ -subsystem. The EST method [67] for constructing separable representations of modern  $NN$  potentials has been applied by the Graz group [48, 49] to cast the Paris potential [68] in separable form. In the meantime these so-called PEST potentials have become of great use in introducing the features of advanced meson-exchange theory [69] into calculations of few-body systems like, e.g., of nucleon-deuteron scattering [70]. They have the general form

$$V_{\ell\ell'}(p', p) = \sum_{i,j=1}^N g_{\ell i}(p') \lambda_{ij} g_{\ell' j}(p), \quad (\text{F.18})$$

where  $N$  and  $\lambda$  specify the rank and the strength of the separable interaction, respectively, in each partial wave. These separable interactions represent a good approximation of the on-shell as well as off-shell properties of the original Paris potential and show a good fit to the modern  $NN$  data base.

The form factors of these separable potentials for each partial wave are given by

$$\begin{aligned} g_{\ell i}(p) &= \sum_{n=1}^4 \frac{C_{\ell in} p^{\ell+2(n-1)}}{(p^2 + \beta_{\ell in}^2)^{\ell+n}}, & (\ell \leq 1) \\ g_{\ell i}(p) &= \sum_{n=1}^4 \frac{C_{\ell in} p^{\ell+2(n-1)}}{(p^2 + \beta_{\ell in}^2)^{\ell+n-1}}, & (2 \leq \ell \leq 3) \\ g_{\ell i}(p) &= \sum_{n=1}^4 \frac{C_{\ell in} p^{\ell+2(n-1)}}{(p^2 + \beta_{\ell in}^2)^{\ell+n-2}}, & (\ell \geq 4) \end{aligned} \quad (\text{F.19})$$

where  $C$  and  $\beta$  are fit parameters of the separable interaction. The values of these parameters in each partial wave are given appendix G. Let us now discuss the partial wave states in detail.

In case of the  ${}^1S_0$  partial wave the Graz group [49] have constructed a modified PEST potential of rank-3. The parameters of this potential are given in Table G.1 for both the (p-p) and (n-p) systems. Fig. F.2 shows that the phase shifts of the (p-p) system<sup>3</sup> are the same for both PEST3 and the original Paris potential.

For the  ${}^3P_0$ ,  ${}^3P_1$  and  ${}^1P_1$  partial waves, they constructed a rank-2 separable approximations. The potential parameters for these three partial waves are given in

---

<sup>3</sup>The Paris potential is given only for the (p-p) system in the  ${}^1S_0$  partial wave.

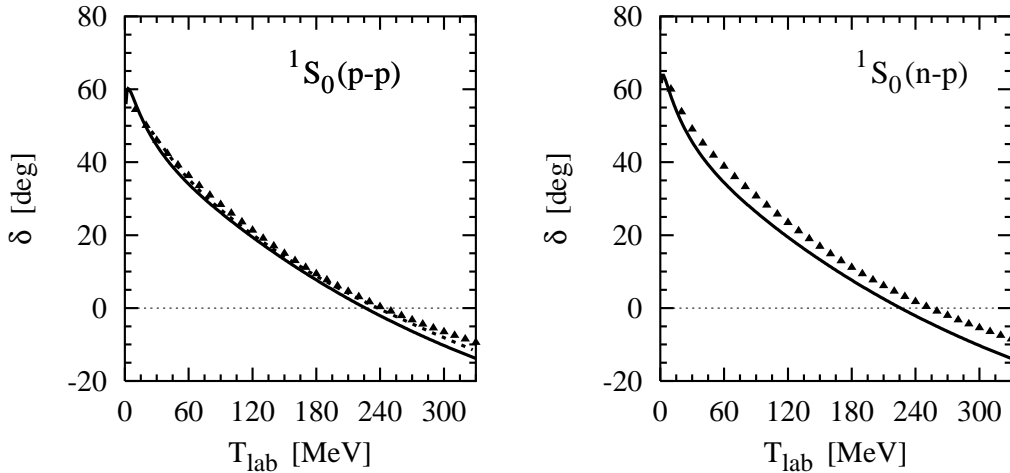


Figure F.2:  $^1S_0$  phase shift using a rank-3 separable potential from [49] (solid curve) in comparison with the original Paris potential (dotted curve) which is given only for the (p-p) system. The data points are from SAID [28] (Solution: SP00).

Table G.2. In this Table we give the modified parameters of the  $^3P_0$  partial wave from Ref. [49] which we use in this work. The on-shell properties of the PEST parametrization for  $^3P_0$  are evident from the phase shift for  $^3P_0$  in the left panel of Fig. F.3. Up to  $T_{lab} \approx 70$  MeV the approximation to the Paris potential is rather good. If we go to higher energies, there is some discrepancy in the phase shifts around  $T_{lab} \approx 100 - 180$  MeV, but the situation improves again at higher energies. For the  $^3P_1$  and  $^1P_1$  partial waves the separable potential is good up to  $T_{lab} \leq 200$  MeV. For  $T_{lab} \geq 200$  MeV the deviation in the  $^3P_1$  and  $^1P_1$  partial waves from the original Paris potential increases strongly.

For the  $^1D_2$  and  $^3D_2$  partial waves the Graz group constructed a rank-2 PEST approximation. The properties of these potentials are practically the same as discussed above for the uncoupled  $P$  waves. The on-shell behaviour of the potentials, whose parameters are given in Table G.3, are evident from the phase shifts shown in Fig. F.4

The coupled  $^3S_1$ - $^3D_1$  partial wave state which acts in the deuteron is crucial for a proper treatment of the  $NN$  interaction. But until now, no satisfactory description of all its aspects has been achieved by means of separable forces. The Graz group tried to remedy this situation by constructing a rank-4 PEST approximation to the Paris potential. This separable interaction, whose parameters are given in Table G.4, yields a correct reproduction of the deuteron properties as well as a fair description of the scattering domain as shown in Fig F.5.

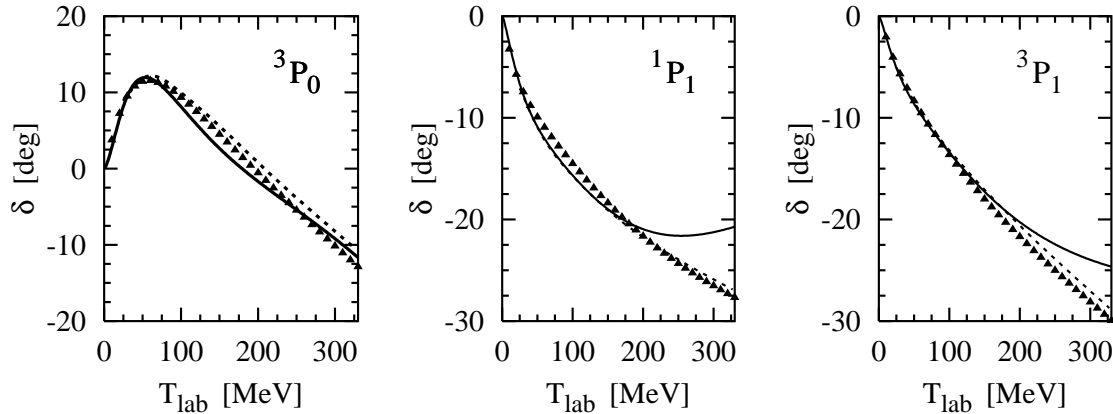


Figure F.3: Same notation as in Fig. F.2 but for the  $^3P_0$ ,  $^1P_1$  and  $^3P_1$  and single channels using a rank-2 separable potential.

For the coupled  $^3P_2$ - $^3F_2$  partial wave, they constructed a rank-3 PEST parametrization, whose parameters are given in Table G.5. The phase shifts and the mixing parameter are shown in Fig. F.6. On the other hand, they designed a rank-4 PEST parametrization for the coupled  $^3D_3$ - $^3G_3$  partial wave. The parameters of the PEST potential are given in Table G.6. The on-shell properties are shown in Fig. F.7; they exhibit a good agreement with the Paris potential.

From the foregoing presentation of the PEST interactions it is clear that these separable representation of the Paris  $NN$  potential are likely to be relevant in few-body problems.

### F.1.3 $NN$ Phase Shifts

The full on-shell  $S$ -matrix in partial wave decomposition is related to the on-shell partial wave  $T$ -matrix by

$$S(E) = \mathbb{1} + 2i T(E), \quad (\text{F.20})$$

with

$$T(E) := -\frac{1}{2}\pi p_0 M_N \mathcal{T}(E), \quad (\text{F.21})$$

in the nonrelativistic kinematics which we use in this work.

The scattering phase shifts for a given partial wave can be calculated from the on-energy-shell  $K$ -matrix (a  $2 \times 2$  matrix) [71, 72] which is expressed in terms of the  $S$ - and  $T$ -matrix by

$$K := i \frac{1 - S}{1 + S} = \frac{T}{1 + i T}. \quad (\text{F.22})$$

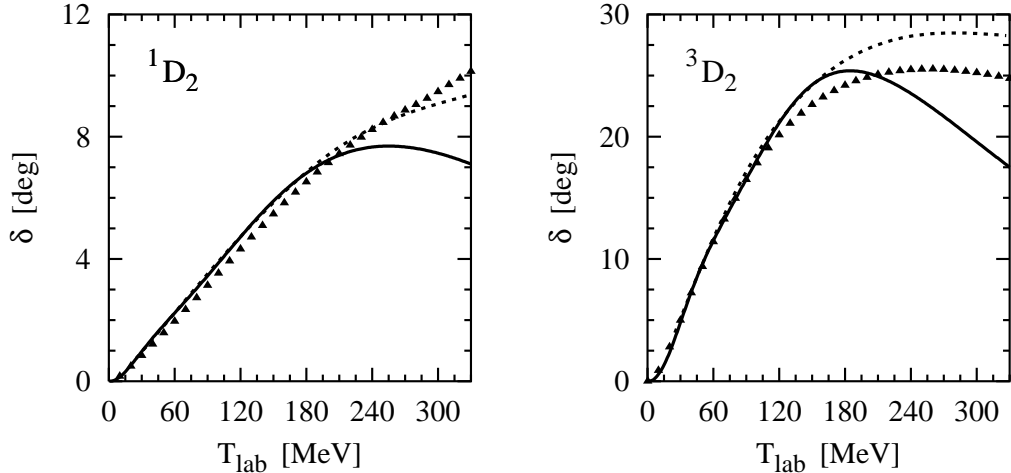


Figure F.4: Same notation as in Fig. F.2 but for the  $^1D_2$  and  $^3D_2$  single channels using a rank-2 separable potential.

For the single channels, the scattering phase shifts are then determined by

$$\tan \delta = \Re e K. \quad (\text{F.23})$$

For the coupled channels, a unitary transformation is needed to diagonalize the two-by-two coupled  $K$ -matrix. This requires an additional parameter, known as the *mixing parameter*  $\epsilon$ . This mixing parameter and the phase shifts of the coupled channels are given in terms of the  $K$ -matrix by

$$\sin(2\epsilon) = \sqrt{\frac{(2\Re e K_0)^2}{[1 + (\Re e K_0)^2 - \Re e K_+ \Re e K_-]^2 + (\Re e K_+ + \Re e K_-)^2}} \quad (\text{F.24})$$

and

$$2\delta_{\pm} = \arcsin\left(\frac{\Re e K_+ + \Re e K_-}{2\Re e K_0} \sin(2\epsilon)\right) \pm \arcsin\left(\frac{\Re e K_+ - \Re e K_-}{2\Re e K_0} \tan(2\epsilon)\right), \quad (\text{F.25})$$

where

$$\begin{aligned} K_0 &:= K_{J+1,J-1} = K_{J-1,J+1}, \\ K_+ &:= K_{J+1,J+1}, \\ K_- &:= K_{J-1,J-1}. \end{aligned} \quad (\text{F.26})$$

In this work, all phase shifts are in the Stapp-Ypsilantis-Metropolis (SYM) or *bar* convention [73].

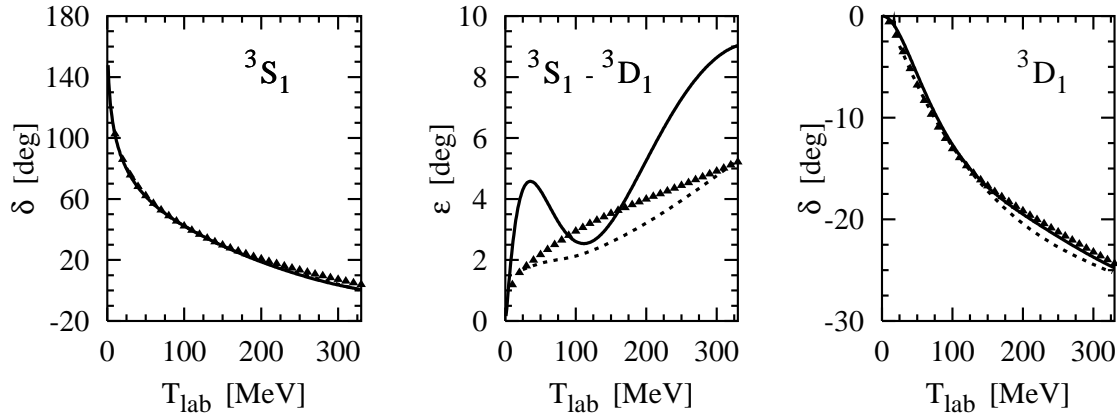


Figure F.5: Same notation as in Fig. F.2 but for the coupled channel  $^3S_1$ - $^3D_1$  using a rank-4 separable potential.

## F.2 The $\pi N$ Subsystem

Analogous to the case of  $NN$ -scattering, the formalism to obtain the full  $\mathcal{T}$ -matrix and the scattering phase shifts for  $\pi N$ -scattering is outlined in this section, but not in more details since we give enough details in case of the  $NN$ -scattering. A partial wave decomposition of the separable  $\pi N$  potential is performed in this section. The  $\pi N$  scattering equation is also given.

### F.2.1 $\pi N$ -Scattering Equation

For a given  $\pi N$  potential  $V$ , the  $\mathcal{T}$ -matrix for  $\pi N$  scattering is obtained from the Lippmann-Schwinger equation which in partial wave decomposition, specified by the orbital angular momentum  $\ell$ , total angular momentum  $J$  and isospin  $t$ , reads<sup>4</sup>

$$\mathcal{T}(p', p; E) = V(p', p) + \int_0^\infty dk k^2 V(p', k) \mathcal{G}_{\pi N}(k, E) \mathcal{T}(k, p; E), \quad (\text{F.27})$$

with the  $\pi N$  propagator

$$\mathcal{G}_{\pi N}(k, E) = \frac{1}{E - E_\pi(k) - E_N(k) + i\epsilon}, \quad (\text{F.28})$$

where  $\vec{p}$ ,  $\vec{k}$  and  $\vec{p}'$  are the  $\pi N$  relative momentum in the initial, intermediate and final state, respectively; and  $p \equiv |\vec{p}|$ ,  $k \equiv |\vec{k}|$  and  $p' \equiv |\vec{p}'|$ .  $E = \sqrt{M_N^2 + p_0^2} + \sqrt{m_\pi^2 + p_0^2}$

<sup>4</sup>The indices  $\ell J t$  are also dropped here for simplicity.

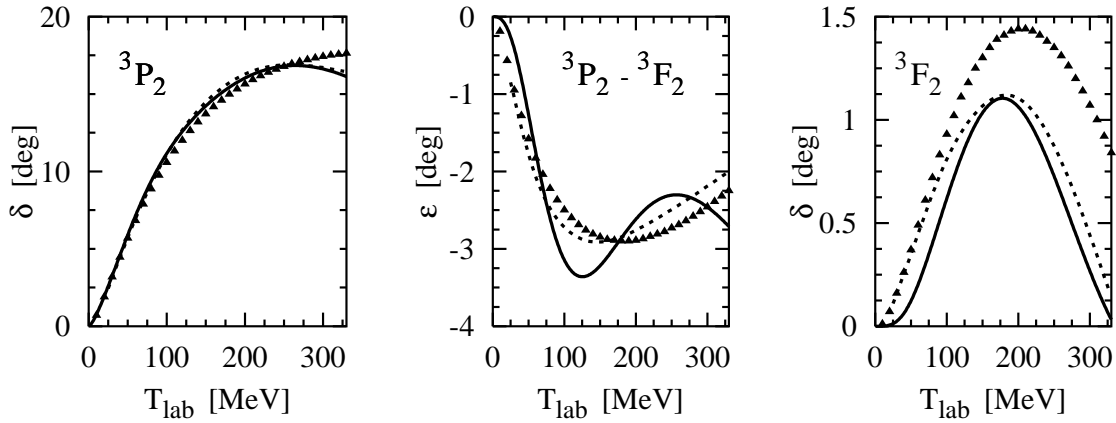


Figure F.6: Same notation as in Fig. F.2 but for the coupled channel  ${}^3P_2$ - ${}^3F_2$  using a rank-3 separable potential.

denotes the total collision energy with on-shell momentum  $p_0$  in the c. m. frame. For our calculations we use relativistic kinematics for both pion and nucleon, thus

$$\begin{aligned} E_\pi(k) &= \sqrt{m_\pi^2 + k^2}, \\ E_N(k) &= \sqrt{M_N^2 + k^2}. \end{aligned} \quad (\text{F.29})$$

The partial wave  $\mathcal{T}$ -matrix for  $\pi N$  scattering is then given by

$$\mathcal{T}(p', p; E) = V(p', p) + \int_0^\infty dk k^2 V(p', k) \frac{G(k)}{p_0^2 - k^2 + i\epsilon} \mathcal{T}(k, p; E), \quad (\text{F.30})$$

where

$$G(k) = \frac{[E_N(p_0) + E_N(k)][E_\pi(p_0) + E_\pi(k)]}{[E_N(p_0) + E_N(k) + E_\pi(p_0) + E_\pi(k)]}. \quad (\text{F.31})$$

To transform this equation into a principle value integral equation, one uses the identity

$$\frac{1}{x^2 - x_0^2 + i\epsilon} = \mathcal{P} \frac{1}{x^2 - x_0^2} - i\pi\delta(x^2 - x_0^2), \quad (\text{F.32})$$

to get the matrix elements in partial wave decomposition as

$$\begin{aligned} \mathcal{T}(p', p; E) &= V(p', p) + \mathcal{P} \int_0^\infty dk k^2 V(p', k) \frac{G(k)}{p_0^2 - k^2} \mathcal{T}(k, p; E) \\ &\quad - \frac{1}{2} i\pi p_0 G(p_0) V(p', p_0) \mathcal{T}(p_0, p; E). \end{aligned} \quad (\text{F.33})$$

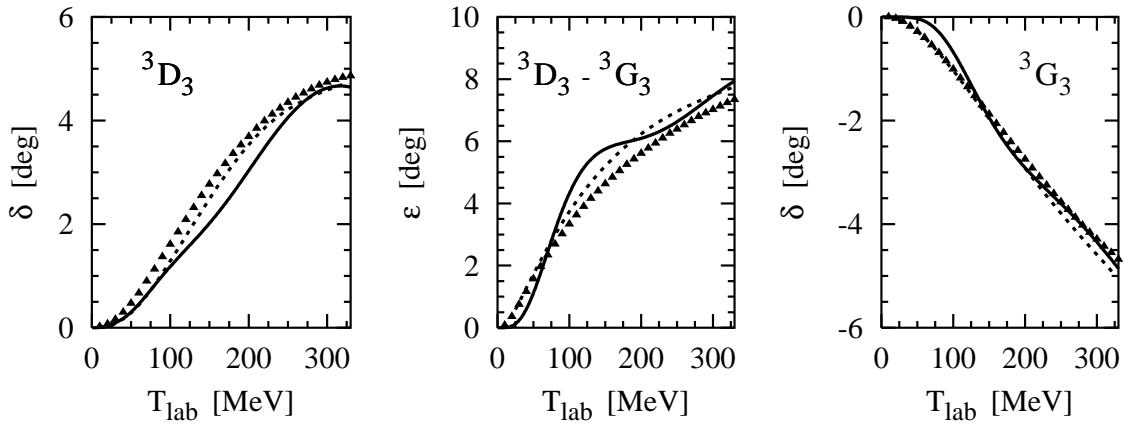


Figure F.7: Same notation as in Fig. F.2 but for the coupled channel  ${}^3D_3$ - ${}^3G_3$  using a rank-4 separable potential.

This one-dimensional integral equation can be solved numerically for a given  $\pi N$  potential model  $V(p', p)$  by using the matrix inversion method which is explained in details in case of  $NN$ -scattering in the previous section. In this work we use the separable  $\pi N$  potential model of Nozawa *et al.* [15]. This model is given in more details in the forthcoming section.

### F.2.2 Separable $\pi N$ Potential Model

In the case of the  $\pi N$  scattering a large number of dynamical models have been developed over the past few years (see for example [15, 74, 75]). Most begin with a separable potential which is iterated in a Lippmann-Schwinger equation to give the scattering amplitude, from which phase shifts and observables are obtained. In this work we use the model of Nozawa *et al.* [15] in order to study the  $\pi N$  interaction in the  $\pi N$ -subsystem. This model is consistent with the existing unitary description of the  $\pi NN$  system and treats the  $\pi N$  interaction dynamically, with all  $S$ -,  $P$ - and  $D$ -wave  $\pi N$  phase shifts being well reproduced below 500 MeV.

For partial wave specified by quantum numbers  $\ell J t$ , the  $\pi N$  scattering equation takes the form given in Eq. (F.27). The  $\pi N$  potential  $V(p', p)$  is given in Ref. [15] due to both a vertex interaction  $f_{\pi N, B}^0$  and a "background" potential  $\mathcal{V}$  (which is assumed to be of a separable form) by

$$V(p', p; E) = \sum_{B=N, \Delta} f_{\pi N, B}^0 g_B^0(E) f_{B, \pi N}^0 + \mathcal{V}, \quad (\text{F.34})$$

where  $g_B^0(E)$  is the free propagator in subspace<sup>5</sup>  $B$  and takes the form

$$g_B^0 = \frac{1}{E - m_{0B}}, \quad (\text{F.35})$$

with  $m_{0B}$  is the bare mass of the baryon  $B$ .

For  $P_{11}$  and  $P_{33}$  channels, both terms in the right-hand-side of Eq. (F.34) are taken into account. Thus the total potential matrix element can be written in terms of *baryon* pole and non-pole parts as follows

$$V(p', p; E) = f_0(p') g_B^0(E) f_0(p) + h_0(p') \lambda_0 h_0(p), \quad (\text{F.36})$$

where  $\lambda_0$  is a phase parameter and it is given in Table H.1. The form factors  $h_0(k)$  and  $f_0(k)$  are parametrized as follows

$$h_0(k) = \frac{a_1 k^{m_1}}{(k^2 + b_1^2)^{n_1}} k^\ell, \quad (\text{F.37})$$

$$f_0(k) = \frac{a_2 k^{m_2}}{(k^2 + b_2^2)^{n_2}} k^\ell. \quad (\text{F.38})$$

The values of the parameters  $n_1$ ,  $n_2$ ,  $m_1$ ,  $m_2$ ,  $a_1$ ,  $a_2$ ,  $b_1$  and  $b_2$  are given in Table H.1 for each partial wave.

By inserting Eq. (F.36) into Eq. (F.27), the  $\pi N$  amplitude can then be written as

$$\mathcal{T}(p', p; E) = T^{NP}(p', p; E) + f(p') g_B(E) f(p). \quad (\text{F.39})$$

The non-pole  $T^{NP}$ -matrix is given by

$$T^{NP}(p', p; E) = h_0(p') \tau_0(E) h_0(p), \quad (\text{F.40})$$

with

$$\tau_0(E) = \frac{\lambda_0}{1 - \lambda_0 \int dk k^2 |h_0(k)|^2 \mathcal{G}_{\pi N}(k, E)}. \quad (\text{F.41})$$

The pole term in Eq. (F.39) consists of a dressed form factor  $f(k_\alpha)$  ( $\alpha = i, f$ ) defined by

$$f(p_\alpha) = f_0(p_\alpha) + \tau_0(E) h_0(p_\alpha) \int dk k^2 h_0(k) f_0(k) \mathcal{G}_{\pi N}(k, E), \quad (\text{F.42})$$

---

<sup>5</sup>Subspace  $S = \sum_{B=N, \Delta} \pi N \oplus B$  describes  $\pi N$  scattering without coupling to photons.

and a dressed propagator  $g_B(E)$  defined by

$$g_B(E) = \frac{1}{E - m_{0B} - \int dk k^2 f(k) f_0(k) \mathcal{G}_{\pi N}(k, E)}. \quad (\text{F.43})$$

For channels other than  $P_{11}$  and  $P_{33}$ , the vertex interaction of Eq. (F.34) does not contribute. The  $\pi N$  potential is then assumed to be of rank 2 separable form

$$\mathcal{V}(p', p) = h_1(p') \lambda_1 h_1(p) + h_2(p') \lambda_2 h_2(p). \quad (\text{F.44})$$

The form factors are parametrized as

$$h_1(k) = \frac{a_1 k^{m_1}}{(k^2 + b_1^2)^{n_1}} k^\ell, \quad (\text{F.45})$$

$$h_2(k) = \frac{a_2 k^{m_2}}{(k^2 + b_2^2)^{n_2}} k^\ell. \quad (\text{F.46})$$

As before, the parameters  $n_1, n_2, m_1, m_2, a_1, a_2, b_1$  and  $b_2$  are given in Table H.1 for each partial wave.

By inserting Eq. (F.44) into Eq. (F.34), one obtains the following analytic solution for the  $\mathcal{T}$ -matrix

$$\begin{aligned} \mathcal{T}(p', p; E) = & h_1(p') \tau_{11}(E) h_1(p) + h_1(p') \tau_{12}(E) h_2(p) \\ & + h_2(p') \tau_{21}(E) h_1(p) + h_2(p') \tau_{22}(E) h_2(p), \end{aligned} \quad (\text{F.47})$$

where

$$\tau_{11}(E) = \frac{\lambda_1(1 - \lambda_2 H_2)}{(1 - \lambda_1 H_1)(1 - \lambda_2 H_2) - \lambda_1 \lambda_2 H_{12}^2}, \quad (\text{F.48})$$

$$\begin{aligned} \tau_{12}(E) &= \tau_{21}(E) \\ &= \frac{\lambda_1 \lambda_2 H_{12}}{(1 - \lambda_1 H_1)(1 - \lambda_2 H_2) - \lambda_1 \lambda_2 H_{12}^2}, \end{aligned} \quad (\text{F.49})$$

$$\tau_{22}(E) = \frac{\lambda_2(1 - \lambda_1 H_1)}{(1 - \lambda_1 H_1)(1 - \lambda_2 H_2) - \lambda_1 \lambda_2 H_{12}^2}, \quad (\text{F.50})$$

with

$$H_1 = \int dk k^2 |h_1(k)|^2 \mathcal{G}_{\pi N}(k, E), \quad (\text{F.51})$$

$$H_2 = \int dk k^2 |h_2(k)|^2 \mathcal{G}_{\pi N}(k, E), \quad (\text{F.52})$$

$$H_{12} = \int dk k^2 h_1(k) h_2(k) \mathcal{G}_{\pi N}(k, E). \quad (\text{F.53})$$

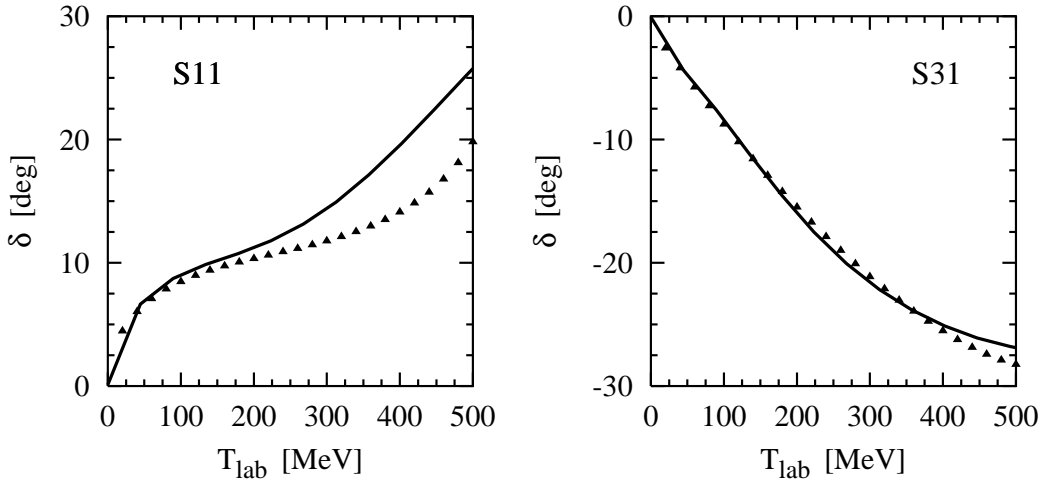


Figure F.8: The  $\pi N$  phase shifts of the  $S$  partial waves obtained from the LS equation using the separable potential model of Nozawa *et al.* [15] shown versus the pion laboratory energy  $T_{lab}$  in MeV. The data points are from the VPI partial wave analysis [28] (Solution: SM99).

### F.2.3 $\pi N$ Phase Shifts

Once the scattering equation given in Eq. (F.33) is solved for the on-shell  $\mathcal{T}$ -matrix, one can obtain the scattering phase shifts. The information about the scattering process is commonly represented by phase shifts  $\delta(E)$  with the on-shell  $S$ -matrix in each channel defined by

$$S(E) = e^{2i\delta(E)}, \quad (\text{F.54})$$

or

$$S(E) = 1 + 2i e^{i\delta(E)} \sin(\delta(E)), \quad (\text{F.55})$$

where  $E(p) = \sqrt{M_N^2 + p^2} + \sqrt{m_\pi^2 + p^2}$  is the invariant total energy of the two interacting particles. The partial wave on-shell  $S$ -matrix is related to the partial wave on-shell  $\mathcal{T}$ -matrix by

$$S(E) = 1 - 2i\pi \rho(p) \mathcal{T}(E), \quad (\text{F.56})$$

where the density of states  $\rho(p)$  is given by

$$\rho(p) = \frac{p^2}{\frac{dE(p)}{dp}} = \frac{pE_N(p)E_\pi(p)}{E_N(p) + E_\pi(p)}. \quad (\text{F.57})$$

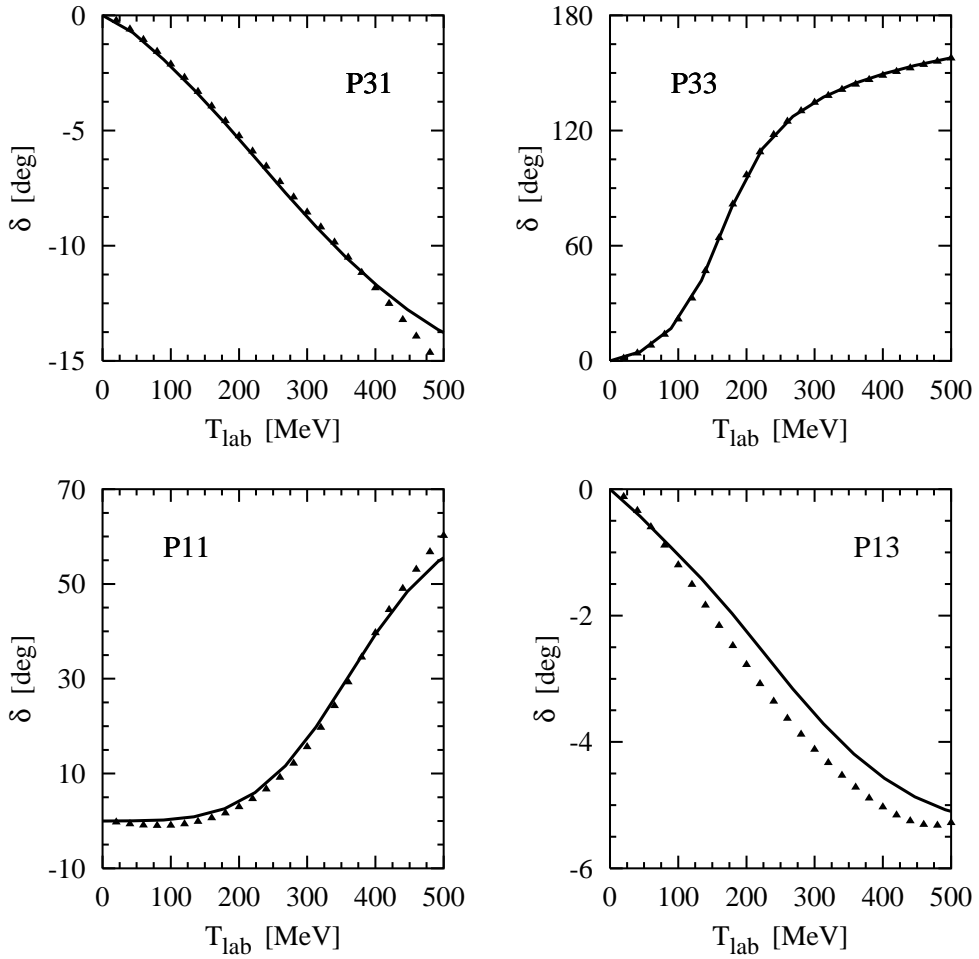


Figure F.9: Same as Fig. F.8 but for the  $P$  partial waves.

Combining Eqs. (F.54) and (F.56) gives

$$\tan(2\delta(E)) = \frac{-2\pi \rho(p) \operatorname{Re}(\mathcal{T}(E))}{1 + 2\pi \rho(p) \operatorname{Im}(\mathcal{T}(E))}. \quad (\text{F.58})$$

Alternatively, we can express the on-shell  $\mathcal{T}$ -matrix in terms of the phase shifts as

$$\mathcal{T}(E) = \frac{-1}{\pi\rho(p)} e^{i\delta(E)} \sin(\delta(E)), \quad (\text{F.59})$$

whence

$$\tan(\delta(E)) = \frac{\operatorname{Im}(\mathcal{T}(E))}{\operatorname{Re}(\mathcal{T}(E))}. \quad (\text{F.60})$$

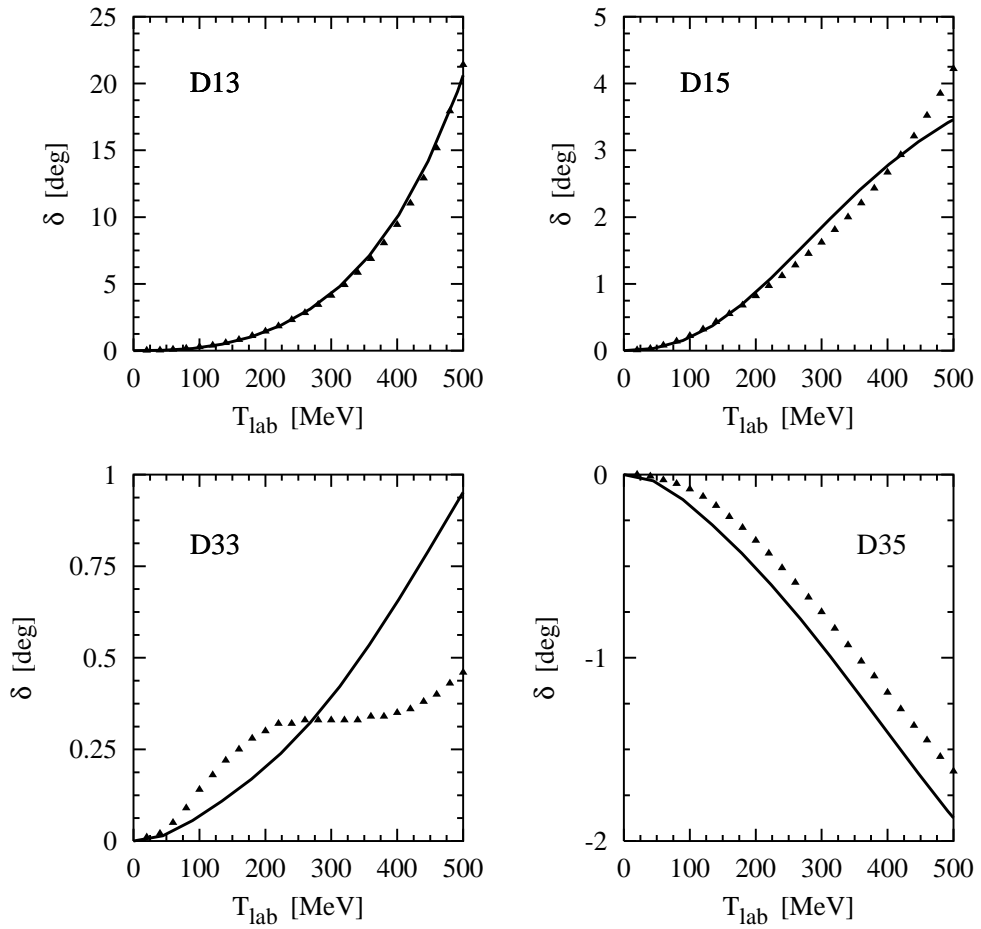


Figure F.10: Same as Fig. F.8 but for the  $D$  partial waves.

The phase shifts calculated from the dynamical model of Nozawa *et al.* [15] for the more important  $\pi N$  partial waves are shown in Figs. F.8-F.10 with the corresponding parameters being given in Table H.1. We see that the Lippmann-Schwinger equation gives a good description of  $\pi N$  phase shifts below 500 MeV. We note in particular the perfect resonance shape of the  $P_{33}$  phase shift (see Fig. F.9) corresponding to the  $\Delta(1232)$  resonance of the nucleon ( $\delta=90^\circ$  at  $T_{lab} \simeq 180$  MeV). The steep rise of the  $P_{11}$  phase shift for  $T_{lab} \rightarrow 500$  MeV is an indication of the Roper resonance  $N(1440)$ . In addition there is some background scattering due to interactions in the  $S_{11}$  and  $S_{31}$  partial waves.

## Appendix G

# Parameters of the $NN$ Separable Potential

We give in this appendix the parameters which we use for the separable  $NN$  interaction of the Graz group [48, 49] in each partial wave.

Table G.1: Parameters of the PEST3 potential in the  $^1S_0$  partial wave.

	$\beta$ (fm $^{-1}$ )	$C$ (fm $^0$ )	$\lambda$ (MeV fm $^{-1}$ )
(p-p)			
	$\beta_{11}=1.1115753$	$C_{11}=-572.29230$	$\lambda_{11}=-0.001021062$
	$\beta_{12}=2.0212320$	$C_{12}=-313.62360$	$\lambda_{12}=0.022965747$
	$\beta_{13}=2.6434278$	$C_{13}=12814.143$	$\lambda_{13}=-0.013907568$
	$\beta_{14}=4.0877911$	$C_{14}=-28477.672$	
	$\beta_{21}=1.0297944$	$C_{21}=-18.494719$	$\lambda_{21}=0.022965747$
	$\beta_{22}=1.5435994$	$C_{22}=-53.628348$	$\lambda_{22}=-0.805816820$
	$\beta_{23}=2.6129194$	$C_{23}=925.42408$	$\lambda_{23}=0.825835300$
	$\beta_{24}=4.0837929$	$C_{24}=-2040.0020$	
	$\beta_{31}=0.8995186$	$C_{31}=-2.8837445$	$\lambda_{31}=-0.013907568$
	$\beta_{32}=2.6843334$	$C_{32}=-84.344154$	$\lambda_{32}=0.825835300$
	$\beta_{33}=3.1505869$	$C_{33}=1163.1547$	$\lambda_{33}=-1.295713900$
	$\beta_{34}=3.9826288$	$C_{34}=-2018.0523$	
(n-p)			
	$\beta_{11}=1.1115753$	$C_{11}=-773.80000$	$\lambda_{11}=-0.000528400$
	$\beta_{12}=2.0212320$	$C_{12}=-424.05244$	$\lambda_{12}=0.015471054$
	$\beta_{13}=2.6434278$	$C_{13}=17326.082$	$\lambda_{13}=-0.008800256$
	$\beta_{14}=4.0877911$	$C_{14}=-38504.839$	
	$\beta_{21}=1.0297944$	$C_{21}=-18.494719$	$\lambda_{21}=0.015471054$
	$\beta_{22}=1.5435994$	$C_{22}=-53.628348$	$\lambda_{22}=-0.742248760$
	$\beta_{23}=2.6129194$	$C_{23}=925.42408$	$\lambda_{23}=0.770689240$
	$\beta_{24}=4.0837929$	$C_{24}=-2040.0020$	
	$\beta_{31}=0.8995186$	$C_{31}=-2.8837445$	$\lambda_{31}=-0.008800256$
	$\beta_{32}=2.6843334$	$C_{32}=-84.344154$	$\lambda_{32}=0.770689240$
	$\beta_{33}=3.1505869$	$C_{33}=1163.1547$	$\lambda_{33}=-1.252847400$
	$\beta_{34}=3.9826288$	$C_{34}=-2018.0523$	

Table G.2: Parameters of the PEST2 potential in the uncoupled  $P$  waves.

	$\beta$ (fm $^{-1}$ )	$C$ (fm $^0$ )	$\lambda$ (MeV fm $^{-3}$ )
$^3P_0$	$\beta_{11} = 1.8691379$	$C_{11} = -189.74407$	$\lambda_{11} = -0.14665888$
	$\beta_{12} = 3.0499866$	$C_{12} = 2096.7281$	$\lambda_{12} = 0.40513783$
	$\beta_{13} = 3.5585752$	$C_{13} = -3066.2694$	
	$\beta_{14} = 1.1596292$	$C_{14} = 102.75384$	
	$\beta_{21} = 2.5512467$	$C_{21} = 59.861550$	$\lambda_{21} = 0.40513783$
	$\beta_{22} = 2.6651826$	$C_{22} = -681.32014$	$\lambda_{22} = -5.47893200$
	$\beta_{23} = 2.9537139$	$C_{23} = 5265.5015$	
	$\beta_{24} = 3.3827130$	$C_{24} = -6825.7570$	
$^3P_1$	$\beta_{11} = 1.6225099$	$C_{11} = 76.181266$	$\lambda_{11} = 0.66973064$
	$\beta_{12} = 2.4712881$	$C_{12} = -381.78599$	$\lambda_{12} = -0.52203105$
	$\beta_{13} = 2.7120059$	$C_{13} = 1471.7803$	
	$\beta_{14} = 3.1642803$	$C_{14} = -1646.4168$	
	$\beta_{21} = 1.7697160$	$C_{21} = 61.335643$	$\lambda_{21} = -0.52203105$
	$\beta_{22} = 2.4049729$	$C_{22} = 1348.5020$	$\lambda_{22} = 0.64075503$
	$\beta_{23} = 1.8631357$	$C_{23} = -842.10204$	
	$\beta_{24} = 4.1084782$	$C_{24} = -1604.2632$	
$^1P_1$	$\beta_{11} = 1.5652079$	$C_{11} = 89.398777$	$\lambda_{11} = 0.44514549$
	$\beta_{12} = 2.0058818$	$C_{12} = -208.13553$	$\lambda_{12} = -0.34067880$
	$\beta_{13} = 2.4100051$	$C_{13} = 425.34413$	
	$\beta_{14} = 4.2981726$	$C_{14} = -630.35239$	
	$\beta_{21} = 1.5463024$	$C_{21} = 43.477263$	$\lambda_{21} = -0.34067880$
	$\beta_{22} = 1.6196926$	$C_{22} = 166.46466$	$\lambda_{22} = 0.44501514$
	$\beta_{23} = 2.0004143$	$C_{23} = -404.03968$	
	$\beta_{24} = 2.1796197$	$C_{24} = 528.13575$	

Table G.3: Parameters of the PEST2 potential in the uncoupled  $D$  waves.

	$\beta$ (fm $^{-1}$ )	$C$ (fm $^0$ )	$\lambda$ (MeV fm $^{-1}$ )
$^1D_2$			
$\beta_{11} = 1.1690501$	$C_{11} = -7.6541157$	$\lambda_{11} = -1.90862530$	
$\beta_{12} = 1.3354235$	$C_{12} = 3.8397789$	$\lambda_{12} = 1.00851240$	
$\beta_{13} = 3.6311131$	$C_{13} = -348.08899$		
$\beta_{14} = 2.9623562$	$C_{14} = 330.93549$		
$\beta_{21} = 0.8715792$	$C_{21} = -1.0867868$	$\lambda_{21} = 1.00851240$	
$\beta_{22} = 1.2853211$	$C_{22} = -22.731322$	$\lambda_{22} = -0.97543827$	
$\beta_{23} = 3.2457085$	$C_{23} = 265.30215$		
$\beta_{24} = 3.8839614$	$C_{24} = -303.60967$		
$^3D_2$			
$\beta_{11} = 1.2055706$	$C_{11} = -40.322168$	$\lambda_{11} = -0.26674102$	
$\beta_{12} = 1.2960008$	$C_{12} = -21.021097$	$\lambda_{12} = 0.14305117$	
$\beta_{13} = 1.6239653$	$C_{13} = 533.48026$		
$\beta_{14} = 1.4452618$	$C_{14} = -436.55162$		
$\beta_{21} = 1.5953203$	$C_{21} = -245.06021$	$\lambda_{21} = 0.14305117$	
$\beta_{22} = 0.3626991$	$C_{22} = 3.0950339$	$\lambda_{22} = -0.15817248$	
$\beta_{23} = 1.7370869$	$C_{23} = 299.77237$		
$\beta_{24} = 0.5873583$	$C_{24} = 42.826073$		

Table G.4: Parameters of the PEST4 potential in the coupled  $^3S_1$ - $^3D_1$  partial wave.

	$\beta$ (fm $^{-1}$ )	$C$ (fm $^0$ )	$\lambda$ (MeV fm $^{-1}$ )
$L = 0$	$\beta_{11} = 1.6855291$	$C_{11} = -51.009539$	$\lambda_{11} = -0.254222420$
	$\beta_{12} = 3.9205339$	$C_{12} = 765.24390$	$\lambda_{12} = -0.171787720$
	$\beta_{13} = 5.7636840$	$C_{13} = -3363.4996$	$\lambda_{13} = 0.071723814$
	$\beta_{14} = 6.0419695$	$C_{14} = 2783.6926$	$\lambda_{14} = 0.005105011$
	$\beta_{21} = 1.7877900$	$C_{21} = -68.041320$	$\lambda_{21} = -0.171787720$
	$\beta_{22} = 2.1759210$	$C_{22} = 488.86119$	$\lambda_{22} = 0.087724390$
	$\beta_{23} = 2.4705717$	$C_{23} = -1199.1640$	$\lambda_{23} = 0.094518781$
	$\beta_{24} = 2.7303931$	$C_{24} = 871.79604$	$\lambda_{24} = -0.079244845$
	$\beta_{31} = 1.5971102$	$C_{31} = -89.517302$	$\lambda_{31} = 0.071723814$
	$\beta_{32} = 9.9678931$	$C_{32} = 2582.2164$	$\lambda_{32} = 0.094518781$
	$\beta_{33} = 4.5948011$	$C_{33} = -3042.3325$	$\lambda_{33} = -0.030645992$
	$\beta_{34} = 2.1206347$	$C_{34} = 1235.3473$	$\lambda_{34} = -0.034997609$
	$\beta_{41} = 4.0268195$	$C_{41} = -382.75856$	$\lambda_{41} = 0.005105011$
	$\beta_{42} = 5.0466356$	$C_{42} = 1005.8091$	$\lambda_{42} = -0.079244845$
	$\beta_{43} = 2.5795951$	$C_{43} = 2298.7534$	$\lambda_{43} = -0.034997609$
	$\beta_{44} = 2.3953665$	$C_{44} = -2718.2533$	$\lambda_{44} = 0.169553430$
$L = 2$	$\beta_{11} = 2.6228398$	$C_{11} = -410.15751$	$\lambda_{11} = -0.254222420$
	$\beta_{12} = 1.8815276$	$C_{12} = 156.64127$	$\lambda_{12} = -0.171787720$
	$\beta_{13} = 3.8346780$	$C_{13} = 888.03985$	$\lambda_{13} = 0.071723814$
	$\beta_{14} = 4.9959386$	$C_{14} = -792.11994$	$\lambda_{14} = 0.005105011$
	$\beta_{21} = 1.9098545$	$C_{21} = 87.065827$	$\lambda_{21} = -0.171787720$
	$\beta_{22} = 1.1170776$	$C_{22} = 20.554605$	$\lambda_{22} = 0.087724390$
	$\beta_{23} = 1.4259853$	$C_{23} = -65.702538$	$\lambda_{23} = 0.094518781$
	$\beta_{24} = 3.0734784$	$C_{24} = -91.839262$	$\lambda_{24} = -0.079244845$
	$\beta_{31} = 2.6431889$	$C_{31} = 143.62150$	$\lambda_{31} = 0.071723814$
	$\beta_{32} = 2.7483825$	$C_{32} = 6.4744841$	$\lambda_{32} = 0.094518781$
	$\beta_{33} = 1.9283993$	$C_{33} = -1384.0981$	$\lambda_{33} = -0.030645992$
	$\beta_{34} = 2.2891433$	$C_{34} = 1550.1289$	$\lambda_{34} = -0.034997609$
	$\beta_{41} = 4.2598369$	$C_{41} = 366.50118$	$\lambda_{41} = 0.005105011$
	$\beta_{42} = 2.1463834$	$C_{42} = 263.87202$	$\lambda_{42} = -0.079244845$
	$\beta_{43} = 2.4905282$	$C_{43} = -611.66811$	$\lambda_{43} = -0.034997609$
	$\beta_{44} = 2.2930841$	$C_{44} = -12.606207$	$\lambda_{44} = 0.169553430$

Table G.5: Parameters of the PEST3 potential in the coupled  ${}^3P_2$ - ${}^3F_2$  partial wave.

	$\beta$ (fm $^{-1}$ )	$C$ (fm $^0$ )	$\lambda$ (MeV fm $^{-3}$ )
$L = 1$			
	$\beta_{11} = 1.4452936$	$C_{11} = -28.609391$	$\lambda_{11} = 0.04672503$
	$\beta_{12} = 2.0173835$	$C_{12} = -186.15068$	$\lambda_{12} = 0.41710484$
	$\beta_{13} = 5.4463467$	$C_{13} = -1094.0574$	$\lambda_{13} = -0.06092248$
	$\beta_{14} = 2.8490316$	$C_{14} = 1022.0712$	
	$\beta_{21} = 1.8993563$	$C_{21} = 65.794074$	$\lambda_{21} = 0.41710484$
	$\beta_{22} = 2.4547294$	$C_{22} = 173.01447$	$\lambda_{22} = 0.25492496$
	$\beta_{23} = 1.5499793$	$C_{23} = -190.40569$	$\lambda_{23} = -0.41481703$
	$\beta_{24} = 5.9773387$	$C_{24} = -217.74704$	
	$\beta_{31} = 2.9659955$	$C_{31} = -327.40790$	$\lambda_{31} = -0.06092248$
	$\beta_{32} = 4.9324835$	$C_{32} = -2950.6615$	$\lambda_{32} = -0.41481703$
	$\beta_{33} = 2.9051889$	$C_{33} = 4127.4473$	$\lambda_{33} = -0.13593596$
	$\beta_{34} = 2.0463803$	$C_{34} = -1298.0249$	
$L = 3$			
	$\beta_{11} = 1.1667491$	$C_{11} = 0.96744407$	$\lambda_{11} = 0.04672503$
	$\beta_{12} = 1.5406619$	$C_{12} = 166.30912$	$\lambda_{12} = 0.41710484$
	$\beta_{13} = 2.3802869$	$C_{13} = -119.42176$	$\lambda_{13} = -0.06092248$
	$\beta_{14} = 4.8335309$	$C_{14} = 366.96981$	
	$\beta_{21} = 1.0955323$	$C_{21} = -0.6386842$	$\lambda_{21} = 0.41710484$
	$\beta_{22} = 1.6020596$	$C_{22} = -37.538146$	$\lambda_{22} = 0.25492496$
	$\beta_{23} = 4.4585234$	$C_{23} = -316.97599$	$\lambda_{23} = -0.41481703$
	$\beta_{24} = 1.8254989$	$C_{24} = 179.59323$	
	$\beta_{31} = 2.1084981$	$C_{31} = -47.364933$	$\lambda_{31} = -0.06092248$
	$\beta_{32} = 3.1977404$	$C_{32} = 2035.5781$	$\lambda_{32} = -0.41481703$
	$\beta_{33} = 3.9573349$	$C_{33} = -5925.4169$	$\lambda_{33} = -0.13593596$
	$\beta_{34} = 4.5120514$	$C_{34} = 5407.1036$	

Table G.6: Parameters of the PEST4 potential in the coupled  $^3D_3$ - $^3G_3$  partial wave.

	$\beta$ (fm $^{-1}$ )	$C$ (fm $^0$ )	$\lambda$ (MeV fm $^{-1}$ )
$L = 2$	$\beta_{11} = 1.7275071$	$C_{11} = -8.6379311$	$\lambda_{11} = -0.09899224$
	$\beta_{12} = 2.5493316$	$C_{12} = 178.84657$	$\lambda_{12} = -0.39484562$
	$\beta_{13} = 1.9111954$	$C_{13} = -114.21507$	$\lambda_{13} = 0.04013528$
	$\beta_{14} = 4.0669172$	$C_{14} = -86.040765$	$\lambda_{14} = 0.11343039$
	$\beta_{21} = 1.9189644$	$C_{21} = -116.07858$	$\lambda_{21} = -0.39484562$
	$\beta_{22} = 2.7381690$	$C_{22} = 354.48169$	$\lambda_{22} = 0.28242764$
	$\beta_{23} = 1.5396020$	$C_{23} = 196.12620$	$\lambda_{23} = 0.40048398$
	$\beta_{24} = 1.9159334$	$C_{24} = -419.69957$	$\lambda_{24} = -0.34677241$
	$\beta_{31} = 3.2277180$	$C_{31} = -110.31148$	$\lambda_{31} = 0.04013528$
	$\beta_{32} = 4.8060158$	$C_{32} = 483.29454$	$\lambda_{32} = 0.40048398$
	$\beta_{33} = 3.1005090$	$C_{33} = 442.80069$	$\lambda_{33} = -0.14224121$
	$\beta_{34} = 3.7214195$	$C_{34} = -903.63957$	$\lambda_{34} = -0.38000970$
	$\beta_{41} = 2.8426813$	$C_{41} = -364.88710$	$\lambda_{41} = 0.11343039$
	$\beta_{42} = 3.3549103$	$C_{42} = 1848.1193$	$\lambda_{42} = -0.34677241$
	$\beta_{43} = 3.2121201$	$C_{43} = 2550.6547$	$\lambda_{43} = -0.38000970$
	$\beta_{44} = 2.7766588$	$C_{44} = -3985.0257$	$\lambda_{44} = 0.50560372$
$L = 4$	$\beta_{11} = 2.4000943$	$C_{11} = 10.076418$	$\lambda_{11} = -0.09899224$
	$\beta_{12} = 1.2830437$	$C_{12} = -90.394797$	$\lambda_{12} = -0.39484562$
	$\beta_{13} = 1.6627122$	$C_{13} = 283.81707$	$\lambda_{13} = 0.04013528$
	$\beta_{14} = 1.5581999$	$C_{14} = -204.52799$	$\lambda_{14} = 0.11343039$
	$\beta_{21} = 3.9194456$	$C_{21} = 10.924992$	$\lambda_{21} = -0.39484562$
	$\beta_{22} = 1.5719585$	$C_{22} = 82.607174$	$\lambda_{22} = 0.28242764$
	$\beta_{23} = 1.6553410$	$C_{23} = -132.30266$	$\lambda_{23} = 0.40048398$
	$\beta_{24} = 2.0963683$	$C_{24} = 47.770331$	$\lambda_{24} = -0.34677241$
	$\beta_{31} = 4.8032746$	$C_{31} = -204.05105$	$\lambda_{31} = 0.04013528$
	$\beta_{32} = 3.6976328$	$C_{32} = -751.61370$	$\lambda_{32} = 0.40048398$
	$\beta_{33} = 2.7214754$	$C_{33} = 1886.8354$	$\lambda_{33} = -0.14224121$
	$\beta_{34} = 1.9739909$	$C_{34} = -954.91540$	$\lambda_{34} = -0.38000970$
	$\beta_{41} = 1.8399157$	$C_{41} = -0.2429913$	$\lambda_{41} = 0.11343039$
	$\beta_{42} = 2.0748484$	$C_{42} = 197.58830$	$\lambda_{42} = -0.34677241$
	$\beta_{43} = 2.2831760$	$C_{43} = -411.75699$	$\lambda_{43} = -0.38000970$
	$\beta_{44} = 2.6095142$	$C_{44} = 229.35025$	$\lambda_{44} = 0.50560372$



## Appendix H

# Parameters of the $\pi N$ Separable Potential

Table H.1: Parameters of the  $\pi N$  separabel potential of Nozawa *et al.* [15] for the  $\pi N$  partial waves. These parameters are determined by fitting the phase shift data [76] up to 500 MeV pion laboratory kinetic energy.

$L_{2t,2J}$	$\ell$	$m_1$	$n_1$	$a_1^\dagger$	$b_1^\S$	$m_2$	$n_2$	$a_2^\ddagger$	$b_2^\S$	$\lambda_0$
$S_{11}$	0	0	3	100.00	2.598	2	2	4.9520	2.877	-1
$S_{31}$	0	0	2	3.0850	1.806	2	2	1.9250	1.275	+1
$P_{11}$	1	2	3	31.623	2.665	0	2	0.5793	1.185	-1
$P_{13}$	1	0	2	0.4269	1.181	2	3	3.9700	1.721	+1
$P_{31}$	1	0	2	1.4730	1.542	2	3	8.0530	1.861	+1
$P_{33}$	1	0	2	2.7700	1.415	0	2	1.7780	1.218	+1
$D_{13}$	2	0	2	1.6390	2.165 $\ddagger$	2	3	9.3120	3.263	-1
$D_{15}$	2	0	2	0.2172	1.175	2	3	1.0110	1.461	-1
$D_{33}$	2	0	2	0.1306	1.128	2	3	1.0810	1.972	-1
$D_{35}$	2	0	2	0.2270	1.168	2	3	1.1510	1.780	+1

$\dagger$   $a_1$  is given in units of  $(\text{fm})^{-2n_1+m_1+\ell+1}$ .

$\ddagger$   $a_2$  is given in units of  $(\text{fm})^{-2n_2+m_2+\ell+\frac{1}{2}}$  for  $P_{11}$  and  $P_{33}$  partial waves, otherwise it is given in units of  $(\text{fm})^{-2n_2+m_2+\ell+1}$ .

$\S$   $b_1$  and  $b_2$  are given in units of  $(\text{fm})^{-1}$ .

$\ddagger$  This value is a missprint in Table 2 of Ref. [15]. We would like to thank Professor S. Nozawa for giving us the correct one.



# Bibliography

- [1] YUKAWA, H., *Photoproduction of Positive Pions*, Proc. Phys. Math. Soc. Japan **17** (1935), 48.
- [2] LATTES, C. M. G., MUIRHEAD, H., OCCHIALINI, G. P. S. AND POWELL, C. F., *Processes Involving Charged Mesons*, Nature **159** (1947), 694.
- [3] CHEW, G. F., GOLDBERGER, M. L., LOW, F. E., AND NAMBU, Y., *Relativistic Dispersion Relation Approach to Photomeson Production*, Phys. Rev. **106** (1957), 1345.
- [4] KROLL, N. M. AND RUDERMANN, M. A., *A Theorem on Photomeson Production Near Threshold and the Suppression of Pairs in Pseudoscalar Meson Theory*, Phys. Rev. **93** (1954), 233.
- [5] FUBINI, S., FURLAN, G. AND ROSSETTI, C., *A Dispersion Theory of Symmetry Breaking*, IL Nuovo Cimento **40** (1965), 1171.
- [6] BERENDS, F. A., DONNACHIE, A. AND WEAVER, D. L., *Photoproduction and Electroproduction of Pions: (I) Dispersion Relation Theory*, Nucl. Phys. **B4** (1967), 1; BERENDS, F. A., DONNACHIE, A. AND WEAVER, D. L., *Photoproduction and Electroproduction of Pions: (II) Photopion Production Below 500 MeV*, Nucl. Phys. **B4** (1967), 54; BERENDS, F. A., DONNACHIE, A. AND WEAVER, D. L., *Photoproduction and Electroproduction of Pions: (III)  $\omega$  and  $B$  Exchange in Low Energy  $\pi^0$  Photoproduction*, Nucl. Phys. **B4** (1967), 103.
- [7] OLSSON, M. G., AND OSYPOWSKI, E. T., *A Pole Model Calculation of the Photoproduction Multipoles in the  $\Delta(1220)$  Region*, Nucl. Phys. **B87** (1975), 399.
- [8] OLSSON, M. G., AND OSYPOWSKI, E. T., *Vector-Meson-Exchange and Unitarity Effects in Low-Energy Photoproduction*, Phys. Rev. **D17** (1978), 174.

[9] TANABE, H. AND OHTA, K., *Dynamical Model for Pion Photoproduction in the Delta Region*, Phys. Rev. **C31** (1985), 1876.

[10] DONNACHIE, A., *Photo- and Electroproduction Processes*, in *High Energy Physics* Vol. 5, edited by E. H. S. Burhop, Academic Press, New York, 1972.

[11] BLOMQVIST, I. AND LAGET, J. M., *A Non-Relativistic Operator Convenient for Analysis of Pion Photoproduction on Nuclei in the  $\Delta(1236)$  Region*, Nucl. Phys. **A280** (1977), 405.

[12] LAGET, J. M., *Pion Photoproduction on Few-Body Systems*, Phys. Rep. **69** (1981), 1.

[13] LAGET, J. M., *Electromagnetic Properties of the  $\pi NN$  System: (I) The Reaction  $\gamma D \rightarrow \pi NN$* , Nucl. Phys. **A296** (1978), 388.

[14] BOSTED, P. AND LAGET, J. M., *Electromagnetic Properties of the  $\pi NN$  system: II. The  $\gamma d \rightarrow d\pi^0$  reaction*, Nucl. Phys. **A296** (1978), 413.

[15] NOZAWA, S., BLANKLEIDER, B. AND LEE, T.-S. H., *A Dynamical Model of Pion Photoproduction on the Nucleon*, Nucl. Phys. **A513** (1990), 459.

[16] GARCILAZO, H. AND MOYA DE GUERRA, E., *A model for Pion Electro- and Photoproduction from Threshold up to 1 GeV*, Nucl. Phys. **A562** (1993), 521.

[17] DRECHSEL, D., HANSTEIN, O., KAMALOV, S. S. AND TIATOR, L., *MAID Program*, Institut für Kernphysik, Johannes Gutenberg-Universität, Mainz, Germany, <http://www.kph.uni-mainz.de/de/MAID/maid2000/>.

[18] CHEW, G. F. AND LEWIS, H. W., *A Phenomenological Treatment of Photomeson Production from Deuterons*, Phys. Rev. **84** (1951), 779.

[19] LAX, M. AND FESHBACH, H., *Photoproduction of Mesons in Deuterium*, Phys. Rev. **88** (1952), 509.

[20] LAGET, J. M., *The Effect of Pion Rescattering Through the  $\Delta(1236)$  on the  $\gamma D \rightarrow pp\pi^-$  Reaction for High Nucleon Momentum*, Phys. Lett. **B68** (1977), 58.

[21] BENZ, P. *et al.*, *Measurement of the Reaction  $\gamma d \rightarrow \pi^- pp$ , and Determination of Cross Sections for the Reaction  $\gamma n \rightarrow \pi^- p$ , at Photon Energies Between 0.2 and 2.0 GeV*, Nucl. Phys. **B65** (1973), 158.

[22] KRUSCHE, B. *et al.*, *Single and Double  $\pi^0$ -Photoproduction from the Deuteron*, Eur. Phys. J. **A6** (1999), 309.

[23] SCHMIDT, R., ARENHÖVEL, H. AND WILHELM, P., *Quasifree Pion Photoproduction on the Deuteron in the  $\Delta$  Region*, Z. Phys. **A355** (1996), 421; SCHMIDT, R., *Photoproduktion geladener Pionen am Deuteron im Bereich der Deltaresonanz*, Diplomarbeit, Institut für Kernphysik, Johannes Gutenberg-Universität, Mainz, 1995.

[24] LEVCHUK, M. I., PETRUN'KIN, V. A. AND SCHUMACHER, M.,  $\pi^0$  Photoproduction on Quasi-Free Neutrons in the Reaction  $\gamma d \rightarrow \pi^0 np$  in the  $\Delta$  Region, Z. Phys. **A 355** (1996), 317.

[25] LEVCHUK, M. I., SCHUMACHER, M. AND WISSMANN, F., The Inclusive Reaction  $d(\gamma, \pi)NN$  in the First Resonance Region, nucl-th/0011041.

[26] BECK, R. *et al.*, Measurement of the  $E2/M1$  Ratio in the  $N \rightarrow \Delta$  Transition using the Reaction  $p(\vec{\gamma}, p)\pi^0$ , Phys. Rev. Lett. **78** (1997), 606; BECK, R. *et al.*, Determination of the  $E2/M1$  Ratio in the  $\gamma N \rightarrow \Delta(1232)$  Transition from a Simultaneous Measurement of  $p(\vec{\gamma}, p)\pi^0$  and  $p(\vec{\gamma}, \pi^+)n$ , Phys. Rev. **C61** (2000), 035204; KRAHN, H.-P., Messung der Photonasymmetrien für die geladene und neutrale Pionphotoproduktion am Proton und das  $E2/M1$  Verhältnis, Dissertation, Institut für Kernphysik, Johannes Gutenberg-Universität, Mainz, 1996.

[27] HANSTEIN, O., DRECHSEL, D. AND TIATOR, L., Multipole Analysis of Pion Photoproduction Based on Fixed  $t$  Dispersion Relations and Unitarity Nucl. Phys. **A632** (1998), 561.

[28] ARNDT, R. A. *et al.*, The Scattering Analysis Interactive Dial-In Program (SAID), data available via telnet to VTINTE.PHYS.VT.EDU, Virginia Polytechnic Institute, Blacksburg, Virginia. For further references see, for example, ARNDT, R. A., STRAKOVSKY, I. I. AND WORKMAN, R. L., Updated Resonances Photodecay Amplitudes to 2 GeV, Phys. Rev. **C53** (1996), 430; ARNDT, R. A., WORKMAN, R. L., LI, Z. AND ROPER, L. D., Partial-Wave Analysis of Pion Photoproduction, Phys. Rev. **C42** (1990), 1853.

[29] BLAAZER, F., Rescattering Effects in Coherent Pion Production on the Deuteron, Nucl. Phys. **A590** (1995), 750.

[30] WILHELM, P. AND ARENHÖVEL, H., Coherent Pion Photoproduction on the Deuteron in the  $\Delta$  Resonance Region, Nucl. Phys. **A593** (1995), 435; WILHELM, P., Kohärente Photopionproduktion am Deuteron und Deuteron-photospaltung im Bereich der Deltaresonanz, Dissertation, Institut für Kernphysik, Johannes Gutenberg-Universität, Mainz, 1992; WILHELM, P. AND ARENHÖVEL, H., Rescattering Effects in Coherent Pion Photoproduction on the Deuteron in the  $\Delta$  Resonance Region, Nucl. Phys. **A609**, (1996) 469.

[31] KAMALOV, S., TIATOR, L. AND BENNHOLD, C., *Coherent  $\pi^0$  and  $\eta$  Photo-production on the Deuteron*, Phys. Rev. **C55**, (1997) 98.

[32] JOACHAIN, C. J., *Quantum Collision Theory*, North-Holland Publishing Company, Amsterdam, New York, Oxford, 1979.

[33] ARNDT, R. A. LI, Z., ROPER, L. D. AND WORKMAN, R. L., *Determination of the  $\pi NN$  Coupling Constant from Elastic Pion-Nucleon Scattering Data*, Phys. Rev. Lett. **65** (1990), 157.

[34] DAVIDSON, R. M., MUKHOPADHYAY, N. C. AND WITTMAN, R. S., *Effective-Lagrangian Approach to the Theory of Pion Photoproduction in the  $\Delta(1232)$  Region*, Phys. Rev. **D43** (1991), 71.

[35] WEBER, H. J. AND ARENHÖVEL, H., *Isobar Configurations in Nuclei*, Phys. Rep. **36** (1978), 277.

[36] KOCH, J. H., OHTSUKA, N. AND MONIZ, E. J., *Nuclear Photoabsorption and Compton Scattering at Intermediate-Energy*, Ann. Phys. **154** (1984), 99.

[37] PÖPPING, H., SAUER, P. U., AND ZHANG, X.-Z., *The Two-Nucleon System above Pion Threshold: A Force Model with  $\Delta$ -Isobar and Pion Degrees of Freedom*, Nucl. Phys. **A474** (1987), 557.

[38] LEUKEL, R., *Photoproduktion neutraler Pionen am Proton mit linear polarisierten Photonen im Bereich der  $\Delta(1232)$ -Resonanz*, Dissertation, Institut für Kernphysik, Johannes Gutenberg-Universität, Mainz, 2001.

[39] PREOBRAJENSKI, I., *Untersuchung der Helizitätsabhängigkeit der Einpionphotoproduktion am Proton*, Dissertation, Institut für Kernphysik, Johannes Gutenberg-Universität, Mainz, 2001.

[40] FUJII, T. *et al.*, *Photoproduction of Charged  $\pi$  Mesons from Protons and Neutrons in the Energy Range Between 250 and 790 MeV*, Nucl. Phys. **B120** (1977), 395.

[41] BAGHERI, A. *et al.*, *Reaction  $\pi^- p \rightarrow \gamma n$  below the  $\Delta$  resonance*, Phys. Rev. **C38** (1988), 875.

[42] HÄRTER, F., *Photoproduktion neutraler Pionen am Proton im ersten und zweiten Resonanzgebiet*, Dissertation, Institut für Kernphysik, Johannes Gutenberg-Universität, Mainz, 1996.

- [43] BJORKEN, J. D. AND DRELL, S. D., *Relativistic Quantum Mechanics*, McGraw-Hill, New York, 1964.
- [44] BYCKLING, E. AND KAJANTIE, K., *Particle Kinematics*, John Wiley & Sons, London, New York, Sydney, Toronto, 1973.
- [45] MACHELEIDT, R., HOLINDE, K. AND ELSTER, CH., *The Bonn Meson-Exchange Model for the Nucleon-Nucleon Interaction*, Phys. Rep. **149** (1987), 1; MACHELEIDT, R., *The Meson Theory of Nuclear Forces and Nuclear Structure*, Adv. Nucl. Phys. **19** (1989), 189.
- [46] MESSIAH, A., *Quantum Mechanics II*, North-Holland Publishing Company, Amsterdam, 1964.
- [47] LIPPMANN, J. AND SCHWINGER, W., *Separable approximations of two-body interactions*, Phys. Rev. **84** (1951), 1232.
- [48] HAIDENBAUER, J. AND PLESSAS, W., *Separable representation of the Paris nucleon-nucleon potential*, Phys. Rev. **C30** (1984), 1822.
- [49] HAIDENBAUER, J. AND PLESSAS, W., *Modified Separable Representation of the Paris Nucleon-Nucleon Potential in the  $^1S_0$  and  $^3P_0$  States*, Phys. Rev. **C32** (1985), 1424.
- [50] BENMERROUCHE, M. AND TOMUSIAK, E.,  $\gamma D \rightarrow \pi^0 D$  Reaction in the Threshold Region, Phys. Rev. **C58** (1998), 1777.
- [51] KOCH, J. H. AND WOLOSHYN, R. M., Near Threshold Photoproduction of Neutral Pions from the Deuteron, Phys. Rev. **C16** (1977), 1968.
- [52] LEVCHUK, M. I., SCHUMACHER, M. AND WISSMANN, F., *The Reaction  $^2H(\gamma, \pi^0)np$  in the Threshold Region*, Nucl. Phys. **A 675** (2000), 621.
- [53] CHIEFARI, G., DRAGO, E., NAPOLITANO, M. AND SCIACCA, C., *Total Cross Section Measurement of  $\pi^-$  Photoproduction on Deuteron in the First Resonance Region*, Lett. Nuovo Cim. **13** (1975), 129.
- [54] ASAI, M. *et al.*, *Total Cross Section for the  $\gamma d \rightarrow \pi^- pp$  Reaction Between 380 and 840 MeV*, Phys. Rev. **C42** (1990), 837.
- [55] SABUTIS, J. I., *Photopion Production with Nonresonant Delta(33) Background Interference*, Phys. Rev. **C27** (1983), 778.

[56] SALAM, A., *Rescattering Effects in Kaon Photoproduction on the Deuteron*, Dissertation, Institut für Kernphysik, Johannes Gutenberg-Universität, Mainz (in preparation).

[57] GERASIMOV, S. B., *A Sum Rule for Magnetic Moments and the Damping of the Nucleon Magnetic Moment in Nuclei*, *Yad. Fiz.* **2** (1965), 598 (Sov. J. Nucl. Phys. **2** (1966), 430).

[58] DRELL, S. D. AND HEARN, A. C., *Exact Sum Rule for Nucleon Magnetic Moments*, *Phys. Rev. Lett.* **16** (1966), 908.

[59] ARENHÖVEL, H., *Electroweak Processes in Few-Nucleon Systems*, *Few-Body Syst.* **26** (1999), 43; ARENHÖVEL, H., KRESS, G., SCHMIDT, R. AND WILHELM, P., *On the Gerasimov-Drell-Hearn Sum Rule for the Deuteron*, *Phys. Lett.* **B407** (1997), 1; ARENHÖVEL, H., KRESS, G., SCHMIDT, R. AND WILHELM, P., *On the Gerasimov-Drell-Hearn Sum Rule for the Deuteron*, *Nucl. Phys.* **A631** (1998), 612c; KRESS, G., *Die Gerasimov-Drell-Hearn-Summenregel am Deuteron*, Diplomarbeit, Institut für Kernphysik, Johannes Gutenberg-Universität, Mainz, 1996.

[60] HORNIDGE, D., *Threshold  $\pi^0$  Production from Deuterium in  $d(\gamma, \pi^0 n)p$* , Invited talk given at the LOwq Workshop on *Electromagnetic Nuclear Reactions at Low Momentum Transfer*, August 23-25, 2001, Halifax, Nova Scotia, Canada.

[61] MERKEL, H., *Threshold Electroproduction of Neutral Pions at Low  $q^2$  Off the Proton and Off the Deuteron*, *Prog. Part. Nucl. Phys.* **44** (2000), 433; MERKEL, H., *Experimental Tests of Chiral Symmetry*, Invited talk given at the 9th International Conference on *The Structure of Baryons*, March 3-8, 2002, JLab, Newport News, Virginia 23606, USA; EWALD, I. *et al.*, *Coherent  $\pi^0$  Threshold Production from the Deuteron at  $Q^2 = 0.1$  Gev $^2/c^2$* , *Phys. Lett. B499* (2001), 238; EWALD, I., *Kohärente Electropproduktion von neutralen Pionen am Deuteron nahe der Schwelle*, Dissertation, Institut für Kernphysik, Johannes Gutenberg-Universität, Mainz, 2000.

[62] ERICSON, T. AND WEISE, W., *Pions and Nuclei*, Clarendon Press, Oxford, 1988.

[63] DRECHSEL, D. AND TIATOR, L., *Threshold Pion Photoproduction on Nucleons*, *J. Phys. G: Nucl. Part. Phys.* **18** (1992), 449.

[64] WEINBERG, S., *The Quantum Theory of Fields I: Foundations*, Cambridge University Press, 1995.

- [65] PILKUN, H. M., *Relativistic Particle Physics*, Springer-Verlag, New York, Heidelberg, Berlin, 1979.
- [66] GARCILAZO, H. AND MIZUTANI, T.,  $\pi NN$  *Systems*, World Scientific, Singapore, 1990 (see also references therein).
- [67] ERNST, D. J., SHAKIN, C. M. AND THALER, R. M., *Separable representation of two-body interactions*, Phys. Rev. **C8** (1973), 46; ERNST, D. J., SHAKIN, C. M. AND THALER, R. M., *Separable representation of T-matrices valid in the vicinity of off-shell points*, Phys. Rev. **C9** (1974), 1780.
- [68] LACOMBE, M. *et al.*, *Parametrization of the Paris NN Potential*, Phys. Rev. **C21** (1980), 861.
- [69] VINH MAU, R., in *Mesons in Nuclei I*, edit by R. D. Wilkinson *et al.*, Plenum, London, 1979.
- [70] ZANKEL, H., PLESSAS, W. AND HAIDENBAUER, J., *Sensitivity of  $N - d$  Polarization Observables on the Off-Shell Behaviour of the NN Interaction*, Phys. Rev. **C28** (1983), 538; ZANKEL, H. AND PLESSAS, W., *Off-Shell Effects in Nucleon-Deuteron Polarization Observables*, Z. Phys. **A317** (1984), 45.
- [71] ARNDT, R. A. *et al.*, *Nucleon-Nucleon Partial-Wave Analysis to 1 GeV*, Phys. Rev. **D28** (1983), 97.
- [72] SCHWAMB, M., *Retardierungseffekte in der Deuteronphotospaltung im Bereich der Deltaresonanz*, Dissertation, Institut für Kernphysik, Johannes Gutenberg-Universität, Mainz, 1999.
- [73] STAPP, H. P., YPSILANTIS, T. J. AND METROPOLIS, N., *Phase Shift Analysis of 310-MeV Proton-Proton Scattering Experiments*, Phys. Rev. **105** (1957), 302.
- [74] ELMESSIRI, Y. AND FUDA, M. G., *Poincare Invariant Coupled Channel Model for the Pion Nucleon System II: An Extended Model*, Phys. Rev. **C57** (1998), 2149.
- [75] FUDA, M. G., *Poincare Invariant Coupled Channel Model for the Pion Nucleon System*, Phys. Rev. **C52** (1995), 2875.
- [76] HÖHLER, G., KAISER, F., KOCH, R. AND PIETARINEN, E., *Handbook of Pion-Nucleon Scattering*, Physics Data 12-1, Karlsruhe, (1979).

# Chapter 1

## Polarization Observables

Polarization observables have the promise of opening a new field in the electromagnetic production of pions from protons and nuclear targets. From this point of view we give in this chapter the formal expressions of all possible polarization observables in the  $\gamma d \rightarrow \pi NN$  reaction with polarized photons and oriented deuterons in terms of the  $\mathcal{M}$ -matrix elements. The importance of this process derives from the fact that the deuteron, being the simplest nuclear system, plays a similar fundamental role in nuclear physics as the hydrogen atom plays in atomic physics.

The initial state for photoproduction of  $\pi$ -mesons on the deuteron is characterized by the incoming photon polarization  $m_\gamma$  and the deuteron spin projection  $m_d$  with respect to a chosen quantization axis, in our case for convenience the incoming photon momentum  $\vec{k}$ . Thus we associate a frame of reference with  $z$ -axis in the direction of  $\vec{k}$ .

The final state is described by the two-nucleon relative momentum  $\vec{p}_r$  having the spherical coordinates  $\theta_r$  and  $\phi_r$  with respect to the chosen frame of reference, by the total spin  $s$  and its spin projection  $m_s$  on  $\vec{p}_r$  and by the pion momentum  $\vec{q}$  having the spherical coordinates  $\theta_\pi$  and  $\phi_\pi$ . The  $x$ - $z$ -plane is determined by the outgoing pion, i.e.  $\phi_\pi = 0$ . This means that the  $\mathcal{M}$ -matrix is spherical harmonics depending on the pion momentum and its direction.

Choosing the  $z$ -axis in the direction of the incoming photon and isolating the azimuthal dependence of the direction of pion momentum, we obtain the following general form for the reaction matrix

$$\mathcal{M}_{sm_s, m_\gamma m_d}^{(t\mu)}(\theta_\pi, \phi_\pi) = \mathcal{O}_{sm_s, m_\gamma m_d}^{(t\mu)}(\theta_\pi) e^{i(m_\gamma + m_d)\phi_\pi}. \quad (1.1)$$

Using parity conservation one can show that the  $\mathcal{M}$ -matrix elements obey the following symmetry relation

$$\mathcal{O}_{s, -m_s, -m_\gamma, -m_d}^{(t\mu)} = (-)^{s+m_s+m_\gamma+m_d} \mathcal{O}_{s, m_s, m_\gamma, m_d}^{(t\mu)}. \quad (1.2)$$

This symmetry relation reduces the number of complex amplitudes from 24 to 12 independent ones. For their determination one needs 23 real observables since a overall phase remains arbitrary.

For a given  $\mathcal{M}$ -matrix one can compute the cross section for arbitrary polarized photons and initial deuterons by applying the density matrix formalism similar to that given by Arenhövel [2] for deuteron photodisintegration. The most general expression for all observables is given by

$$\mathcal{O} = \rho_s \sum_{\substack{sm_s t, m_\gamma m_d \\ s' m'_s t', m'_\gamma m'_d}} (\mathcal{M}_{s' m'_s, m'_\gamma m'_d}^{(t' \mu')})^* \vec{\Omega}_{s' m'_s sm_s} \mathcal{M}_{sm_s, m_\gamma m_d}^{(t\mu)} \rho_{m_\gamma m'_\gamma}^\gamma \rho_{m_d m'_d}^d d\Omega_{\vec{p}_r}, \quad (1.3)$$

where  $\rho_{m_\gamma m'_\gamma}^\gamma$  and  $\rho_{m_d m'_d}^d$  denote the density matrices of initial photon polarization and deuteron orientation, respectively, and  $\vec{\Omega}$  is an operator associated with the observable which acts in the two-nucleon spin space. The kinematical phase space factor  $\rho_s$  is given in [1]. For more details about the density matrices we refer to [2].

For a given  $\mathcal{M}$ -matrix all polarization observables can be expressed in terms of the following quantities

$$\begin{aligned} V_{IM} &= \frac{1}{\sqrt{3}} \sum_{m'_d m_d} \sum_{sm_s t, m_\gamma} (-)^{1-m'_d} \hat{I} \begin{pmatrix} 1 & 1 & I \\ m_d & -m'_d & -M \end{pmatrix} \\ &\quad \times \int \rho_s (\mathcal{M}_{sm_s, m_\gamma m_d}^{(t\mu)})^* \mathcal{M}_{sm_s, m_\gamma m'_d}^{(t\mu)} d\Omega_{\vec{p}_r}, \end{aligned} \quad (1.4)$$

and

$$\begin{aligned} W_{IM} &= \frac{1}{\sqrt{3}} \sum_{m'_d m_d} \sum_{sm_s t, m_\gamma} (-)^{1-m'_d} \hat{I} \begin{pmatrix} 1 & 1 & I \\ m_d & -m'_d & -M \end{pmatrix} \\ &\quad \times \int \rho_s (\mathcal{M}_{sm_s, m_\gamma m_d}^{(t\mu)})^* \mathcal{M}_{s-m_s, m_\gamma -m'_d}^{(t\mu)} d\Omega_{\vec{p}_r}, \end{aligned} \quad (1.5)$$

where  $\hat{I} = \sqrt{2I+1}$ .

The unpolarized differential cross section is then given by

$$\frac{d\sigma}{d\Omega_\pi dq} = V_{00}. \quad (1.6)$$

The photon asymmetry for linearly polarized photons is given by

$$\sum^\ell(\theta_\pi) = - \left( \frac{d\sigma}{d\Omega_\pi dq} \right)^{-1} W_{00}. \quad (1.7)$$

The target asymmetries are given by

- The vector target asymmetry:

$$T_{11}(\theta_\pi) = \left( \frac{d\sigma}{d\Omega_\pi dq} \right)^{-1} 2 \Im m V_{11} , \quad (1.8)$$

- The tensor target asymmetries:

$$T_{2M}(\theta_\pi) = \left( \frac{d\sigma}{d\Omega_\pi dq} \right)^{-1} (2 - \delta_{M0}) \Re e V_{2M} , \quad (M = 0, 1, 2) . \quad (1.9)$$

The photon and target asymmetries are given by

- Circular:

$$\begin{aligned} T_{1M}^c(\theta_\pi) &= \left( \frac{d\sigma}{d\Omega_\pi dq} \right)^{-1} (2 - \delta_{M0}) \Re e V_{1M} , \quad (M = 0, 1) \\ T_{2M}^c(\theta_\pi) &= \left( \frac{d\sigma}{d\Omega_\pi dq} \right)^{-1} 2 \Im m V_{2M} , \quad (M = 0, 1, 2) , \end{aligned} \quad (1.10)$$

- Longitudinal:

$$\begin{aligned} T_{1M}^\ell(\theta_\pi) &= \left( \frac{d\sigma}{d\Omega_\pi dq} \right)^{-1} i W_{1M} , \quad (M = 0, \pm 1) , \\ T_{2M}^\ell(\theta_\pi) &= - \left( \frac{d\sigma}{d\Omega_\pi dq} \right)^{-1} W_{2M} , \quad (M = 0, \pm 1, \pm 2) . \end{aligned} \quad (1.11)$$



# Bibliography

- [1] DARWISH, E., *Rescattering Effects in Incoherent Photoproduction of  $\pi$ -Mesons off Deuterium in the  $\Delta(1232)$  Resonance Region*, Dissertation, Institut für Kernphysik, Johannes Gutenberg-Universität, Mainz, 2002.
- [2] ARENHÖVEL, H., *General Formulae for Polarization Observables in Two-Body Break-Up of Deuteron Photodisintegration*, Few-Body Systems **4** (1988), 55.